Survey of single-particle states in the mass region $A > 228$*

R. R. Chasman, I. Ahmad, A. M. Friedman, and J. R. Erskine

Argonne National Laboratory, Argonne, Illinois 60439

A deformed single-particle potential mode, with residual interactions, is applied to an analysis of states in odd-mass nuclides with $A > 228$, and configuration assignments are presented for many levels. The systematics of energy level spacings throughout the actinides are studied, and the values of the nuclear deformation parameters that are appropriate to these nuclides are discussed. Tables of occupation probabilities and single-particle matrix elements are provided to facilitate the comparison of future measurements with theoretical expectations.

CONTENTS

*Work performed under the auspices of the Division of Physical Research of the U. S. Energy Research and Development Administration.

I. INTRODUCTION

The heavy element region constitutes one of the frontiers of nuclear research. If the study of odd-mass nuclides with $A > 228$ were confined to those found in nature, our task would consist of the study of the single nuclide ^{235}U. However, the situation is now vastly different. Almost 100 odd-mass nuclides with $A > 228$ are known. The study of the systematics of these nuclides has led to considerable advances in the understanding of the alpha-decay process (Rasmussen, 1965), the fission process, nuclear shapes, and the limits of nuclear stability (Hill and Wheeler, 1953; Mottelson and Nilsson, 1959; Myers and Swiatecki, 1966; Strutinsky, 1967; Bolsterli *et al.*, 1972; Brack *et al.*, 1972). Underlying all of these problems are the concepts of the nuclear single-particle state and the nuclear central potential.

The single-particle potential plays a central role in our understanding of nuclear structure. It both generates and is generated by the motion of nucleons in the nucleus. Through a proper choice of the effective single-particle potential many aspects of nuclear structure can be simply understood. Low-lying nuclear eigenstates can often be well described as single-particle excitations. A systematic study of these excitations determines the parameters of the single-particle potential. The single-particle eigenstates obtained from such a potential provide the basic building block for the microscopic description of more complicated nuclear eigenstates. The few-particle excitations and also the coherent modes are described in terms of these single-particle eigenstates. In this work, we examine the low-lying excitations in the heavy element region and the interactions that best describe these states.

The first triumph of the single-particle approach was the explanation of the phenomenon of "magic numbers," i.e., the unusual stability of nuclei with certain numbers of protons and neutrons. By including a one-body spin-orbit term in a spherically symmetric single-particle potential, Mayer (1949) and Haxel, Jensen, and Suess (1950) were able to correlate magic numbers of protons and neutrons with the complete filling of shells in the single-particle potential. This potential also explained the spins and magnetic moments of magic and near magic nuclides, as well as the occurrence of nuclear isomerism. However, this model did not account for the large observed nuclear quadrupole moments (Townes *et al.*, 1949). The large quadrupole moments led to the postulate (Rainwater, 1950; Bohr, 1951; Bohr, 1952) of

permanently deformed nuclides. This model was developed by Bohr and Mottelson (1953) to provide a detailed picture of nuclear structure in many regions of the Periodic Table, most notably the rare earths and the actinides. The concept of a permanently deformed nucleus is a most fruitful one for the elucidation of low-lying states in odd-mass nuclides in the region that we consider here. An interesting summary of the early history (Rainwater, 1976), as well as the development (Bohr, 1976; Mottelson, 1976) of this picture can be found in the Nobel laureate addresses of Rainwater, Bohr, and Mottelson.

The single-particle states generated from an axially symmetric spheroidal potential (Nilsson, 1955; Moszkowski, 1955; Gottfried, 1955) provided a fairly accurate picture of level spins and level spacings in the actinides. An improved description of the single-particle states has been achieved with the introduction of a Woods-Saxon potential (Woods and Saxon, 1954; Chepurnov and Nemirovskii, 1963). The structure of odd-mass nuclides has been further clarified with the consideration of two-body interactions such as the pairing force (Bardeen *et al.*, 1957a, 1957b; Bogoliubov, 1958a, 1958b; Bohr *et al.*, 1958), and particle–hole interactions (Brown and Bolsterli, 1959; Arvieu and Veneroni, 1960; Baranger, 1960; Kisslinger and Sorensen, 1963; Bohr and Mottelson, 1975).

In the 1950s sophisticated experimental techniques were extremely difficult to apply to the actinides. Precision measurements of alpha and electron energies were done using relatively low transmission magnetic spectrometers. Precise photon energies could be determined only by diffraction techniques. Ground-state spins and magnetic moments were determined by optical spectroscopy and direct measurements for long-lived nuclei. A good survey of this situation was given by Perlman and Rasmussen (1957). Nevertheless, sufficient data had been obtained by 1959 (Mottelson and Nilsson, 1959) to establish good agreement with the single-particle model in the rare-earth region. While evidence for specific assignments of the single-particle states in the actinide elements was much more indirect, Mottelson and Nilsson (1959) and Stephens *et al.* (1959) assigned about 40 single-particle states in that mass region on the basis of energy orderings and inferred spins. They were able to confirm half of the assignments by correlations between theoretical and observed alpha decay, beta or electromagnetic transition rates, and/or agreement between calculated and observed magnetic moments or decoupling parameters.

Semiconductor detector and multichannel analyzer development provided enormous advances in nuclear instrumentation in the 1960s; and a great deal of new data was obtained concerning the structure of the actinides. However, most of this information was restricted to levels below ~600 keV.

It became apparent from the studies of Vergnes and Sheline (1963) that reaction spectroscopy was a feasible technique to use in investigating levels of deformed nuclei, and that this technique would yield nuclear structure information not available from radioactive decay studies. The earliest attempt to adapt this technique to the heavy elements was performed by Macefield and Middleton (1964). A more comprehensive study was presented the following year by Braid *et al.* (1965) on neutron states observed in many of the lighter odd-neutron actinides. Ellis and Schmorak (1972), in their tabulation of the systematics of $A > 229$ nuclei, were able to list 120 assigned single-particle states in the heavy elements. The vast majority of these assignments were based on data obtained using reaction spectroscopy to populate odd-neutron species. Our survey contains well over 200 assignments of single-particle states.

As noted above, a comparison of experimental data with the predictions of the deformed oscillator model was made by Mottelson and Nilsson (1959) and by Stephens *et al.* (1959). A later review was given by Nathan and Nilsson (1965). An extensive review of the rare-earth region of the Periodic Table was written by Bunker and Reich (1971). In a companion paper, these data were comprehensively analyzed by Ogle *et al.* (1971) for the purpose of determining the parameters of the single-particle potential in the rare earths. In this work, we treat the actinides in much the same spirit as the latter two surveys of the rare earths. Much of the material discussed in this study was covered in a preliminary form in talks at the International Symposium on Transplutonium Elements (Erskine, 1972; Chasman, 1972). Also, much of this information has been summarized by Hoff (1972; 1975). In this survey, we have organized the information in the form of tables, both of experimental data and of calculated matrix elements.

Many excellent discussions have been published of the single-particle model, the one-nucleon transfer reaction, and residual interaction effects (Nilsson, 1955; Moszkowski, 1957; Kerman, 1959; Nathan and Nilsson, 1965; Elbek and Tjøm, 1969; Bès and Sørenson, 1969; Kumar, 1975; Nemirovskii, 1963; Lane, 1964; Brown, 1967; Davidson, 1968; Rowe, 1970; de Shalit and Feshbach, 1974; Bunker and Reich, 1971; Ogle *et al.*, 1971). An exceptionally valuable text is that of Bohr and Mottelson (1969; 1975). We shall refer to the appropriate sections of this text throughout this paper.

Our survey of the experimental literature has a cutoff date of December 1976, although there are some references to later data.

II. NUCLEAR MODEL

As the nuclear model we use here has been extensively discussed elsewhere, we present a summary, with relevant formulas. In this model, we assume that the actinide nuclides are nonspherical in shape and have rotational symmetry about an intrinsic z axis and reflection symmetry through the intrinsic x–y plane. The model is one of a deformed core with rotational degrees of freedom and valence nucleons that move in the field of the deformed core. At a more microscopic level, the deformed core must also be described in terms of the motions of individual nucleons (Bohr and Mottelson, 1975).

A. Rotational Hamiltonian

The Hamiltonian that describes this model is (Bohr, 1952; Bohr and Mottelson, 1953)

$$H = H_{\text{rotor}} + H_{\text{intrinsic}}, \tag{2.1}$$

with

$$H_{\text{rotor}} = \sum_{K=1}^{3} \frac{\hbar^2}{2\mathcal{I}_K} R_K^2 \tag{2.2}$$

and

$$H_{\text{intrinsic}} = \sum_{\alpha} \left[\left(\sum_{L=1}^{3} \frac{(P_\alpha)_L^2}{2m} + \right) + V_c(\mathbf{r}_\alpha, \mathbf{P}_\alpha, \sigma_\alpha, \tau_\alpha) + \sum_{\beta} V_{\alpha\beta}(\mathbf{r}_{\alpha\beta}, \mathbf{R}_{\alpha\beta}, \mathbf{P}_{\alpha,\beta} \ldots) \right] . \tag{2.3}$$

In Eq. (2.2), $\mathcal{I}_K$ denotes the moment of inertia of the rotating core and R_K is the Kth component of the core angular momentum. In Eq. (2.3) the indices α and β denote nucleon orbitals; $(P_\alpha)_L$ is a component of the nucleon momentum; V_c is the effective central nucleon potential; and $V_{\alpha\beta}$ is the residual interaction between nucleons. Both V_c and $V_{\alpha\beta}$ may depend on position, momentum, spin, and isospin variables.

The relevant angular momentum variables in this model are **R**, the core angular momentum; **J**, the angular momentum of the individual nucleons; and **I**, the total angular momentum of the nucleus. Of these, only **I** is a conserved quantity and the relation between the angular momentum variables is

$$\mathbf{I} = \mathbf{R} + \mathbf{J} . \tag{2.4}$$

In Fig. 1, we display (as given in Nilsson, 1955) the angular momentum vectors and their projections on space-fixed and intrinsic axes. We shall use indices 1, 2, 3 to denote intrinsic axes and x, y, z to denote the space-fixed axes.

Substituting Eq. (2.4) into Eq. (2.2), one obtains

$$H_{\text{rotor}} = \sum_{K=1}^{3} \frac{\hbar^2}{2\mathcal{I}_K} (I_K - J_K)^2 . \tag{2.5}$$

As the core is symmetric about the 3 axis, the moment of inertia about that axis vanishes and we have

$$H_{\text{rotor}} = \frac{\hbar^2}{2\mathcal{I}_\perp} (I^2 - I_3^2) - \frac{\hbar^2}{2\mathcal{I}_\perp} (I^+ J^- + I^- J^+) + \frac{\hbar^2}{2\mathcal{I}_\perp} (J^2 - J_3^2) . \tag{2.6}$$

The final term of Eq. (2.6) is called the recoil term, and

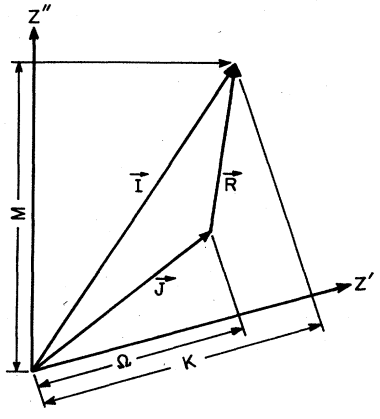

FIG. 1. Angular momenta couplings in the rotational model and their projections (Nilsson, 1955). **R** is the core angular momentum and **J** is the particle angular momentum.

it has usually been ignored in studies of the actinides. It can be readily absorbed into $H_{\text{intrinsic}}$, and presumably the parameters of the effective potential are adjusted to take it into account. This term should not give rise to serious problems in the actinides, where the moments of inertia are large and do not vary excessively. At the edges of deformed regions, where the moments of inertia are changing, this term will cause shifts in the relative single-particle energies. The effects of this term have been treated roughly in the analysis of the rare earths by Ogle *et al.* (1971). This term has been treated in more detail in a recent study of the rare earths (Nielsen and Bunker, 1975) and a study of the transition nuclides (Osnes *et al.*, 1975). We do not consider this term explicitly here.

The first term of Eq. (2.6) gives the rotational spectrum of the symmetric top. The second term, often called the Coriolis interaction term (Bohr, 1952; Kerman, 1956), gives rise to particle–rotation interactions.

Because we assume that the 3 axis is a rotational symmetry axis and the x–y plane is reflection symmetric in the intrinsic potential, the eigenstates of $H_{\text{intrinsic}}$ will have $\Omega(J_3)$ and parity as good quantum numbers. Further, because of the time reversal symmetry of the Hamiltonian, all intrinsic eigenstates are doubly degenerate, with the two degenerate states having projections $+\Omega$ and $-\Omega$ on the 3 axis; we denote these states by χ_Ω and $\chi_{-\Omega}$.

Taking the first term of H_{rotor} and $H_{\text{intrinsic}}$ as the unperturbed Hamiltonian, the eigenstates are of the form (Bohr and Mottelson, 1953)

$$\phi^I_{M,\Omega} = \left(\frac{2I+1}{16\pi^2} \right)^{1/2} \left[\chi_\Omega D^I_{M\Omega}(\omega_i) + (-1)^{I+\Omega} \chi_{-\Omega} D^I_{M-\Omega}(\omega_i) \right] , \tag{2.7}$$

where the functions $D^I_{M\Omega}(\omega_i)$ are symmetric top eigenfunctions [Bohr and Mottelson, 1969 (Appendix 1A)] whose arguments are the Euler angles ω_i. These eigenstates are mixed by the Coriolis interaction term of Eq. (2.6) (Kerman, 1956).

The main concern of this review is the nature of $H_{\text{intrinsic}}$. H_{rotor} modifies our perceptions of the effective nuclear interaction through the Coriolis term. We present here the relevant matrix elements of H_{rotor} and can then focus exclusively on the intrinsic Hamiltonian. The relevant relations are [Bohr and Mottelson, 1969 (Appendix 1A)]

$$I^2 D^I_{M\Omega}(\omega_i) = I(I+1) D^I_{M\Omega}(\omega_i) , \tag{2.8a}$$

$$I_3 D^I_{M\Omega}(\omega_i) = \Omega D^I_{M\Omega}(\omega_i) , \tag{2.8b}$$

$$I_Z D^I_{M\Omega}(\omega_i) = M D^I_{M\Omega}(\omega_i) , \tag{2.8c}$$

$$I_\pm D^I_{M\Omega}(\omega_i) = [(I \pm \Omega)(I \mp \Omega + 1)]^{1/2} D^I_{M\Omega \mp 1}(\omega_i) . \tag{2.8d}$$

One also needs $J_\pm$ matrix elements to calculate Coriolis interaction effects. For systems with spherical symmetry, J is a good quantum number, and the analog of Eq. (2.8d) is

$$J_\pm |J, \Omega\rangle = [(J \mp \Omega)(J \pm \Omega + 1)]^{1/2} |J, \Omega \pm 1\rangle . \tag{2.9}$$

However, the eigenstates of the nonspherically symmetric $H_{\text{intrinsic}}$ do not have a conserved angular momentum, and the matrix elements of $J_\pm$ depend on the details of these eigenstates. We have tabulated matrix elements

of J_+ for all of the orbitals that are expected to be found in the actinide nuclides, and these quantities are presented in Appendix C. Because of the core's rotational degrees of freedom, there is a rotational band built on each intrinsic configuration χ_Ω with an energy spectrum that is proportional to $I(I+1)$ in lowest order. This rotational spectrum is modified for configurations with $\Omega = \frac{1}{2}$ by the Coriolis interaction term, as there are nonvanishing diagonal matrix elements in this instance. For $\Omega = \frac{1}{2}$ configurations, the rotational spectrum is given as (Bohr, 1952; Nilsson, 1955)

$$E^I_{1/2} = \frac{\hbar^2}{2\mathcal{I}_\perp}\left[I(I+1) + (-1)^{I+1/2}(I+1/2)\mathbf{a}\right], \tag{2.10}$$

with the decoupling parameter $\mathbf{a}$ given by

$$\mathbf{a} = -\langle \chi_{1/2}|J_+|\chi_{-1/2}\rangle . \tag{2.11}$$

The decoupling parameter often provides a characteristic signature for $\Omega = \frac{1}{2}$ configurations.

B. Intrinsic Hamiltonian

The aim of this section is the characterization of the intrinsic Hamiltonian. We first discuss the single-particle potential and then consider the residual interactions.

1. Single-particle Hamiltonian

In the spherical limit, the single-particle potentials that we consider are of the general form

$$H_{\text{s.p.}} = \frac{p^2}{2m} + V_0 v(r) F(p^2) + K\frac{1}{r}\frac{dv(r)}{dr}\,\mathbf{l}\cdot\mathbf{s} + \frac{(1+\tau_3)}{2}V^{(r)}_{\text{Coul}} . \tag{2.12}$$

There are several different ways of generalizing a Hamiltonian of this form for nonspherical potentials. There is some confusion in the literature on the relations between different parametrizations of the deformation of the single-particle potential. In an attempt to clarify these relations, we discuss this problem in Appendix A, where all deformation parameters used in this paper are defined.

The most important deformation mode in the actinides is the quadrupole deformation mode; however, this is not the only deformation mode with axial and reflection symmetry. Other deformation modes can be introduced into the potential, by expansions in a series of Legendre polynomials, or by rather different characterizations of the nuclear surface shape, as done in studies of the fission process (Bolsterli *et al.*, 1972; Brack *et al.*, 1972). In most studies of the actinides, at stable values of the deformation parameters, the Legendre expansion of the potential shape is used. Because of the assumed symmetry, only even Legendre polynomials are included. The deformations characterized by $P_4(\cos\theta)$ turn out to be important in the actinides, but are considerably smaller than the quadrupole deformations. The evidence for higher multipole deformation modes is weak.

Qualitatively, the various treatments of a deformed single-particle potential give similar results in terms of single-particle wave functions and energy level spacings. This is because the potential parameters are adjusted to the same set of experimental data.

The first extensively used single-particle potential model for the actinides was the modified oscillator potential of Nilsson and co-workers (Nilsson, 1955; Mottelson and Nilsson, 1959). This potential has been modified and improved (Gustafson *et al.*, 1967; Lamm, 1969; Bengtsson, 1975) in recent years. We shall discuss this potential in some detail, since the same terminology is used for other single-particle potentials as well. In the first and simplest version, the modified oscillator Hamiltonian is (Nilsson, 1955)

$$H = \frac{p^2}{2m} + \frac{m}{2}(\omega_\perp^2\rho^2 + \omega_Z^2 z^2) - K(2\mathbf{l}\cdot\mathbf{s} + \mu l^2) , \tag{2.13}$$

with the parameters $\omega_\perp^2$ and ω_Z^2 defined in terms of the constant $\hbar\omega_0 \approx 41/A^{1/3}$ MeV, as

$$\omega_\perp^2 = \omega_0^2(1 + \tfrac{1}{3}\epsilon)^2 \tag{2.14}$$

and

$$\omega_Z^2 = \omega_0^2(1 - \tfrac{2}{3}\epsilon)^2 , \tag{2.15}$$

with ϵ being the parameter describing the magnitude of the quadrupole deformation of the single-particle potential. The eigenstates of this Hamiltonian are normally obtained by diagonalization with a harmonic oscillator basis set—either the spherical basis set (Nilsson, 1955) or the cylindrical oscillator basis set (Nilsson, 1955; Rassey, 1958; Boisson and Piepenbring, 1971). The role of the l^2 term in the modified oscillator potential is to give a potential that is somewhat steeper than the simple oscillator.

The cylindrical oscillator basis set plays a key role in the description of deformed single-particle eigenstates as the cylindrical oscillator quantum numbers provide a labeling of these states. To obtain the cylindrical solutions, one transforms

$$\begin{aligned} x' &= \sqrt{\omega_\perp m/\hbar}\; x , \quad P_{x'} = \frac{1}{\sqrt{\omega_\perp m/\hbar}}\,P_x ; \\ y' &= \sqrt{\omega_\perp m/\hbar}\; y , \quad P_{y'} = \frac{1}{\sqrt{\omega_\perp m/\hbar}}\,P_y ; \\ z' &= \sqrt{\omega_z m/\hbar}\; z , \quad P_{z'} = \frac{1}{\sqrt{\omega_z m/\hbar}}\,P_z . \end{aligned} \tag{2.16}$$

The eigenstates of $H_\perp$ are designated by $|n_\perp, \Lambda\rangle$ and those of H_z by $|n_z\rangle$. The basis states for the diagonalization in the cylindrical oscillator representation are labeled as $\Omega^\pi[Nn_Z\,\Lambda]$. N, the oscillator shell number, is the sum of the two oscillator quantum numbers $n_\perp$ and n_Z. The quantity Λ denotes the projection of single-particle orbital angular momentum on the 3 axis. Because of the spin-orbit interaction, Λ is no longer the conserved quantity, rather $\Lambda + S_3$ is conserved. This conserved projection j_3 is denoted by Ω; π denotes parity. In the limit of large quadrupole deformations the eigenstates of the modified oscillator Hamiltonian are well described by a single basis state $\Omega^\pi[Nn_Z\Lambda]$, where N, n_Z, and Λ are the asymptotic quantum numbers. The stretched spherical coordinates are obtained by defining the variables (Nilsson, 1955; Moszkowski, 1955)

$$\begin{aligned} (r')^2 &= (\rho')^2 + (z')^2 , \\ \cos\theta' &= z'/r' , \end{aligned} \tag{2.17}$$

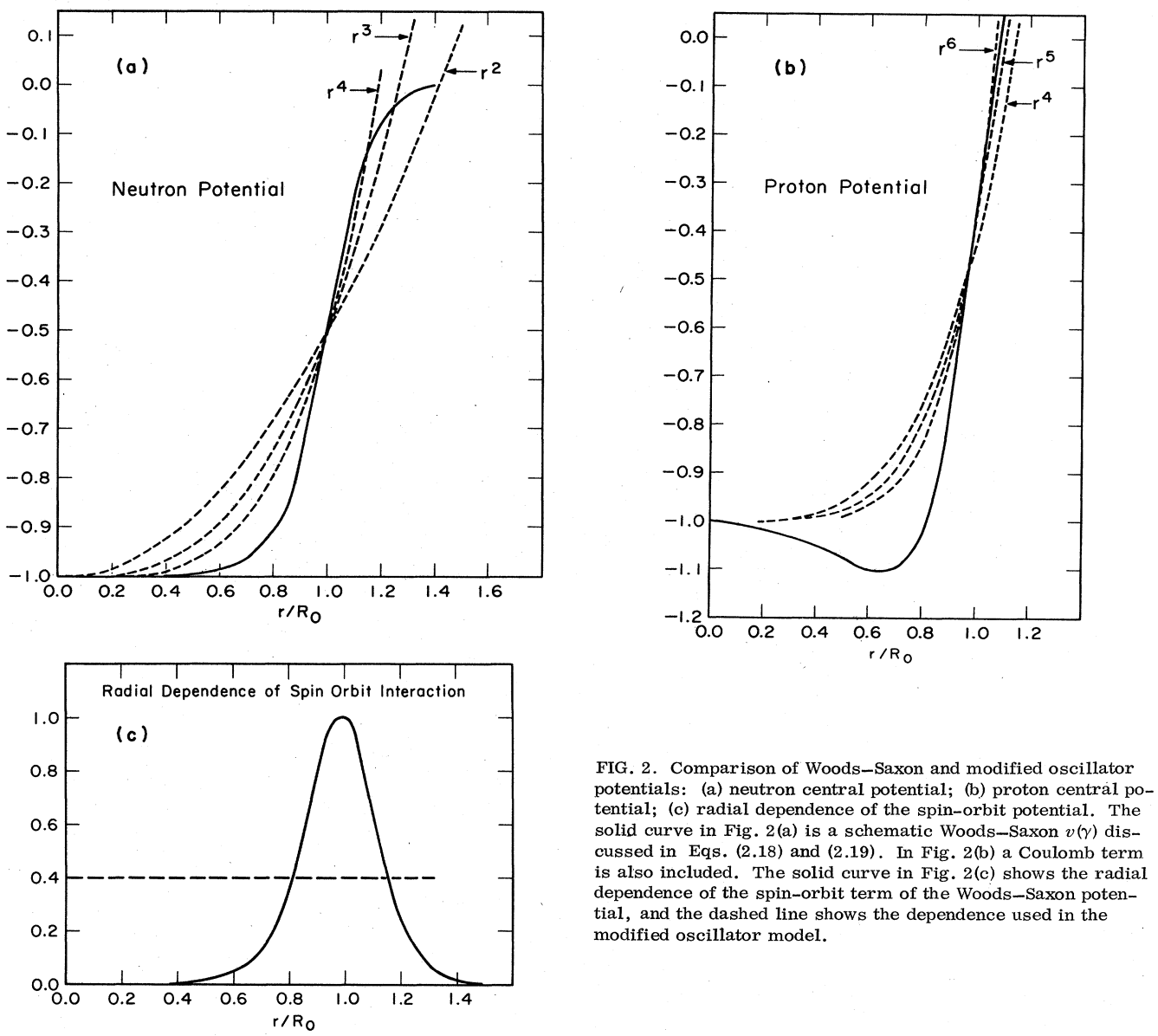

FIG. 2. Comparison of Woods–Saxon and modified oscillator potentials: (a) neutron central potential; (b) proton central potential; (c) radial dependence of the spin-orbit potential. The solid curve in Fig. 2(a) is a schematic Woods–Saxon $v(\gamma)$ discussed in Eqs. (2.18) and (2.19). In Fig. 2(b) a Coulomb term is also included. The solid curve in Fig. 2(c) shows the radial dependence of the spin-orbit term of the Woods–Saxon potential, and the dashed line shows the dependence used in the modified oscillator model.

and the corresponding basis set is called the stretched spherical basis, denoted by $\Omega^{\pi}[N'l'\Lambda]$. The advantage of this basis is that states having different values of N' are not mixed by the first terms of the central potential, in contrast to the situation that obtains for an unstretched spherical basis set.

A more realistic approach to single-particle potentials is the Woods–Saxon potential (Woods and Saxon, 1954; Blomquist and Wahlborn, 1960; Chepurnov and Nemirovskii, 1963). The single-particle Hamiltonian $H_{\rm WS}$ in the spherical limit is

$$H_{\rm WS} = \frac{p^2}{2m} + V_0 v(r) + V_{LS}\frac{1}{r}\frac{dv(r)}{dr}\mathbf{l}\cdot\mathbf{s} + \frac{1+\tau_3}{2}V_{\rm Coul}(r) \quad (2.18)$$

with

$$v(r) = \{1+\exp[(r-R_0)/a]\}^{-1}. \quad (2.19)$$

The essential differences relative to the modified oscillator potential are (1) the well is finite rather than infinite; (2) the spin-orbit radial form factor is surface peaked; (3) Coulomb forces are taken into account explicitly. In Fig. 2, we compare the two potentials. The parameter R_0 is usually taken as $r_0 A^{1/3}$, with $r_0 \approx 1.25$ fm; and a, which determines the steepness of the potential, is 0.6–0.8 fm (Ehrling and Wahlborn, 1972).

Deformations are introduced into the Woods–Saxon potential either as (Chasman, 1970; Ogle *et al.*, 1971; Ehrling and Wahlborn, 1972)

$$r^2 \to r^2[1+\sum_l \lambda_l P_l(\cos\theta)] \quad (2.20a)$$

or (Nemirovskii and Chepurnov, 1966; Faessler and Sheline, 1966; Rost, 1967; Gareev *et al.*, 1967, 1971; Møller *et al.*, 1974; Brack *et al.*, 1974)

$$R_0 \to R_0[1+\sum_l \beta_l Y_l^0(\cos\theta)]. \quad (2.20b)$$

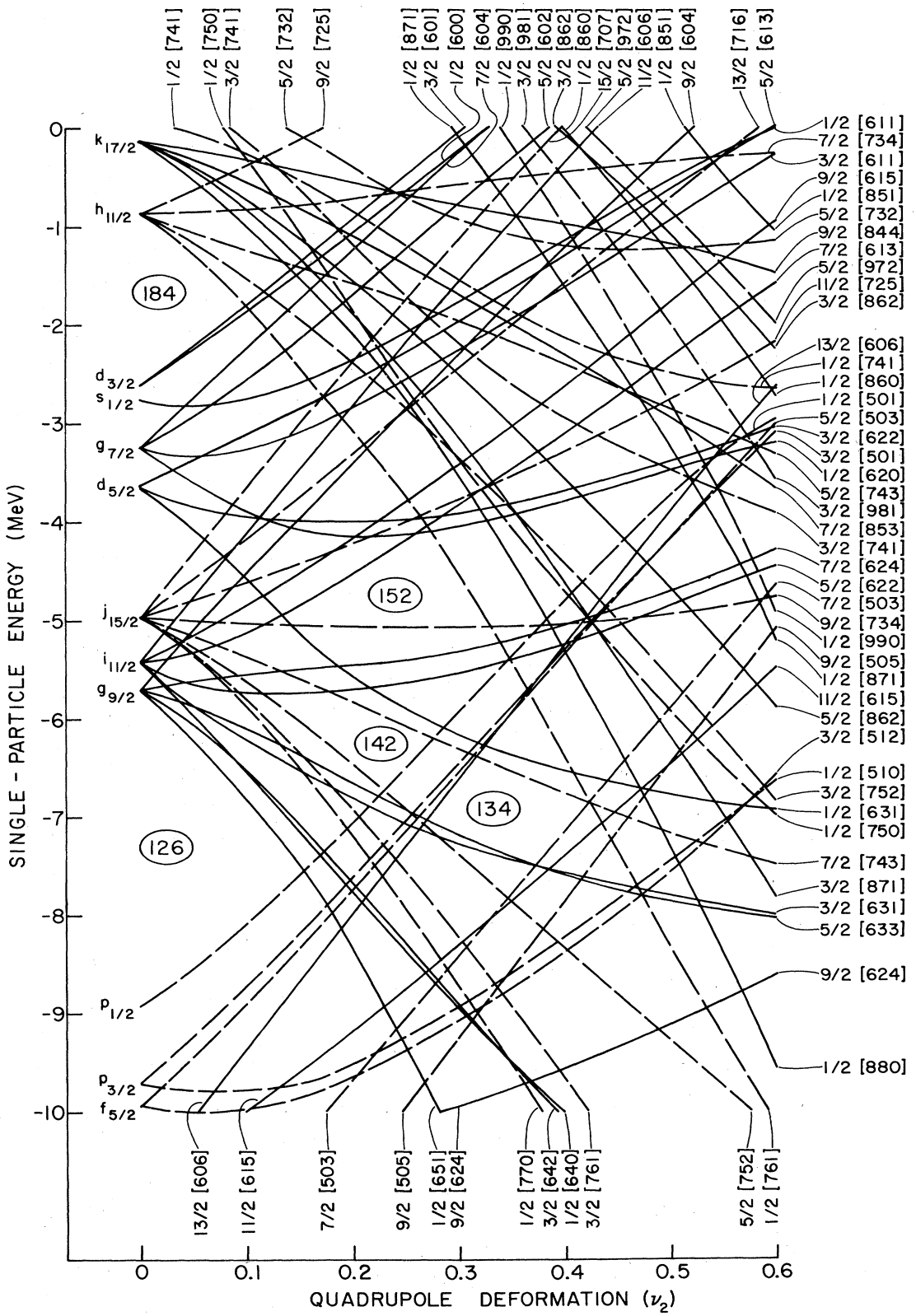

FIG. 3. Actinide neutron single-particle levels obtained from momentum-dependent Woods–Saxon potential as a function of quadrupole deformation, ν_2. Deformation parameters are defined in Appendix A. Asymptotic labels are used for levels, but they do not always characterize levels well at the equilibrium deformation.

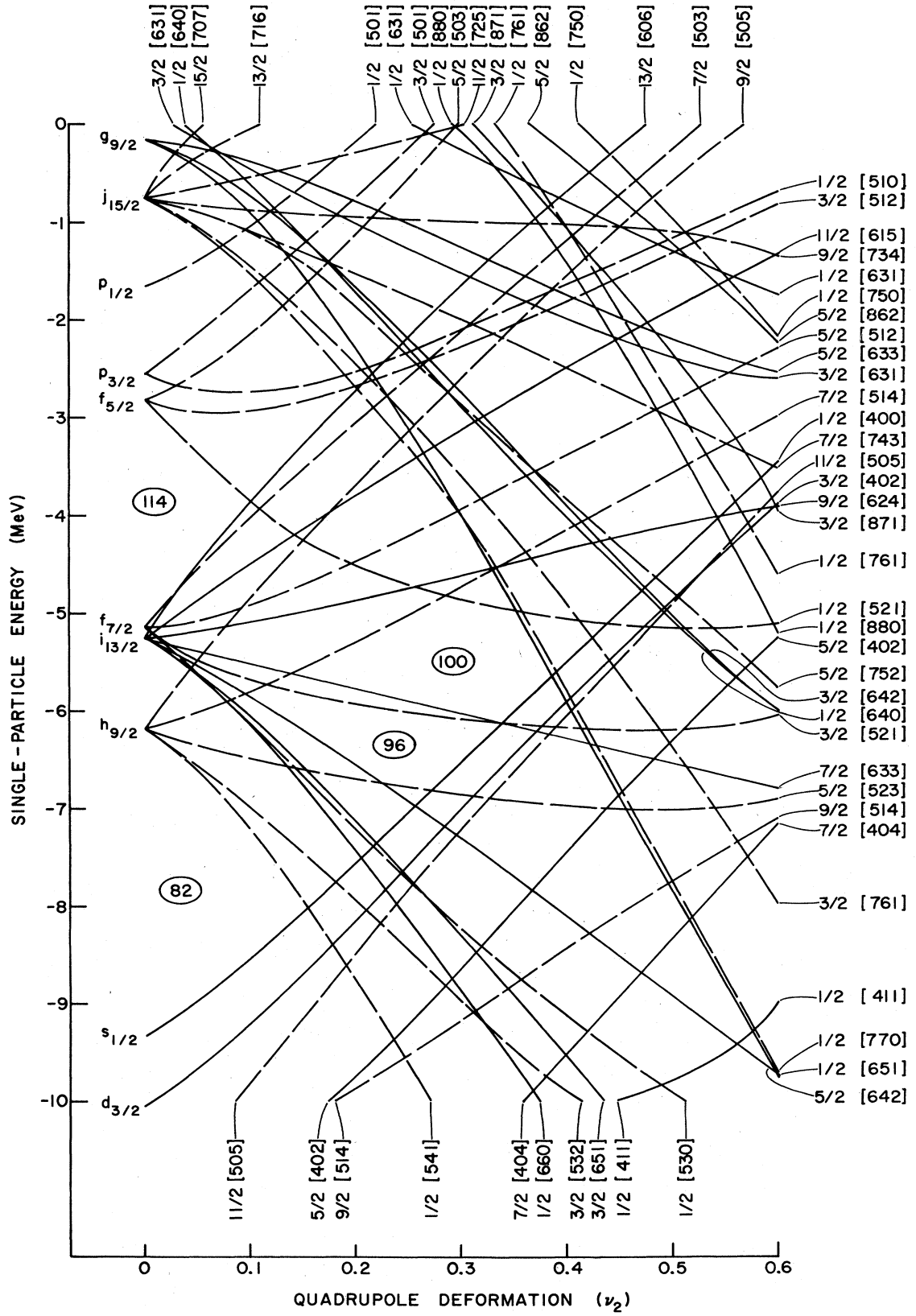

FIG. 4. Actinide proton single-particle levels obtained from momentum-dependent Woods–Saxon potential as a function of quadrupole deformation, ν_2. Also see caption for Fig. 3.

The first of these is analogous to the treatment of deformations in the modified oscillator model. The second is specialized for the Woods–Saxon form of the potential.

There are several ways to calculate the eigenvalues of the deformed Woods–Saxon potential. One is to use the spherical Woods–Saxon eigenfunctions as a basis set for the deformed potential calculation (Faessler and Sheline, 1966). Another is the coupled-channel method of calculating Woods–Saxon eigenvalues (Rost, 1967). This latter technique gives accurate wave functions, including the tail region, but it is quite time consuming. For most purposes, e.g., energy level spacings and transition matrix elements, it is not necessary to calculate the tail of the wave function accurately. For transfer reaction studies the tails are important; and this approach, or the use of Sturmian functions (Anderson *et al.*, 1970; Schultz *et al.*, 1972; Bang and Gareev, 1974), is warranted. In general, however, it is most convenient to calculate the single-particle states of the Woods–Saxon potential using a large harmonic oscillator basis set. The cylindrical oscillator basis set is particularly useful for this purpose. One chooses the basis set frequencies as given in Eqs. (2.14) and (2.15) (Damgaard *et al.*, 1969; Chasman, 1970). The choice of stretched spherical oscillator eigenfunctions would also require a basis set of the same size as the cylindrical oscillator eigenfunctions. The use of ordinary spherical oscillator eigenfunctions requires a larger basis set. For deformations of the magnitude that one encounters in the actinide region ($|\epsilon_2| \lesssim 0.30$, $|\epsilon_4| \lesssim 0.10$), we find that the cylindrical basis set for neutrons should consist of at least 14 oscillator shells and that for protons should consist of at least 13 oscillator shells. The wave functions that are obtained from the Woods–Saxon potential agree better with experimental data than those obtained from the modified oscillator potential.

In the Woods–Saxon potential that we have so far discussed, the calculated binding energy of the 0s (orbital) neutron is roughly 35 MeV. High-energy proton scattering experiments indicate, however, that the 0s proton is bound by ~50 MeV (James *et al.*, 1969). If one adjusts the parameters of the Woods–Saxon well to reproduce the 0s binding energies and keep the Fermi level at ~−6 MeV, one finds (Wyatt *et al.*, 1960; Brown *et al.*, 1963) that the energy spacings of the eigenvalues in the vicinity of the Fermi level are roughly twice as large as those given by the conventional Woods–Saxon parameter choices, or as indicated by experiment. There are two ways to look at this difficulty: (1) there is a real momentum or energy dependence of the effective single-particle potential that gives level compressions in the vicinity of the Fermi level (Wyatt *et al.*, 1960; Brown *et al.*, 1963) or (2) residual interaction effects cause the level compression in the vicinity of the Fermi level. These effects are in no way mutually exclusive. In either event, the observed level compression can be simply incorporated into the Woods–Saxon potential, together with physically correct 0s eigenvalues, by making the potential momentum dependent using a polynomial in p^2 (Chasman, 1971). By adding a term $V_2(p^2/m)v(r)$ to the potential, it is possible to lower the 0s binding energy and keep the Fermi level at ≈−6 MeV. This is the effective mass approximation, and it gives level spacings in the vicinity of the Fermi level that are too large (Brown *et al.*, 1963). The counterterm $-V_4(p^2/m)^2v(r)$ gives the level compression at the Fermi level required by experiment, but it has the catastrophic feature that infinite momentum states are infinitely bound. To remove this catastrophe, an additional term $V_6(p^2/m)^3v(r)$ is needed. Sets of parameters V_0, V_2, V_4, and V_6 for proton and neutron potentials have been given (Chasman, 1971). We have incorporated this feature into our potential, and the matrix elements tabulated in this work are obtained using wave functions calculated with this momentum-dependent Woods-Saxon single-particle potential. In the vicinity of the Fermi level, the spacings and wave functions are similar to those of a conventional Woods–Saxon potential. Single-particle matrix elements obtained with these wave functions are tabulated in Appendix C.

In Figs. 3 and 4, we show the variation of proton and neutron eigenvalues with changes in the quadrupole deformation parameter. In Figs. 5–10, we display the variation of these eigenvalues with deformations in the $P_2(\cos\theta)$, $P_4(\cos\theta)$, and $P_6(\cos\theta)$ modes over the ranges of deformation appropriate to the actinides (Braid *et al.*, 1971; Chasman, 1972; Erskine *et al.*, 1975). In these figures there is no volume conservation correction for the P_4 and P_6 deformations.

2. Residual interactions

a. Pairing

The observed properties of the actinide levels are not given simply by the central interaction that we have discussed above. Two-body interactions may modify level properties substantially. The most important of the residual interactions is the pairing interaction. The pairing interaction (Bardeen *et al.*, 1957a; 1957b; Bogoliubov, 1958), first used to describe superconductivity, was

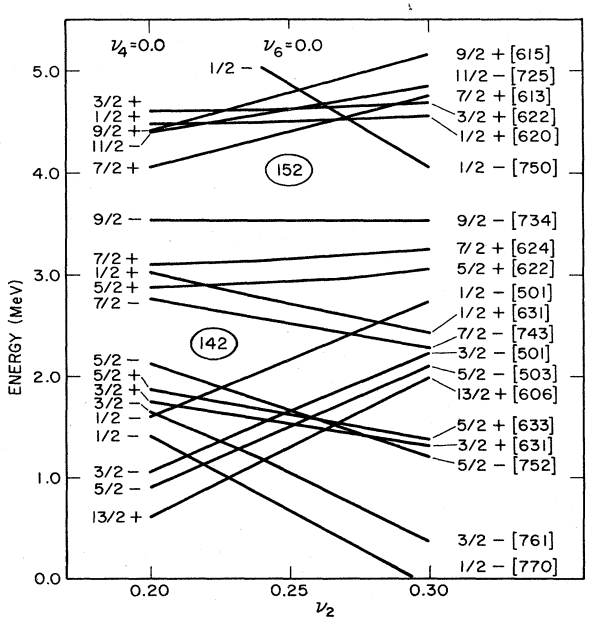

FIG. 5. Actinide neutron single-particle levels as a function of ν_2, reduced range; $\nu_4 = 0.0, \nu_6 = 0.0$.

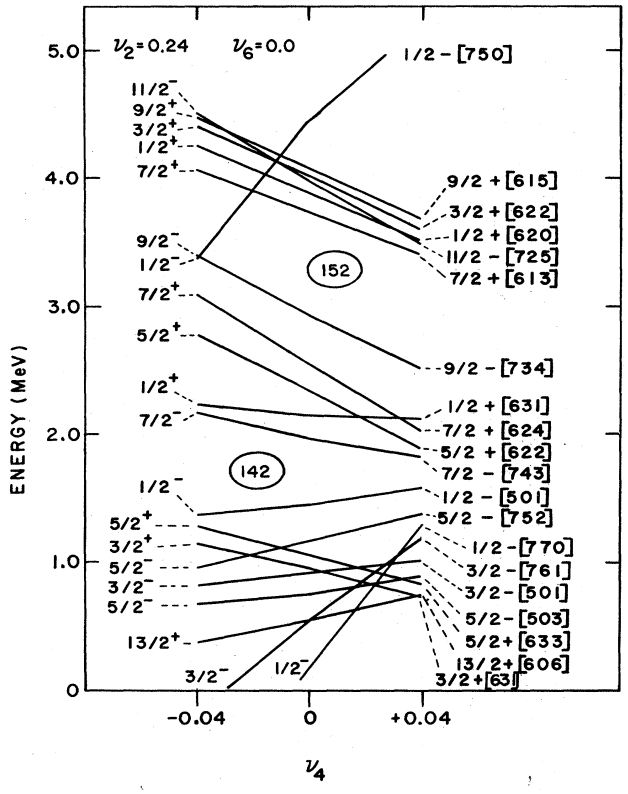

FIG. 6. Actinide neutron single-particle levels as a function of ν_4; $\nu_2 = 0.24, \nu_6 = 0.0$.

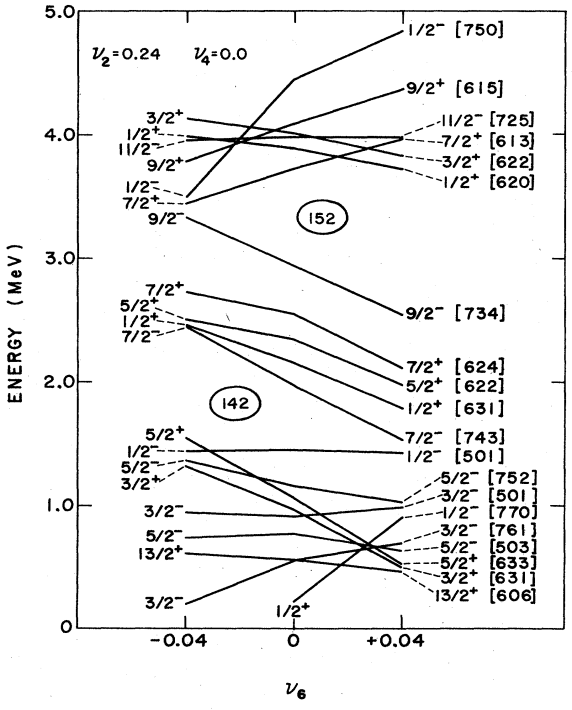

FIG. 7. Actinide neutron single-particle levels as a function of ν_6; $\nu_2 = 0.24, \nu_4 = 0.0$.

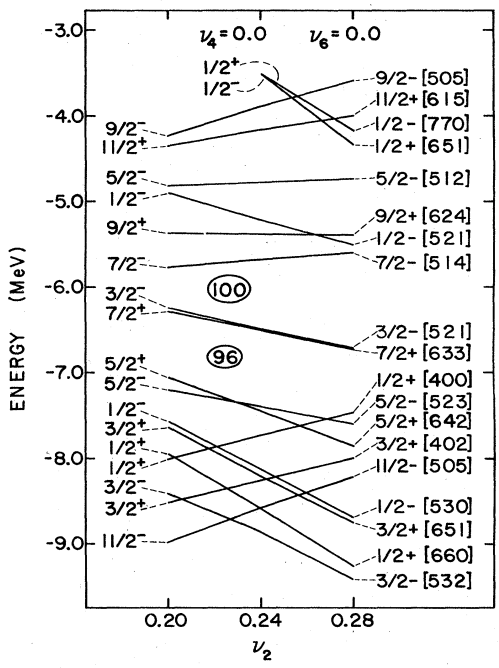

FIG. 8. Actinide proton single-particle levels as a function of ν_2; $\nu_4 = 0.0, \nu_6 = 0.0$.

applied to the nuclear problem (Bohr *et al.*, 1958; Belyaev, 1959; Soloviev, 1958/59; Kisslinger and Sorensen, 1960) and explains in a rather simple way the gap in the spectrum of intrinsic states in even–even deformed nuclei. An examination of states in odd-mass actinides indicates that the single-particle level spacings are roughly 300 keV, and one would expect the excited non-

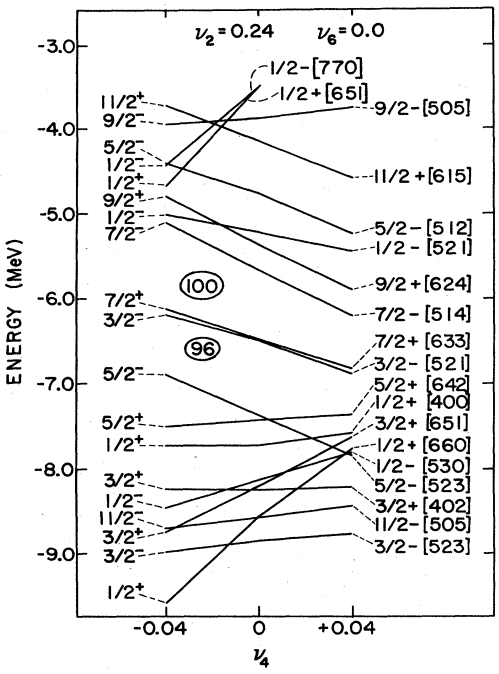

FIG. 9. Actinide proton single-particle levels as a function of ν_4; $\nu_2 = 0.24, \nu_6 = 0.0$.

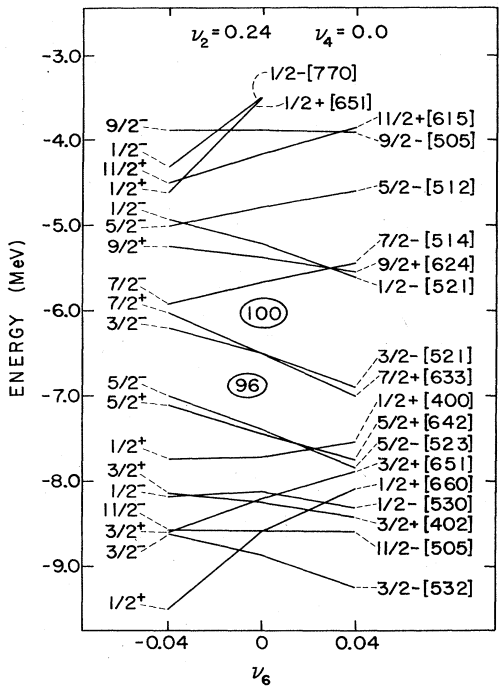

FIG. 10. Actinide proton single-particle levels as a function of ν_6; $\nu_2 = 0.24$, $\nu_4 = 0.0$.

rotational states in even nuclides to appear at about this energy. In fact, these lowest excited noncollective states occur at roughly 1 MeV excitation energy (Lederer *et al.*, 1967). This difference is accounted for by the strong ground-state correlations induced by the pairing force. These correlations give rise to a large depression in the energy of the ground state. Promoting a particle which involves breaking a pair weakens these correlations and the energy of the excited state is much less depressed.

It is most convenient to describe two-body interactions in the second quantized representation. In this representation the pairing force is

$$H_{\text{pairing}} = -\sum_{i,j>0} G_{i,j} a_i^+ a_{-i}^+ a_{-j} a_j , \tag{2.21}$$

where the antisymmetrized matrix element $G_{i,j}$ is

$$G_{i,j} = \int d^3 r_1 d^3 r_2 \psi_i(r_1)\psi_{-i}(r_2) V(r_{12}) \times \{\psi_j(r_1)\psi_{-j}(r_2) - \psi_j(r_2)\psi_{-j}(r_1)\} \tag{2.22}$$

and the quantities $a_i^+(a_i)$ are the usual fermion creation (annihilation) operators. For a short-range attractive interaction, all of the pairing matrix elements are assumed to be negative ($G_{i,j} \geq 0$). This can be verified explicitly in the case of a delta force interaction, for which the matrix element is proportional to the integral of the product of the densities of the wave functions i and j. In most calculations, the pairing force matrix elements are taken as constant ($G_{ij} = G$).

Calculations have also been carried out with nonconstant pairing force matrix elements (Mang *et al.*, 1965; Griffin *et al.*, 1971; van Rij and Kahana, 1972; Chasman, 1972; Bès *et al.*, 1972; Immele and Struble, 1973; Glas and Mosel, 1973; Chasman, 1976). One such approach is to assume that the pairing matrix elements are relatively enhanced for orbitals with similar values of $\langle n_z \rangle / \langle N \rangle$ and diminished for values that differ substantially, i.e., large matrix elements between orbitals with good angular overlap (Bès, 1966; Griffin *et al.*, 1971). This sort of matrix element correlation comes naturally from the surface delta residual interaction (Green and Moszkowski, 1965; Immele and Struble, 1973), and can also be obtained by assuming a quadrupole component of the pairing force (Bès *et al.*, 1972). If one uses a conventional delta interaction, rather than the surface delta interaction, the radial correlations also determine the magnitude of the matrix elements (Mang *et al.*, 1965; Glas and Mosel, 1973) and there are no simple rules for the matrix elements. The surface delta type of interaction can be made somewhat less schematic using a density-dependent delta interaction (Chasman, 1976), with the interaction taking place outside of the nuclear interior. Comparisons with the experimental data (Chasman, 1976) indicate that this form of the pairing interaction provides a much better description of the actinides than is provided by constant pairing matrix elements or by the conventional delta interaction.

There is a considerable literature on techniques for obtaining solutions to the pairing Hamiltonian. The first and simplest method of solution is the BCS method (Bardeen, Cooper, and Schrieffer, 1957a, b; Bogoliubov, 1958; Belyaev, 1959). The accuracy of this method is rather marginal for studies of odd-mass nuclides. The BCS wave function is

$$\psi_{\text{BCS}} = \prod^{K} (U_K + V_K a_K^+ a_{-K}^+) |0\rangle , \tag{2.23}$$

where V_K^2 is the joint occupation probability of the orbits K and $-K$ and

$$U_K^2 \equiv 1 - V_K^2 \tag{2.24}$$

is the probability that the orbits K and $-K$ are not occupied by a pair. The wave function ψ_{BCS} contains configurations with different numbers of particles, but U_K and V_K are chosen such that the expectation value of the number operator is the correct particle number. The distribution about the average value is of little concern in the case of electronic superconductivity, where one is dealing with $\sim 10^{20}$ electrons. However, in the nuclear case one is dealing with only tens of nucleons, and the deviation of the particle number from the correct value implies significant corrections to BCS wave functions and energies. Also, in odd-mass systems there is (at least) one unpaired nucleon. The orbital containing the unpaired particle is blocked for occupation by a pair of particles and should not be included in the BCS wave function. This same blocking effect is equally applicable to all other techniques for dealing with pairing forces and plays an important role in the energy level spacing calculations. For completeness, we note the BCS relations

$$\left.\begin{matrix} U_K^2 \\ V_K^2 \end{matrix}\right\} = \frac{1}{2}\left[1 \pm \frac{(\epsilon_K - \lambda)}{[(\epsilon_K - \lambda)^2 + \Delta_K^2]^{1/2}}\right] , \tag{2.25}$$

where λ, the Fermi level, is a Lagrange multiplier

chosen to give a wave function with the correct average particle number, and ϵ_K is the single-particle energy. Δ_K, the gap parameter, is defined as

$$\Delta_K = \sum_L G_{K,L} U_L V_L . \tag{2.26}$$

The excitation energy of an unpaired particle is given as

$$\mathcal{E}_K = [(\epsilon_K - \lambda)^2 + \Delta_K^2]^{1/2} . \tag{2.27}$$

In odd systems, we are interested in the configurations with one unpaired particle. The effect of pairing forces is to reduce the level spacings of orbitals relative to those obtained from the pure single-particle potential (Mottelson, 1959; Bakke, 1958/59; Soloviev, 1961; Wahlborn, 1962). The reason for this compression is that blocking a level far from the Fermi level destroys much less of the pairing correlation than blocking a level near the Fermi level. In even nuclides, the promotion of a particle causes two orbitals to be blocked, and as can be seen from Eq. (2.27), the minimum excitation is $\Delta_K + \Delta_{K'}$.

The BCS solutions are notoriously poor when the ground-state correlations are weak. Below a critical interaction strength, the BCS method gives only the uncorrelated solutions ($V^2 = 0$ or 1). This makes BCS results somewhat more suspect when the blocked level is near the Fermi level. To get more meaningful results, we must utilize other methods of solving the pairing problem. However, the qualitative features that we have noted in the BCS solutions apply also when other methods are used.

Analytic solutions of the pairing problem for constant pairing matrix elements have been obtained by Richardson and Sherman (1964). This approach has not been used in actinide studies, but has provided useful test cases for approximate treatments of the pairing force problem (Richardson, 1966). Exact solutions for spherical nuclides have been given using quasispin methods (Kerman *et al.*, 1961).

Accurate solutions to the pairing problem have been obtained by the fixed particle number methods (Dietrich *et al.*, 1966; Mang *et al.*, 1965, 1966), and/or by projecting states of good particle number from BCS solutions (Lande, 1965). Another approach is that of generator coordinates. One uses the interaction strength as the generator coordinate. Another accurate technique is to assume a semiseparable product form for the wave function amplitudes (Chasman, 1964) and to minimize the energy directly with respect to the parameters determining the configuration amplitudes. Other methods have also been proposed (Giu Do Dang and Klein, 1965/1966; Wahlborn, 1966; Sorensen, 1972). All of the above methods give accurate solutions in odd-mass systems.

In the calculations that are presented in this work, we have used the correlated quasiparticle method (Chasman, 1972) which gives quick and accurate solutions to the pairing problem. This approach takes into account the correlations, neglected in the BCS solution, between pairs of particles that arise in the paired wave function because of fixed particle number.

It can be easily shown that the results of the BCS method follow from the approximation

$$\langle a_i^+ a_{-i}^+ a_{-j} a_j \rangle = [\langle N_i \rangle \langle 1 - N_i \rangle \langle N_j \rangle \langle 1 - N_j \rangle]^{1/2} , \tag{2.28a}$$

where the angled brackets indicate ground-state expectation values and N_i is a pair occupation probability. In this approximation, the pair occupation probabilities of levels i and j are uncorrelated in the ground-state wave function. However, there is, in fact, a correlation. If we pick out those configurations in the ground-state wave function in which level i is occupied by a pair, the occupation probability of level j will usually be reduced relative to the value of $\langle N_j \rangle$. The reason for this reduction is that the total number of particles in the system is fixed, and increasing the occupation of level i means that the occupation probability of other levels is decreased. Because of this correlation effect, a more accurate approximation than Eq. (2.28a) is (Chasman, 1972)

$$\langle a_i^+ a_{-i}^+ a_{-j} a_j \rangle = [\langle N_i (1 - N_j) \rangle \langle N_j (1 - N_i) \rangle]^{1/2} . \tag{2.28b}$$

This approximation takes the correlation of occupation probabilities into account. The magnitude of these correlations is obtained from the exact sum rule relation

$$\sum_{j \neq i} \langle N_i N_j \rangle = \langle N_i \rangle \sum_{j \neq i} \langle N_j \rangle - \langle N_i \rangle \langle 1 - N_i \rangle . \tag{2.29a}$$

Examination of numerically exact solutions of model pairing systems, and considerations of lowest-order perturbation theory, show that the major part of this correlation is between orbitals on opposite sides of the Fermi level. This feature, together with Eq. (2.29a), gives rise to the approximation (Chasman, 1972)

$$\langle N_i (1 - N_j) \rangle = \langle N_i \rangle \langle 1 - N_j \rangle + \frac{G_{i,j}}{2} \langle N_i \rangle \langle 1 - N_i \rangle \langle N_j \rangle \langle 1 - N_j \rangle S_{i,j} \times \left[\frac{1}{\sum_{k \neq i} G_{i,k} \langle N_k \rangle \langle 1 - N_k \rangle S_{i,k}} + \frac{1}{\sum_{k \neq j} G_{j,k} \langle N_k \rangle \langle 1 - N_k \rangle S_{j,k}} \right] , \tag{2.29b}$$

where $S_{i,j}$ is a particle–hole correlation enhancement factor and is given by

$$S_{i,j} = [\langle N_i \rangle \langle 1 - N_j \rangle + \langle N_j \rangle \langle 1 - N_i \rangle] . \tag{2.29c}$$

The ground-state energy and occupation probabilities are obtained by substituting Eq. (2.29b) into (2.28b) and solving the set of coupled equations

$$\frac{\partial \langle H \rangle}{\partial \langle N_i \rangle} = 0 \tag{2.30}$$

as is done in the standard BCS treatment.

The correlation effect of Eq. (2.29b) is particularly important in deformed nuclides, where the level density is often low in the vicinity of the Fermi level. This level density is further lowered in odd-mass systems, since levels are blocked. In such cases, the conventional BCS treatment often does not give any solution other than the trivial one. In the results that we present here, the blocking effect is taken fully into account.

The strength of the pairing interaction has often been determined by relating the gap parameter Δ to odd-even mass differences, i.e., setting (Nilsson and Prior, 1961)

$$\Delta = \Delta M_{o-e}, \tag{2.31}$$

which is an approximate relation. This relation was used in the analysis of the rare earths (Ogle *et al.*, 1971). There it was found that the pairing interaction constant did not decrease with increasing A, as is expected (Bès and Sorensen, 1969). Another way to determine the overall pairing interaction strength is to calculate the energies of seniority two (i.e., two unpaired particles) states in the even actinides. Changes of 5 keV in G give changes of ~100 keV in these excitation energies. It is best to use high spin states for this purpose, as they are more likely to be pure configurations. We have used this approach to estimate pairing strengths in the actinides and find no trend of G with mass. We emphasize that the value of G to be used in a calculation depends on the number of levels used. In the calculations presented here, we use 30 levels for both protons and neutrons. We have adopted the values

$$G_{\text{proton}} = 0.135 \text{ MeV},$$
$$G_{\text{neutron}} = 0.095 \text{ MeV} \tag{2.32}$$

for calculations with constant pairing matrix elements in the actinides.

In addition to the calculations with constant pairing matrix elements, we also present here the results of pairing calculations carried out with matrix elements obtained from a density-dependent delta interaction. The matrix elements used in these calculations have been tabulated and analyzed in considerable detail (Chasman, 1976).

We compare the single-particle level spacings obtained with the constant G and density-dependent delta interaction pairing matrix elements in Sec. IV.A for both odd-neutron and odd-protron nuclides in the actinides. In Appendix B, we have tabulated level occupation probabilities using both types of pairing matrix elements.

b. Particle-hole interactions

Although the pairing force plays a major role in determining the structure of configurations in the actinides, it is not the whole story. One must consider other interaction modes as well. The importance of other coherent residual interaction modes is signaled experimentally, in even nuclides, by the appearance of nonrotational excited states with energies below 2Δ and/or by enhanced electromagnetic transition rates. Such states are called vibrational states or phonon excitations.

There are several approaches to the problem of particle–hole interactions in even systems that take these features more or less into account. The simplest are the Tamm–Dancoff (Tamm, 1945; Dancoff, 1950) approximation and the random-phase approximation (RPA) (Ferrell, 1957). The RPA takes the ground-state correlations induced by the particle–hole interaction into account to some extent and is the starting point for the more modern treatments of particle–hole interactions. The RPA and the improvements to it are limited in their radius of effective convergence, as they are perturbation expansions in the parameter $(\Omega\overline{V}/\overline{E})$, where Ω is the number of particle–hole pairs, $\overline{V}$ is the average particle–hole matrix element, and $\overline{E}$ is an average energy difference of the particle and hole eigenvalues.

Improvements on the RPA have been made using boson expansion techniques in which equations of motion are obeyed exactly to higher and higher orders in successive approximations (Belyaev and Zelevinsky, 1962; Marumori *et al.*, 1964; Sørensen, 1967, 1968; Marshalak, 1974). The boson expansion methods are closely related to the generator coordinate method (Hill and Wheeler, 1953; Griffin and Wheeler, 1957; Jancovici and Schiff, 1964; Brink and Weiguny, 1968; Wong, 1975) and can be derived with this technique (Holzworth, 1972; da Providencia, 1974).

A second approach to improving the RPA is the diagrammatic perturbation theory or diagrammatic Green's function approach. This approach appears to provide a convenient and systematic method of making higher-order corrections to the RPA (Migdal, 1962, 1967, 1968; Mattuck, 1967; Mills, 1969; Brown, 1972; Parry, 1973; Hamamoto, 1974; Bohr and Mottelson, 1975). The diagrammatic calculations can be carried out either in the time representation or in the energy representation.

Beyond the range of utility of the perturbation schemes, it appears that the best hope is to take the ground-state correlations into account as well as possible and generate excited states from the correlated ground state.

The problem of particle–hole correlations is further complicated by the presence of pairing forces. This problem is dealt with in much the same way as the simple particle–hole interactions. The RPA is replaced by the quasiparticle RPA (QRPA) (Arvieu and Veneroni, 1960; Bès, 1961; Kisslinger and Sorensen, 1963; Soloviev and Vogel, 1967). Boson expansions are replaced by quasiboson expansions (Belyaev and Zelevinsky, 1962), and the particle propagators of the Green's function method are replaced by quasiparticle propagators (Migdal, 1962).

The particle–hole interactions that have been considered in the actinides are of the multipole–multipole type [Elliot, 1958a, b; Belyaev, 1959; Kisslinger and Sorensen, 1963: Bohr and Mottelson, 1975 (Chap. 6)]. The consideration of particle–hole interactions has been mainly confined to the quadrupole and octupole modes (Malov and Soloviev, 1966; Bès and Cho, 1966; Neergaard and Vogel, 1970a, b). The λth multipole of this interaction is

$$H^{\lambda}_{\text{p-h}} = V_{\lambda} \sum_{\mu} \left[\sum_{i,j} \langle i | f(r) Y^{\mu}_{\lambda} | j \rangle a^{+}_{i} a_{j} \right] \left[\sum_{k,l} \langle k | f(r) Y^{-\mu}_{\lambda} | l \rangle a^{+}_{k} a_{l} \right] \tag{2.33}$$

with

$$\mu = \Omega_i - \Omega_j = \Omega_l - \Omega_K . \tag{2.34}$$

In a series of papers, the Dubna group has treated both quadrupole and octupole modes of the residual interaction (Soloviev and Vogel, 1967; Gareev *et al.*, 1970; Komov *et al.*, 1971; Ivanova *et al.*, 1972) together with pairing forces in the actinides. Much of this work is summarized in the publication of Gareev *et al.* (1971). In this work, the QRPA is used to calculate phonons in the even deformed nuclides, and Eq. (2.33) is used to calculate particle phonon mixings, taking into account matrix elements of the type

$$\langle i, n_\lambda^\mu = 0 | H_{\text{p-h}}^\lambda | j, n_\lambda^\mu = 1 \rangle , \tag{2.35}$$

where n_λ^μ indicates the number of phonons of type (λ, μ) in the configuration. This is an oversimplification of the problem; the correlations associated with the particle–hole mode must be more adequately taken into account, i.e., one must consider backward diagrams in the time representation.

To illustrate this point, as well as the general features of particle–hole interactions, we consider an extension of a schematic particle–hole model presented previously (Chasman and Durso, 1975). The significant features can be seen by examining energy shifts to order V^2 in the residual interaction. By confining our discussion to lowest-order effects, we can analyze the problem of particle–hole interactions in a simple way. Our goal here is to illustrate the sources of the self-energy shift rather than to derive any new results. The Hamiltonian we consider is

$$H = \sum_K \epsilon_K N_K - V \sum_{\alpha,\beta} [(a_\alpha^+ a_\beta + a_{-\beta}^+ a_{-\alpha})]_\mu \sum_{\gamma,\delta}{}' (a_\gamma^+ a_\delta + a_{-\delta}^+ a_{-\gamma})_{-\mu} , \tag{2.36}$$

where ϵ_K is a single-particle energy and N_K is the occupation number of level K. In the model we consider here, there are Ω doubly degenerate levels at the energy $\epsilon = 0$, 2Ω doubly degenerate levels at the energy $\epsilon = 1$, 2Ω doubly degenerate levels at the energy $\epsilon = 2$, and Ω doubly degenerate levels at the energy $\epsilon = 3$. We first consider an even system with 6Ω particles, i.e., all orbitals at the energy $\epsilon = 0$ and $\epsilon = 1$ are occupied and all orbitals at the energy $\epsilon = 2$ and $\epsilon = 3$ are unoccupied. The orbitals at $\epsilon = 0$ are A-shell orbitals; those at $\epsilon = 1$ are B- and C-shell orbitals; those at $\epsilon = 2$ are D- and E-shell orbitals; and those at $\epsilon = 3$ are F-shell orbitals. In this model, each orbital has a unique partner in the residual interaction term. Each of the Ω A-shell orbitals at $\epsilon = 0$ has as its partner one of the Ω B-shell orbitals at $\epsilon = 1$; the Ω C-shell orbitals at $\epsilon = 1$ have as their partners the Ω D-shell orbitals at $\epsilon = 2$. The remaining Ω E-shell orbitals at $\epsilon = 2$ have as their residual interaction partners the F-shell orbitals at $\epsilon = 3$. In order to avoid irrelevant Hartree–Fock-type correlations, we exclude all terms with $a_\alpha^+ a_\beta a_\beta^+ a_\alpha$; this is indicated by the prime on the third summation of Eq. (2.36). In Fig. 11, we show the various groups of orbitals; the connections for nonvanishing residual interaction matrix elements are indicated by arrows. The dashed line indicates the Fermi level for the even system.

In lowest order, the residual interaction modifies the ground-state wave function by admixing configurations with two particles in the D-shell levels and two holes in the C-shell levels. Denoting a two-particle, two-hole amplitude as C_1, and the ground-state amplitude as C_0, one has in lowest order

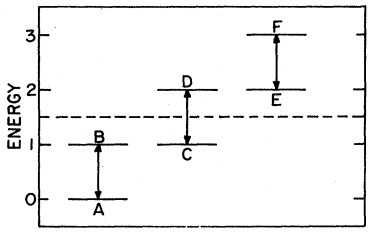

FIG. 11. Energies of levels in schematic calculation. The lateral displacements are made for clarity. The nonzero particle–hole matrix elements are indicated by arrows. The dashed line indicates the Fermi level.

$$C_0(4\Omega - \omega_0) = \Omega^2 V C_1 , \tag{2.37a}$$

$$C_1(4\Omega + 2 - \omega_0) = V C_0 . \tag{2.37b}$$

In lowest order, these equations give

$$C_1 = \tfrac{1}{2} V C_0 , \tag{2.37c}$$

$$\omega_0 = 4\Omega - \tfrac{1}{2}\Omega^2 V^2 . \tag{2.37d}$$

ω_0 makes a convenient zero of energy.

Next, we discuss the problem of particle addition (self-energy shift). First consider a particle added in one of the D-shell orbitals. Because this orbital is now occupied, the three-particle, two-hole amplitudes with a particle in this specific D orbital and a hole in the corresponding C-shell orbital cannot be formed. Accordingly, we have

$$C'_D(4\Omega + 2 - \omega') = \Omega(\Omega - 1) V C'_{D^3C^{-2}} , \tag{2.38a}$$

$$C'_{D^3C^{-2}}(4\Omega + 4 - \omega') = V C'_D \tag{2.38b}$$

with the indices on the amplitudes denoting the changes from the particle–hole vacuum. Solving for ω', we have to order V^2

$$\omega' = 4\Omega + 2 - \tfrac{1}{2}\Omega(\Omega - 1) V^2 . \tag{2.38c}$$

Comparing Eqs. (2.38c) and (2.37d), we note

$$\omega' = \omega_0 + 2 + \tfrac{1}{2}\Omega V^2 . \tag{2.39}$$

We next consider the case in which the odd particle is added to one of the E-shell orbitals. In this instance, the situation is reversed. Not only are all configurations with two holes in the C shell and two particles in the D shell available, there are additional configurations that couple here. The new configurations are those with one particle in the D shell, one hole in the C shell, and one particle in the F shell. For this case, we have the amplitude relations

$$C''_E(4\Omega + 2 - \omega'') = (\Omega^2) V C''_{D^2C^{-2}E} + \Omega V C''_{DC^{-1}F} . \tag{2.40a}$$

We also have, to lowest order,

$$C''_{D^2C^{-2}E}(4\Omega + 4 - \omega'') = V C''_E , \tag{2.40b}$$

$$C''_{DC^{-1}F}(4\Omega + 4 - \omega'') = V C''_E \tag{2.40c}$$

giving

$$\omega'' = \omega_0 + 2 - \tfrac{1}{2}\Omega V^2 . \tag{2.41}$$

In contrast to Eq. (2.39), the self-energy shift is down.

An entirely different situation obtains when we add the odd particle to the F shell. In this instance, relations in lowest order are

$$C_F(4\Omega + 3 - \omega''') = \Omega^2 V C_{D^2C^{-2}F} + \Omega V C_{DC^{-1}E}\,, \tag{2.42a}$$

$$C_{D^2C^{-2}F}(4\Omega + 5 - \omega''') = V C_F + V C_{DC^{-1}E}\,, \tag{2.42b}$$

$$C_{DC^{-1}E}(4\Omega + 3 - \omega''') = V C_F + \Omega V C_{D^2C^{-2}F} + (\Omega - 1) V_{DC^{-1}E^{-1}}\,. \tag{2.42c}$$

The unperturbed energies of the configurations F and $DC^{-1}E$ are degenerate, and a perturbation approach is no longer valid. In this case, the first corrections to the energy are of order V rather than V^2. With the lowest-order correction, the energy is

$$\omega''' = \omega_0 + 3 - \Omega V\,. \tag{2.43}$$

We shall pass over this sort of situation in the discussion of self-energy corrections. Also, the introduction of pairing forces into the Hamiltonian guarantees that this sort of degeneracy is broken at low energies in the odd-mass spectrum ($DC^{-1}E$ is a seniority-three configuration, whereas F is a seniority-one configuration).

The point of this illustration is that the same attractive interaction can shift the single-particle states either up [Eq. (2.39)] or down [Eq. (2.41)], depending on the relevant occupation probabilities, by virtue of changes in the correlations due to the particle addition. The self-energy shift to order V^2 is of magnitude ΩV^2. This is the leading term in the diagrammatic expansion of the self-energy. In higher orders, one gets corrections to the self-energy of the form $(1/\Omega)(\Omega V)^N$.

With this illustration in mind, we turn to the situation that is more typical of deformed nuclides. Here the pairing interaction is the important residual interaction and the particle–hole interaction is considered a perturbation. In such a case, we must consider the mixing of pairing eigenstates due to the particle–hole interaction, and the associated energy shifts. Qualitatively, there is a resemblance to the results obtained in the absence of pairing. To make the qualitative features transparent, we introduce some quasiparticle-like approximations. We assume that the occupation probability of a given level is the same in all the pairing eigenstates that enter our analysis, except for a particular orbital that is blocked. This can be rationalized by assuming that the number of levels in each shell, Ω, is infinite. In the treatment here, we also assume that the eigenvalues used for the pairing states are simple sums of quasiparticle-like energies which we denote as $\mathcal{E}_i$. We take the particle–hole interaction as being electric in character under time reversal, i.e.,

$$\langle \alpha|\theta|\beta\rangle = \langle -\alpha|\theta|-\beta\rangle\,, \tag{2.44}$$

where $\theta \cdot \theta$ is the separable residual interaction and $-\alpha$ indicates the orbital that is the time-reversed partner of α. The pairing factors that enter the calculation are of two types:

(1) Seniority two to seniority zero transitions, i.e.,

$$\begin{array}{ccc} \beta\ \text{X O} & \beta\ \text{X X} & \beta\ \text{O O} \\ \alpha\ \text{O X} & \alpha\ \text{O O} & \alpha\ \text{X X} \end{array} \tag{2.45}$$

with associated pairing factor $(U_\alpha V_\beta + U_\beta V_\alpha)$ where X denotes a particle and O denotes the absence of a particle;

(2) Seniority one to seniority one transitions, i.e.,

$$\begin{array}{cc} \beta\ \text{X O} & \beta\ \text{O O} \\ \alpha\ \text{O O} & \alpha\ \text{X O} \end{array} \tag{2.46}$$

with pairing factor $U_\alpha U_\beta$, and

$$\begin{array}{cc} \beta\ \text{X O} & \beta\ \text{X X} \\ \alpha\ \text{X X} & \alpha\ \text{X O} \end{array} \tag{2.47}$$

with pairing factor $-V_\alpha V_\beta$.

We note also that all residual interaction terms of the form $a^+_\alpha a_\beta a^+_{-\alpha} a_{-\beta}$ should be excluded from the perturbation, as they are simply reorderings of terms in the pairing Hamiltonian. In writing out our equations, however, we shall ignore this fact, as it simplifies the writing of equations. The errors are of the order $1/\Omega$. Here we label amplitudes with subscripts that denote the shells of unpaired particles.

For the ground state of the even nucleus, we have the amplitude relation

$$C_0(E_0 - \omega_0) = \mathcal{V}\Omega^2 \begin{bmatrix} (U_A V_B + U_B V_A)^2 C_{A^2B^2} \\ + (U_C V_D + U_D V_C)^2 C_{C^2D^2} \\ + (U_E V_F + U_F V_E)^2 C_{E^2F^2} \\ + (U_A V_B + U_B V_A)(U_C V_D + U_D V_C) C_{ABCD} \\ + (U_A V_B + U_B V_A)(U_E V_F + U_F V_E) C_{ABEF} \\ + (U_C V_D + U_D V_C)(U_E V_F + U_F V_E) C_{CDEF} \end{bmatrix}. \tag{2.48a}$$

For the seniority four amplitudes, we use, e.g.,

$$C_{A^2B^2}(E_0 + 2\mathcal{E}_A + 2\mathcal{E}_B - \omega_0) = \mathcal{V}(U_A V_B + U_B V_A)^2 C_0\,. \tag{2.48b}$$

Eliminating the amplitudes gives the shift of ω_0 to order $\mathcal{V}^2$. We use a script $\mathcal{V}$ for the interaction strength here to avoid confusion with the occupation probabilities.

Again, we add a particle to the system, say in the D shell. This gives the set of equations

$$\begin{aligned} C'_D(E + \mathcal{E}_D - \omega') = {} & \mathcal{V}\Omega^2 \begin{bmatrix} (U_A V_B + U_B V_A)^2 C'_{A^2B^2D} \\ + (U_E V_F + U_F V_E)^2 C'_{E^2F^2D} \\ + (U_A V_B + U_B V_A)(U_E V_F + U_F V_E) C'_{ABEFD} \end{bmatrix} + \mathcal{V}\Omega(\Omega - 1)(U_C V_D + U_D V_C) \begin{bmatrix} (U_A V_B + U_B V_A) C'_{ABCD^2} \\ + (U_E V_F + U_F V_E) C'_{EFCD^2} \end{bmatrix} \\ & + \mathcal{V}\Omega(U_C U_D - V_C V_D) \begin{bmatrix} (U_A V_B + U_B V_A) C'_{ABC} \\ + (U_E V_F + U_F V_E) C'_{EFC} \end{bmatrix} + \mathcal{V}(\Omega - 1)^2 (U_C V_D + U_D V_C)^2 C'_{C^2D^3} \\ & + \mathcal{V}(\Omega - 1)[(U_C U_D - V_C V_D)(U_C V_D + U_D V_C)]\, C'_{C^2D} \end{aligned} \tag{2.49}$$

By relating the amplitudes of the high seniority states to C'_D with equations similar to Eq. (2.48b), we get a relation for ω'.

Comparing ω_0 and ω', we get the result of interest

$$\omega' = \omega_0 + \mathcal{E}_D + \frac{v^2(\Omega - \frac{1}{2})}{\mathcal{E}_C + \mathcal{E}_D}(U_C V_D + U_D V_C)^4 - \frac{(\Omega - 1)v^2}{2\mathcal{E}_C}(U_C U_D - V_C V_D)^2(U_C V_D + U_D V_C)^2$$
$$+\Omega v^2(U_C V_D + U_D V_C)^2\left[\frac{(U_A V_B + U_B V_A)^2}{\mathcal{E}_A + \mathcal{E}_B + \mathcal{E}_C + \mathcal{E}_D} + \frac{(U_E V_F + U_F V_E)^2}{\mathcal{E}_E + \mathcal{E}_F + \mathcal{E}_C + \mathcal{E}_D}\right]$$
$$-\Omega v^2(U_C U_D - V_C V_D)^2\left[\frac{(U_A V_B + U_B V_A)^2}{\mathcal{E}_A + \mathcal{E}_B + \mathcal{E}_C - \mathcal{E}_D} + \frac{(U_E V_F + U_F V_E)^2}{\mathcal{E}_E + \mathcal{E}_F + \mathcal{E}_C - \mathcal{E}_D}\right]. \quad (2.50)$$

We can simplify Eq. (2.50) considerably by exploiting the particle–hole symmetry of the model that we are using. The relevant relations are

$$U_A = V_F, \quad (2.51a)$$
$$\mathcal{E}_A = \mathcal{E}_F, \quad (2.51b)$$
$$U_B = U_C = V_D = V_E, \quad (2.52a)$$
$$\mathcal{E}_B = \mathcal{E}_C = \mathcal{E}_D = \mathcal{E}_E. \quad (2.52b)$$

Making use of these relations, we note that $(U_C U_D - V_C V_D)$ vanishes and $U_C V_D + U_D V_C = 1$, giving

$$\omega' = \omega_0 + \mathcal{E}_D + \frac{(\Omega - \frac{1}{2})v^2}{2\mathcal{E}_D} + \frac{2\Omega v^2}{\mathcal{E}_A + \mathcal{E}_B + 2\mathcal{E}_D}(U_A V_B + U_B V_A)^2, \quad (2.53)$$

which is quite similar to (2.39). A general feature that emerges from this case is that when the particle and hole are symmetric about the Fermi level, the self-energy corrections are positive. One cautionary note: in quantitative calculations, one must use the U and V values appropriate to the specific eigenstates that are interacting, rather than using ground-state occupation probabilities everywhere.

To determine the self-energy shift when the unpaired particle is put in the E shell, we can again use Eq. (2.50), making the interchanges of indices $C \rightarrow F$ and $D \rightarrow E$. If we make this interchange, and consider the limit of weak pairing, the largest contribution to the self-energy shift comes from the final term of Eq. (2.50) in its interchanged form. This gives

$$\omega' = \omega + \mathcal{E}_E - \frac{\Omega v^2(U_E U_F - V_E V_F)^2}{\mathcal{E}_C + \mathcal{E}_D + \mathcal{E}_F - \mathcal{E}_E}, \quad (2.54)$$

and the shift is downward, as was the case with no pairing. For physically reasonable values of G, it is hard to make any quantitative general statements based on Eq. (2.50); rather, the specifics of the U_i's and V_i's determine the direction and magnitude of the shifts.

The shifts of order v^2 that we have been discussing are described diagramatically, in the energy representation, by the relation

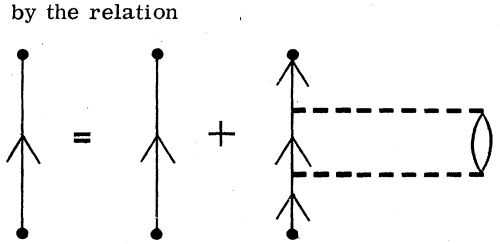

(2.55)

The higher-order terms of order $(1/\Omega)(\Omega V)^n$, as well as the terms of order ΩV^2, are described by the diagrammatic relation

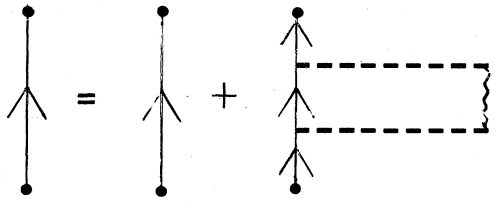

(2.56)

in the energy representation where the propagators are either particle propagators or quasiparticle propagators, depending on the system being studied. The matrix elements are antisymmetrized in actual calculations.

The vertical wavy line in Eq. (2.56) denotes a phonon propagator. The energy shifts that we have discussed here can be thought of as arising from interactions of a single particle and a phonon.

In the calculations of the Dubna group, only the terms in Eq. (2.50) that are multiplied by $(U_C U_D - V_C V_D)^2$ appear. The counterterms, those multiplied by $(U_C V_D + U_D V_C)^2$, are not present. The decrease in correlations due to the occupation of orbitals C and D [the effect illustrated in Eq. (2.39)] is neglected. We conclude that these calculations exaggerate the downward shift of low-lying single-particle states arising from the particle–hole interaction. A second problem with these calculations is that the exclusion principle is not taken properly into account in intermediate states, e.g., the component of the phonon having a particle in the same D-shell orbital is not excluded. This correction is made to order V^2, automatically, when one uses antisymmetrized matrix elements in the diagrammatic approach. The calculations of the Dubna group nevertheless give a good qualitative insight into which states are strongly mixed by particle–hole residual interactions.

Some of these neglected effects were taken into account in early calculations in the rare-earth region (Bès and Cho, 1966). More recently calculations taking all of these effects into account have been performed (Immele and Struble, 1975) for rare earths. Hopefully such calculations will soon be carried out for the actinides.

The problem of taking the changes in occupation probabilities properly into account for the excited configurations is yet to be dealt with.

III. PROPERTIES USED TO DEDUCE LEVEL ASSIGNMENTS

A. Ground-state spin and magnetic moment

The first step in the characterization of a single-particle state is the determination of its spin and parity. The nuclear ground-state spin can be experimentally measured by several techniques; for example atomic beam, optical spectroscopy, etc. (Nierenberg and Lindgren, 1965; Fuller and Cohen, 1969). These experiments also provide the magnetic moment of the ground state. Once the nuclear spin of the ground state is known, an energy level diagram can usually be used to determine its asymptotic quantum numbers, because states of the same spin and parity seldom lie next to each other. Further, the magnetic moment of an orbital can be calculated from the nuclear wave function and compared with the experimental value. This comparison can then be used to choose between various possible assignments. The nuclear ground-state spins and magnetic moments thus far measured for actinides have been recently summarized by Shirley and Lederer (1975) and Ellis and Schmorak (1972). In Table I we present the measured and calculated magnetic moments for actinide nuclei. These calculations were performed with our wave functions (Chasman, 1971) using $g_s^{\text{eff}} = 0.6\, g_s^{\text{free}}$. Our calculations reproduce the measured magnetic moments rather well. There are large discrepancies for the neutron orbital $5/2+[622]$ and the proton orbitals $1/2-[530]$ and $7/2+[633]$.

B. Alpha decay

Alpha decay populates several members of a rotational band with gradually decreasing intensity. Thus α spectroscopy can provide level energies, rotational constants, and decoupling parameters. In addition, the α transition probability is helpful in making single-particle assignments.

The α-decay reduced transition probability is the reciprocal of the hindrance factor, which is defined as the ratio of the experimental partial half-life to the theoretical value. The theoretical half-life is calculated from the spin-independent theory of Preston (1947). The hindrance factor is defined with respect to the $L = 0$ α wave because an α transition from an odd-mass nucleus usually occurs by several L waves and it is difficult to determine their amplitudes.

TABLE I. Magnetic moments.

Nuclide	Spin	Assignment	Magnetic moment Exptl.	References	Magnetic moment calculated value[s] $\nu_2=0.19$ $\nu_4=-0.04$	0.22 −0.02	0.25 0.0
^{229}Th	5/2	$5/2+[633]$	+0.45 ±0.04	a	+0.43	+0.54	+0.59
^{233}U	5/2	$5/2+[633]$	+0.55	b,c			
^{235}U	7/2	$7/2-[743]$	−0.35	b,c	−0.23	−0.23	−0.23
^{239}Pu	1/2	$1/2+[631]$	+0.203 ±0.004	d	+0.20	+0.22	+0.23
^{241}Pu	5/2	$5/2+[622]$	−0.718 ±0.017	e	−0.03	−0.16	−0.23
^{243}Cm	5/2	$5/2+[622]$	0.40[t]	f			
^{245}Cm	7/2	$7/2+[624]$	0.5 ±0.1[t]	g	+0.38	+0.68	+0.80
^{247}Cm	9/2	$9/2-[734]$	0.36[t]	f	−0.32	−0.34	−0.34
^{231}Pa	3/2	$1/2-[530]$	2.01 ±0.02[t]	h	+0.76	+0.78	+0.78
^{233}Pa	3/2	$1/2-[530]$	+3.5 ±0.8	i			
^{237}Np	5/2	$5/2+[642]$	+3.14 ±0.04	j,k	+2.51	+2.51	+2.50
^{239}Np	5/2	$5/2+[642]$	not measured	l			
^{241}Am	5/2	$5/2-[523]$	+1.61 ±0.03	m	+1.57	+1.56	+1.57
^{243}Am	5/2	$5/2-[523]$	+1.61 ±0.04	m,n			
^{249}Bk	7/2	$7/2+[633]$	2.2 ±0.4[t]	o	+3.62	+3.62	+3.63
^{253}Es	7/2	$7/2+[633]$	+4.10 ±0.07	p			

[a] Gerstenkorn *et al.* (1974).
[b] Dorain *et al.* (1957).
[c] Van der Sluis (1956).
[d] Faust *et al.* (1965).
[e] Edelstein (1970).
[f] Abraham *et al.* (1973).
[g] Abraham *et al.* (1970).
[h] Axe *et al.* (1961).
[i] Marrus *et al.* (1961).
[j] Hutchison and Weinstock (1960).
[k] Lewis *et al.* (1970).
[l] Hubbs and Marrus (1958).
[m] Armstrong and Marrus (1966).
[n] Manning *et al.* (1956).
[o] Boatner *et al.* (1972).
[p] Goodman *et al.* (1975).
[s] These values were calculated with $g_s^{\text{eff}} = 0.6 g_s^{\text{free}}$ and $g_R = 0.39$.
[t] For these magnetic moments the sign is not known.

Hindrance factors (HF) of observed transitions between odd-A nuclei can be divided into four categories (Prior, 1959):

1. If the HF is between 1 and 4, the transition is called a favored transition (Rasmussen, 1953) and in such α decays the unpaired nucleon remains in the same orbital in the parent and daughter nuclei. Thus a definite identification of either state can be made if the other state has already been characterized.
2. A HF value of 4–10 indicates strong Coriolis mixing between the state fed by the particular α group and the state fed by the favored α transition, and/or mixing of the analogous single-particle states in the parent nucleus. Low hindrance factors are also expected for some vibrational states, in particular the $K\pi = 0+$ phonon, coupled to the favored band. In this case, the K value of the vibrational band will be the same as that of the favored band whereas if the source of the reduction in the hindrance factor is Coriolis coupling, the two bands will differ in K quantum number by unity (except for $K = 1/2$ bands).
3. Hindrance factors of 10–100 imply that the projections of the intrinsic spin, Σ, for the two states involved in the α decay are parallel.
4. Hindrance factors of >1000 suggest that the Σ values for the parent and daughter states are antiparallel.

In the present paper only favored α transitions have been used in the characterization of single-particle states. Rules 2–4 are used to support assignments deduced by other means.

The relative α-transition probabilities to various members of a band can be calculated semiempirically as suggested by Bohr *et al.* (1955). Their formula is based on the assumption that each partial L wave is divided among the members of a band in proportion to the squares of the appropriate Clebsch–Gordan coefficients and that the α-decay matrix elements remain constant for transitions to all members of the band. For favored α decay, since the unpaired nucleon does not participate in the α-particle formation, K remains unchanged. Hence only transitions $K \to K$ are allowed, but $K \to -K$ are forbidden. On the other hand, in unfavored α decay, the unfavored α transitions will involve $K_i \to K_f$ as well as $K_i \to -K_f$ matrix elements, if the latter process is allowed by angular momentum selection rules.

The α-transition probability P to a member of the favored band is given by (Bohr *et al.*, 1955; Fröman, 1957)

$$P = \frac{P_E}{N} \sum_{L=0,2,4} \frac{|\langle I_i L K_i (K_f - K_i) | I_i L I_f K_f \rangle|^2}{(\mathrm{HF}_L)_{e-e}} , \tag{3.1}$$

where P_E is the α-transition probability expected from the spin-independent theory of Preston (1947) [(P_E/P) is the hindrance factor]. The term in the angular bracket is the Clebsch–Gordan coefficient; i and f refer to the initial and final states; $(\mathrm{HF}_L)_{e-e}$ is the hindrance factor determined for the α transition of that L in the adjacent even–even nuclei; and N is an adjustable parameter with value between 1 and 2. The parameter N is introduced because the hindrance factors in even–even and odd-A nuclei are not exactly the same. In fact, higher hindrance factors are expected for the favored α transitions of odd-A nuclei because of the blocking effect (see Sec. II.B.2.a).

It is found that the relative α intensities calculated with the above equation do not agree well with observed values (Ahmad and Milsted, 1975a). In general the calculated relative α intensity to the $K+1$ member is too low, and that to the $K+2$ member is too high. Until recently this behavior was believed to be caused by the interaction of the nuclear quadrupole moment with the outgoing α waves (Chasman and Rasmussen, 1959). However, recent comprehensive calculations (Soinski *et al.*, 1973) indicate that this effect alone does not reproduce the observed relative intensities.

The relative α-transition probabilities to members of an unfavored band are given by the expression (Bohr *et al.*, 1955; Fröman, 1957)

$$P = P_E \sum_L \frac{|\langle I_i L K_i (K_f - K_i) | I_i L I_f K_f \rangle + b_L (-)^{I_f + K_f} \langle I_i L K_i (-K_f - K_i) | I_i L I_f - K_f \rangle|^2}{\mathrm{HF}_L} , \tag{3.2}$$

where b_L and HF_L are adjustable parameters and their values are determined from known α intensities. The second term in the above equation has nonzero value only when $L \geq K_i + K_f$. Although experimental relative intensities are often compared with intensities calculated with the above equation for a given K_f, the calculated intensities do not vary significantly for different K_f values. Consequently such analyses can be used only as corroborative evidence for assignments already deduced from other experimental data.

As has been pointed out by Rasmussen (1965), Eqs. (2.1) and (3.2) are exact only in the limit of infinite nuclear moment of inertia or vanishing nuclear quadrupole moment.

Alpha-decay transition probabilities have been calculated by Poggenburg *et al.* (1969) using Nilsson single-particle wave functions modified by the pairing force. The calculated intensities were normalized to the experimental transition probability of the ^{238}Pu α_0 group. These intensities agree only approximately (within a factor of 10) with the measured intensities of α groups for unfavored bands and thus are not accurate enough for the characterization of single-particle states. However, these numbers are helpful in deciding between possible assignments.

C. Beta decay

The β-decay transition probabilities (or the closely related logft values) can be used to set limits on the relative spins of the initial and final states involved in a transition. The logft values are usually calculated by nomograms (Lederer *et al.*, 1967), but in cases where the electron capture (EC) decay energy is close to the K-electron

binding energy the nomogram fails to give the correct logft. For such transitions logft values are calculated using a procedure given by Major and Biedenharn (1954) or Gove and Martin (1971). The reduced transition probability for first-forbidden unique ($\Delta I = 2$, yes) transitions is expressed by logf_1t, where $f_1t = (q_K^2/12)ft$; q_K being the neutrino energy in unit of m_0c^2.

In the actinides, logft values for allowed transitions ($\Delta I = \Delta K = 0$ or 1; no) and those first-forbidden transitions characterized by ($\Delta I = \Delta K = 0$ or 1; yes) lie between 5.5 and 8.6. For all other transitions, the logft value is greater than 8.0. A logft value of <8.0 thus indicates that the β transition involves a spin change of 0 or 1. Hence, if the ground state of the parent nucleus is known, the daughter state can have only three possible spin values, or vice versa. This severely limits the possible single-particle orbital assignments.

The reduced β-transition probability, which is given by the reciprocal of the ft value, is a product of two terms: the single-particle term and the pairing factor P_β^2. Thus,

$$\frac{1}{(ft)_{\rm obs}} = \frac{1}{(ft)_{\rm sp}} P_\beta^2 , \tag{3.3}$$

where P_β is defined in Appendix B. We expect the $(ft)_{\rm sp}$ value between any two given configurations to remain nearly constant in the actinide region. However, the observed logft values may change significantly because of the pairing effect.

β transitions which violate selection rules (Alaga, 1955) in the asymptotic quantum numbers n_z and Λ do not show any systematic trend. On the other hand, transitions which violate the selection rule in the principal quantum number N usually have high logft values. For example, allowed transitions with $\Delta N = 2$ have logft values as high as 8.6 (Porter *et al.*, 1972).

In the actinide region no β^+ decay of an odd-mass nucleus has yet been observed.

It was first pointed out by Alaga *et al.* (1955) that β-decay reduced transition probabilities to members of a rotational band should be proportional to the squares of their respective Clebsch–Gordan coefficients. However, this rule is seldom used since β transitions usually involve more than one transition operator and more than one angular momentum value. Also, there is difficulty in the measurement of the β intensities to members of a rotational band because of the difficulty in determining the intensity of the low-energy intraband γ transitions. The ft values measured for actinides are given in Table II.

TABLE II. logft values for β^- and EC decays.

Initial state	Final state	Nuclear decay	logft [a]
n[631] 1/2+	p[530] 1/2 3/2−	^{233}Thβ^-	5.9
	p[651] 3/2+		6.5
	p[660] 1/2+		~7
	p[530] 1/2 3/2−	^{237}Uβ^-	6.3
	p[530] 1/2 1/2−		6.5
	p[400] 1/2+		7.3
	p[521] 3/2−	^{241} Cm EC	7.7
	p[400] 1/2+		8.0
	p[530] 1/2 3/2−		6.2
	p[530] 1/2 1/2−		6.2
	p[651] 3/2+		7.7
n[633] 5/2+	p[651] 3/2 5/2+	^{231}Thβ^-	5.6
	p[523] 5/2−		6.8
	p[642] 5/2+		5.7
n[743] 7/2−	p[642] 5/2+	^{237}Pu EC	~6.8
	p[523] 5/2−		~6.8
n[622] 5/2+	p[642] 5/2+	^{239}Uβ^-	6.7
	p[523] 5/2−		6.0
	p[523] 5/2−	^{241}Puβ^-	5.8
n[624] 7/2+	p[523] 5/2−	^{243}Puβ^-	6.1
	p[642] 5/2+		6.1
	p[633] 7/2+		5.5
n[734] 9/2−	p[633] 7/2+	^{245}Puβ^-	7.3
	p[633] 7/2+	^{251}Fm EC	6.7
n[620] 1/2+	p[521] 3/2−	^{249}Cmβ^-	5.9
	p[530] 1/2 3/2−		~7
	p[521] 1/2−		5.9
p[530] 1/2 3/2−	n[631] 3/2+	^{233}Paβ^-	7.3
	n[631] 1/2 3/2+		6.6
p[642] 5/2+	n[743] 7/2−	^{235}Np EC	6.8
	n[622] 5/2+	^{239}Npβ^-	7.1
	n[743] 7/2−		6.3
	n[624] 7/2+	^{245}Amβ^-	6.3
	n[622] 5/2+		6.4
p[523] 5/2−	n[622] 5/2+	^{237}Am EC	6.0
	n[631] 3/2+		7.3
	n[633] 5/2+		6.8
	n[624] 7/2+		6.7
	n[752] 5/2−		7.2
	n[613] 7/2+		6.4
	n[622] 5/2+	^{239}Am EC	6.0
	n[743] 7/2−		8.6
	n[624] 7/2+		5.8
p[521] 3/2−	n[622] 5/2+	^{245}Bk EC	6.9
	n[631] 1/2+		8.0
	n[620] 1/2+		6.0
	n[620] 1/2+	^{251}Es EC	6.2
	n[622] 3/2+		~5.7
p[633] 7/2+	n[734] 9/2−	^{249}Bkβ^-	6.8
	n[734] 9/2−	^{249}Es EC	6.7
	n[622] 5/2+		7.3
	n[624] 7/2+		6.2
	n[613] 7/2+		7.2
	n[615] 9/2+		6.6

[a] For references see Tables V–XXXVII.

D. Electromagnetic transitions

The single-particle estimate of a γ-ray lifetime is calculated using equations given by Moszkowski (1965). In these calculations the statistical factor "S" is usually taken as unity. The single-particle estimate represents an upper limit for the transition probability per second unless there is collective enhancement of the transition rate.

In the actinide region, the multipolarity of a transition can be uniquely determined by measuring its absolute conversion coefficients and comparing them with the theoretical values (Hager and Seltzer, 1968). For low-energy (<100 keV) transitions, the ratios of subshell conversion coefficients are used for this purpose. Since an excited state can decay to one or more members of a rotational band, the spin of the parent state can be uniquely determined from the multipolarities of the de-exciting transitions, when the K value of the lower band is already known from other measurements.

In actinide nuclei, the γ-ray lifetimes are such that the excited states usually decay by $E1$, $M1$, and/or $E2$ transitions. $E1$ transitions are always retarded relative

to single-particle estimates; the retardation factors lie in the range of 10^3–10^7 (Asaro *et al.*, 1960). The retardation factors for $M1$ and $E2$ transitions are between 10 and 1000. Only a few cases of K-forbidden transitions have been observed in odd-mass actinide nuclei. These transitions display retardation factors of 100–1000, for each unit of K-forbiddenness.

The observed transition rate $T(\lambda)$ and the reduced transition probability $B(\lambda)$ are related by the following expression (Nilsson, 1955)

$$T(\lambda)=\frac{8\pi(\lambda+1)}{\lambda[(2\lambda+1)!!]^2}\frac{1}{\hbar}\left[\frac{E_\gamma}{\hbar c}\right]^{2\lambda+1}B(\lambda)\,. \tag{3.4}$$

In the above equation E_γ is the transition energy, $T(\lambda)$ the gamma emission rate per second, λ the transition multipole order, and the term $(2\lambda+1)!!=1\cdot3\cdot5\cdots(2\lambda+1)$. For $M1$, $E1$, and $E2$ transitions the above equation reduces to

$$T(M1)=(16\pi/9\hbar)[E_\gamma/\hbar c]^3B(M1)\,, \tag{3.5a}$$

$$T(E1)=(16\pi/9\hbar)[E_\gamma/\hbar c]^3B(E1)\,, \tag{3.5b}$$

and

$$T(E2)=(4\pi/75\hbar)[E_\gamma/\hbar c]^5B(E2)\,. \tag{3.5c}$$

The expressions for calculating $B(\lambda)$ values from transition matrix elements are given in Appendix C. The single-particle matrix element G_λ should be multiplied by a pairing term P before it is inserted in the expression for $B(\lambda)$.

Because of the high retardation of $E1$ transition rates, it has been possible to measure the lifetimes of several $E1$ transitions in the actinide region. In most cases the transition rates calculated with the $E1$ matrix elements of Appendix C and the pairing factors of Appendix B agree within a factor of 3 with the experimental transition rates. Similar results were also obtained (Perdrisat, 1966) using $E1$ matrix elements calculated with Nilsson (1955) wave functions. However, the calculated rates in both cases for the $\frac{5}{2}\,\frac{3}{2}+[651]\rightarrow\frac{3}{2}\,\frac{1}{2}-[530]E1$ transitions in ^{231}Pa and ^{233}Pa are 500 times larger than the measured values.

Lifetimes of only a limited number of $E2$ and $M2$ transitions between one-quasiparticle states have been measured.

Because $M1$ lifetimes are so short (less than 10^{-10}s), no measurement of interband $M1$ transition probabilities has been possible. However, lifetimes of intraband $M1$ transitions in ^{229}Th and ^{235}U have been measured, and g_K values were extracted (Höjeberg and Malmskog, 1970; Ton *et al.*, 1970). These g_K values were found to be in good agreement with values calculated using Nilsson (1955) wave functions. The g_K value can also be derived from the $M1$–$E2$ mixing ratio of intraband transitions, as has been done by Kroger and Reich (1976) and Ahmad *et al.* (1976b).

According to Alaga *et al.* (1955), the ratio of the reduced transition probabilities, $B(\lambda)$, for γ rays between two bands is given by

$$\frac{B(\lambda,I_i\rightarrow I_f)}{B(\lambda,I_i\rightarrow I_f')}=\left[\frac{\langle I_i\lambda K_i(K_f-K_i)|I_i\lambda I_fK_f\rangle+b(-)^{I_f+K_f}\langle I_i\lambda K_i(-K_f-K_i)|I_i\lambda I_f-K_f\rangle}{\langle I_i\lambda K_i(K_f-K_i)|I_i\lambda I_f'K_f\rangle+b(-)^{I_f'+K_f}\langle I_i\lambda K_i(-K_f-K_i)|I_i\lambda I_f'-K_f\rangle}\right]^2, \tag{3.6}$$

where λ is the multipole order of the transition and b is the ratio of matrix elements, $G_\lambda(K_i\rightarrow-K_f)/G_\lambda(K_i\rightarrow K_f)$. In general, the agreement between experiment and theory for $M1/E2$ ratios is fairly good. On the other hand, large deviations from the Alaga rules are often observed for $E1$ γ rays. Again, the γ-ray branching ratios are used only to decide between various possible K assignments.

E. One-nucleon transfer reactions

The single-particle transfer reaction [e.g., (d,p), (d,t), and $(^3\mathrm{He},d)$ reactions] has proved to be the most useful tool for the identification of single-particle energy levels. This utility arises from the sensitivity of the cross sections to the single-particle wave function.

1. First-order theory

The usefulness of transfer reactions depends on the fact that a simple, first-order theory can explain most features of the data. In this theory the assumption is made that the cross section is a product of two factors. The first factor describes the reaction mechanism for transfer of a nucleon into a single-particle orbital; the second factor, the spectroscopic factor, is a measure of the overlap between initial and final nuclear states. In this approximation the differential cross section to a given final state for an even target with spin zero can be written as

$$d\sigma/d\Omega=(2I+1)S_j\theta_j^{\mathrm{DW}}\,, \tag{3.7}$$

where I is the total angular momentum of the final state, j the total angular momentum of the transferred nucleon, θ_j^{DW} the intrinsic single-particle differential cross section, and S_j the spectroscopic factor, which contains information about internal nuclear structure. In this case I always equals j. The advantage of factoring the cross section in this way is that all the effects involving bombarding energy, scattering angle, projectile mass, etc., are separated, isolating the factor S_j. For a spin-zero target the spectroscopic factor can be written

$$S_j^\kappa=[2/(2I+1)](C_j^\kappa)^2P_\kappa^2\,, \tag{3.8}$$

where κ denotes the specific orbital being populated, P_κ is the pairing factor for that orbital in the target, and C_j^κ is an expansion coefficient of the deformed single-particle wave function in terms of a spherical basis set. These wave functions are written

$$\chi^\kappa=\sum_j C_j^\kappa\phi_j\,. \tag{3.9}$$

The pairing factor P_κ in (3.8) describes the overlap between the pairing parts of the wave functions of the target and final state. For the (d,p) reaction on an even–even target, this factor can be written exactly as

$$P_\kappa^2=[\langle\phi_\kappa(A+1)|\alpha_\kappa^\dagger|\phi_0(A)\rangle]^2\,, \tag{3.10}$$

where ϕ_κ indicates the state in the final nucleus in which the single-particle level κ is blocked, and $\phi_0(A)$ designates the wave function of the even-A nucleon target. The overlap integral is complicated to compute, since one needs complete wave functions for the target and for each final state studied. A good approximation is

$$P_\kappa^2 \approx [1 - \langle N_\kappa(A)\rangle] R_\kappa^2 , \tag{3.11}$$

where the overlap factor R_κ is defined in Appendix B, and $\langle N_\kappa(A)\rangle$ is the occupation probability for level κ in the target nucleus. In the simplest approximation $R_\kappa = 1$, and $P_\kappa^2 = U_\kappa^2$ for a (d,p) reaction where U_κ^2 is the emptiness of level κ in the initial system.

The intrinsic single-particle differential cross section θ_j^{DW} contains all the details of the transfer process other than information about the nuclear structure of the initial and final states. The distorted-wave Born approximation (DWBA) theory is usually used to calculate θ_j^{DW}. Satchler (1964) provides a thorough discussion of DWBA theory. The codes DWUCK (Kunz, 1969) and JULIE (Bassel *et al.*, 1962) are frequently used distorted wave codes. Detained agreement with experiment has never been achieved because a variety of second-order effects, to be discussed below, are ignored. A further difficulty is that the optical-model potentials needed are difficult to measure, since the elastic-scattering angular distributions are relatively structureless. Nevertheless DWBA calculations are of great value since they can usually be relied on to reproduce the energy and angular-momentum dependence of the cross sections. However, they cannot be trusted to give the absolute differential cross section to better than a factor of 2 for (d,p) and (d,t) reactions and are less reliable for other transfer reactions.

Equations (3.7) and (3.8) combine to give the following very useful expression for the differential cross section

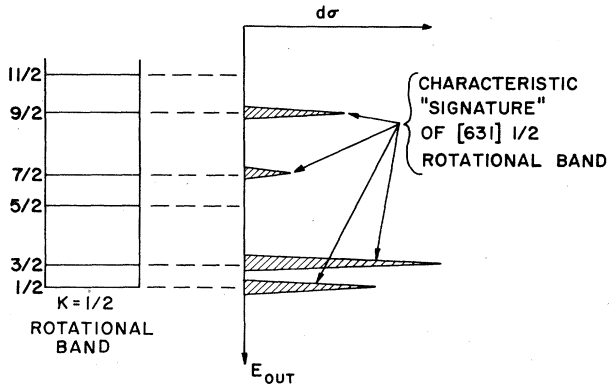

FIG. 12. Illustrative signature for the neutron orbital 1/2 + [631] in single-nucleon transfer reaction.

to an energy level with spin $I = j$:

$$d\sigma/d\Omega = 2(C_j^\kappa)^2 \theta_j^{\mathrm{DW}} P_\kappa^2 . \tag{3.12}$$

For further information on transfer reactions on deformed nuclei see Siemssen and Erskine (1966), Elbek Tjøm (1969), and Braid *et al.* (1970).

2. Signature patterns in the relative differential cross sections

The cross section for populating a level in a rotational band is proportional to the square of only one expansion coefficient, C_j^κ, in the wave function of that single-particle orbital. In general the coefficients C_j^κ are distinctive for each orbital. Hence, the relative cross sections for populating the members of a rotational band make a unique signature or fingerprint for that state [see Eq. (3.12)]. A schematic example of these signatures is presented in Fig. 12. Figure 13, taken from Braid *et al.*

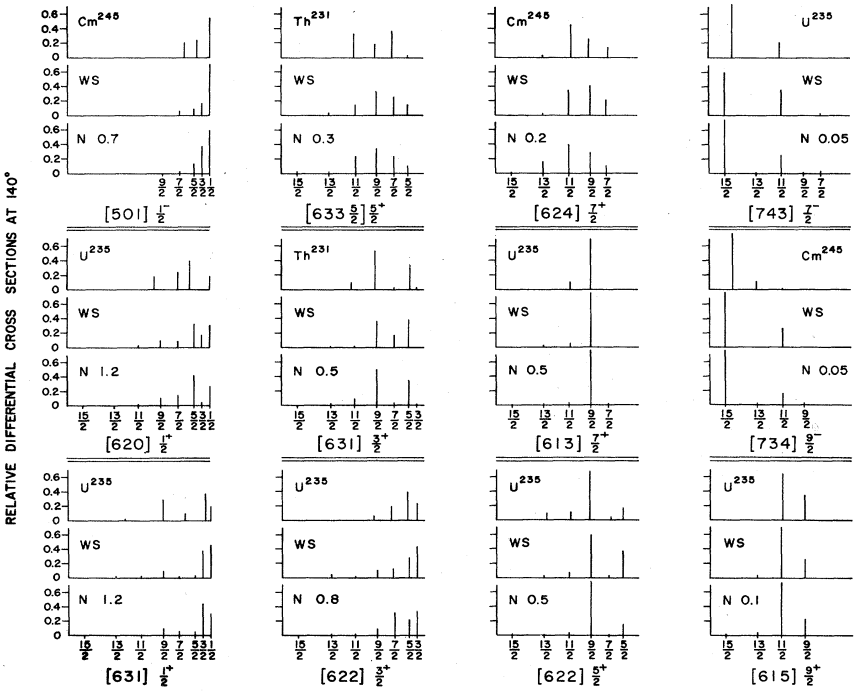

FIG. 13. Catalog of signatures. The experimental signature as measured at 140° with 12 MeV deuterons is the upper figure in each group. The middle member of the group is the signature calculated with the Woods–Saxon wave functions (Rost, 1967). The lower member is the signature calculated with modified oscillator wave functions (Nilsson, 1955). The DWBA code JULIE was used for both calculated differential cross sections. The number in each figure is the total cross section (calculated or measured) in (μb/sr). All bar graphs are normalized to a total cross section of unity for convenience in comparing relative cross sections to members of each band.

(1970), compares the signatures calculated for 12 single-particle states using modified oscillator (Nilsson, 1955) and Woods–Saxon (Rost, 1967) wave functions, as well as those signatures experimentally observed with the (d,p) and (d,t) reactions on various actinide targets. As can be seen, the major features of the signatures are reproduced by the calculations, but there are minor discrepancies. However, for many of these states the signatures, especially when previously verified by experiment, serve to identify a group of levels as being part of the rotational band of a specific single-particle state.

3. Angular-momentum dependence of the angular distributions

Most studies of transfer reactions on heavy elements have been performed with beams from tandem Van de Graaff accelerators with the projectile energies for deuterons 12–16 MeV, and for ^{3}He or ^{4}He, 24–30 MeV. At these energies the transfer process is strongly dominated by Coulomb effects. The angular distributions tend to peak near 90° and show no forward oscillatory structure which would be useful to measure the orbital angular momentum transfer l. Macefield and Middleton (1964) have measured complete angular distributions for (d,p) reactions on ^{238}U. In some circumstances the overall shape provides a clue to the l value of the transfer. For example, for (d,p) and (d,t) reactions at 12 MeV, the cross section at backward angles is larger for high l transfer than for small l transfer. In practice there are exceptions, presumably caused by second-order effects. Figure 14 illustrates an example of this type of l dependence. It is taken from Braid *et al.* (1970) and shows the ratio of the ^{234}U$(d,p)^{235}$U cross sections at 90° and 140° for angular momentum transfer l. This ratio does not change greatly with excitation energy. However, as is also shown, the same ratios for the ^{236}U$(d,t)^{235}$U reaction are not strongly l dependent, and change appreciably with excitation energy, making these ratios much less useful for the assignment of states.

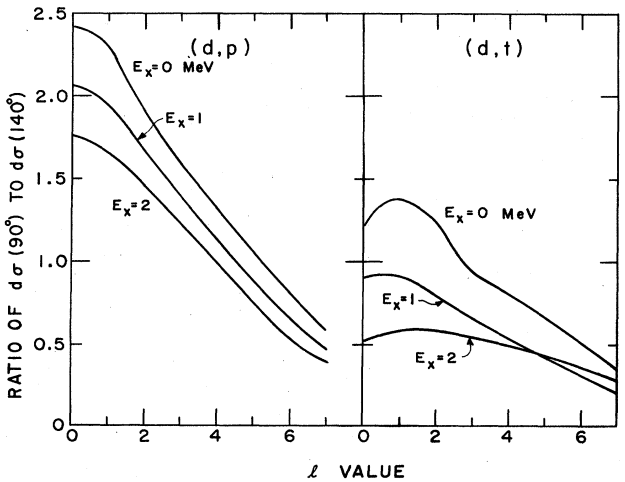

FIG. 14. Calculated values of ratio of differential cross sections at 90° to that at 140°, as a function of angular momentum transfer, l. Values are for ^{234}U$(d,p)^{235}$U and ^{236}U$(d,t)^{235}$U reactions with 12 MeV deuterons.

4. l-value determination from the cross-section ratio of different reactions

Another technique which has been used to establish l values is to observe the same levels with two reactions having a different dependence on l value. The reaction with the larger momentum mismatch between entrance and exit channels tends to emphasize levels with high l transfer. For neutron transfer the (d,t), $(^3\text{He},\alpha)$ combination works well, as shown in the study of high spin states in ^{241}Pu by Elze and Huizenga (1971). A combination of limited use for proton transfers are the (α,t) and $(^3\text{He},d)$ reactions (Elze and Huizenga, 1970b; Erskine *et al.*, 1975).

In this survey we have used the data on the angular momentum dependence of the levels only as a means of verifying assignments based on other evidence.

5. Distinguishing particle and hole states

The ratio of (d,p) to (d,t) cross sections leading to the same level serves as a useful guide to the particle or hole character of a single-particle state (Braid *et al.*, 1970). Under the assumption that the intrinsic single-particle cross section θ_j^{DW} has the same j dependence for (d,p) and (d,t) reactions, the ratio of (d,p) to (d,t) cross sections is proportional to $[1-\langle N_\kappa(A-1)\rangle]/\langle N_\kappa(A+1)\rangle$, where A is the nucleon number of the odd-A product nucleus. For a particle state this ratio is large and for a hole state it is small.

6. Corrections to the first-order theory

There are a number of effects not included in the simple theory discussed above which complicate the transfer process to the extent that really good agreement between theory and data is difficult to achieve. The calculations which have been performed to date usually treat the various effects separately. Obviously a proper calculation which included all of these effects on a consistent basis would be very difficult and would need to be performed for every case. Fortunately in most cases these second-order effects do not obscure the main features of the transfer reactions predicted by Eq. (3.12). Some of the neglected effects follow.

a. Coriolis mixing

Coriolis mixing among the various single-particle states (see Sec. II) may considerably change the signature of an orbital. The expression for a mixed spectroscopic factor is (Siemssen and Erskine, 1966)

$$S_j^\kappa = [2/(2I+1)]\left[\sum_i a_i^\kappa C_j^i P_i\right]^2, \tag{3.13}$$

where the mixing coefficients a_i are usually obtained from a fit to the measured level energies. Signatures calculated with Eq. (3.13) generally give improved agreement with the data (Erskine, 1965).

b. Coupled-channel effects

Inelastic excitation of the target (or residual nucleus) by the beam projectile (or emitted particle) is an important feature of the reaction mechanism. Population of

weakly excited levels in the residual nucleus frequently occurs by means of multistep processes in which the target or residual nucleus is excited to an intermediate state during the transfer process. In some situations this indirect transfer amplitude may exceed that of the direct transfer. The multistep contributions are usually weak and therefore the main features of the signatures of orbitals do not change from one nucleus to the next. There may be instances in which the multistep contributions are large, but do not vary from one nucleus to another. It is difficult to distinguish between these two possibilities. Multistep transfer has been discussed in some detail by Tamura *et al.* (1970), by Ascuitto *et al.* (1972), and by Glendenning (1975).

c. Uncertainties in the tails of the nuclear wave functions

At the bombarding energies used in the typical transfer reaction experiments on actinide nuclei, transfer occurs mostly in the region 2–8 fm beyond the nuclear surface (Erskine, 1972). Since only a small part of the single-particle wave function lies beyond the nuclear surface, very careful calculations are needed to accurately compute the nuclear wave function at the radius where the reaction occurs, and such calculations are not usually available. One procedure for obtaining good wave functions is to solve the general coupled-channel eigenvalue problem (Rost, 1967; Tamura, 1971). Another procedure, which involves the use of Sturmian functions, has been given by Anderson *et al.* (1970) and by Schulz *et al.* (1972).

d. Particle-hole interaction

The presence of coherent particle–hole modes, particularly the quadrupole or octupole modes, causes the mixing of single-particle states (see Secs. II.B.2.b and III.F), which changes the observed differential cross sections. This effect is minimal for the ground state and increases with excitation energy. In the calculations of Gareev *et al.* (1971) the ground states of a variety of actinides show admixtures which range from 2% to 25%. At higher excitation energies the admixing becomes very large.

It is very difficult at present to make quantitative comparison of these calculations with the data. However, the fact that the cross-section signatures of many single-particle states can be recognized up to excitation energies of 1 MeV suggests that the calculations of Gareev *et al.* (1971) tend to overemphasize the degree of phonon–quasiparticle mixing.

F. Vibrational states

In deformed actinide nuclei there are really no pure single-particle states. Calculations, such as those of Gareev *et al.* (1971), indicate that phonon admixtures in the single-particle states vary from a few percent to over 90%.

Schematically we define a single-particle wave function as

$$\phi_{\rm sp}=a_i^+|0\rangle, \tag{3.14}$$

and a particle-plus-phonon wave function as

$$\phi_{\rm ph}=a_j^+\sum_{k,l}T_{k,l}a_k^+a_l|0\rangle, \tag{3.15}$$

where $|0\rangle$ denotes the particle–hole vacuum. The states discussed in Sec. II.B.2.b were of the form

$$\Psi=b\phi_{\rm sp}+\sqrt{1-b^2}\,\phi_{\rm ph}, \tag{3.16}$$

with $b\approx 1$, i.e., primarily single-particles states. In this section we discuss briefly those states for which $(1-b^2)\simeq 1$. Such states we denote as vibrational. There is no sharp demarcation between these two categories.

The vibrational states that have been identified in the odd-mass actinides are given in Table III. The identification of these states was made either through decay scheme studies or through nuclear reactions that preferentially excite the collective states. Studies of radioactive decay provide spin-parity, logft value, rotational constant and gamma-decay pattern of the state. Assignments to vibrational states based on radioactive decay studies are made only when no reasonable single-particle orbital assignments are possible near the observed excitation energies.

Coulomb excitation preferentially populates collective states because of the enhanced $B(E2)$ and $B(E3)$ values. Only one odd-A nucleus, ^{235}U, has been studied in detail by Coulomb excitation (Stephens *et al.*, 1968). Recently, the (d,d') reaction has been utilized to investigate the collective states of odd-mass nuclei. The (d,d') reaction preferentially excites the octupole bands. So far deuteron inelastic scattering experiments have been performed with targets of ^{249}Cf (Yates *et al.*, 1975b), ^{233}U, ^{235}U, ^{237}Np, and ^{239}Pu (Thompson *et al.*, 1976). In these studies octupole bands corresponding to the $K\pi=0-$, $1-$, $2-$, and $3-$ excitations of even–even nuclei have been identified. The rotational constants of the vibrational bands identified are very similar to those of the base states.

Vibrational states have also been studied by (p,t) reactions (Friedman *et al.*, 1973). These reactions preferentially excite the 0+ phonon coupled to the ground-state configuration of the target nucleus.

In principle, the magnitudes of particle-plus-phonon admixtures of type $\phi_{\rm ph}$ can be determined from measurements of cross sections in reactions such as the (d,d') and (p,t) reactions if the index j in Eq. (3.15) is the ground state of the odd-A system. This is done by measuring the ratio of the cross section to the state of interest in the odd-A nucleus and the cross section to the corresponding phonon state in the neighboring even-A nucleus. Another approach which was used by Yates *et al.* (1975b) is to assume equal cross sections to the $(K+\nu)$ and $(K-\nu)$ bands and then assume that the $(K+\nu)$ band is a pure particle-plus-phonon state. However, both procedures suffer from considerable uncertainties because of inadequacies in the theoretical cross-section calculations.

In general, the γ-de-excitation process cannot be used to deduce the magnitudes of phonon components in the single-particle wave functions. Although the phonon admixture enhances the probability for a γ-transition of the phonon multipolarity, it is still usually small compared to transitions of lower multipolarities. Unless lower multipole order transitions are K-forbidden or retarded, it is not possible to deduce the phonon admixture

TABLE III. Vibrational states in actinide nuclei.

Nucleus	Bandhead energy (keV)	$K\pi$	$[A_{vib}/A_{gs}]$ [s]	Assignment	Method	References
^{233}U	748	5/2−	1.04 ±0.06	{5/2+[633]⊗0−}	(d,d')	a
^{235}U	444	7/2+	1.4	{7/2−[743]⊗0−}	(d,d')	a
	637.9	3/2−	1.04 ±0.02	{7/2−[743]⊗2+}	Coul, (d,d')	a,b
	920.7	11/2−	1.001±0.009	{7/2−[743]⊗2+}	Coul, (d,d')	a,b
	1053	7/2−		{7/2−[743]⊗0+}	Coul	b
^{235}Np	834	5/2+		{5/2+[642]⊗0+}	(p,t)	c
^{237}Np	721	5/2−	1.02 ±0.07	{5/2+[642]⊗0−}	(d,d')	a
^{237}Pu	800	1/2+		{1/2+[631]⊗0+}	(p,t)	c
^{239}Pu	470	1/2−[t]		{1/2+[631]⊗0−}	(d,d')	a
^{241}Am	952	5/2−		{5/2−[523]⊗0+}	(p,t)	c
^{243}Pu	703.9	3/2−		{7/2+[624]⊗2−}	(n,γ)	d
^{245}Cm	663.7	3/2−	0.917±0.004	{7/2+[624]⊗2−}	Decay scheme	e
^{249}Cf	668	13/2−	0.97 ±0.04	{9/2−[734]⊗2+}	(d,d')	f
	813.2	5/2−	0.981±0.006	{9/2−[734]⊗2+}	(d,d') Decay scheme	f,g
	920	11/2+	0.98 ±0.03	{9/2−[734]⊗1−}	(d,d')	f
	1063	13/2+	0.96 ±0.04	{9/2−[734]⊗2−}	(d,d')	f
	1078	15/2+	1.04 ±0.04	{9/2−[734]⊗3−}	(d,d')	f
	1415	7/2+	1.00 ±0.07	{9/2−[734]⊗1−}	(d,d')	f
^{251}Es	889.1	11/2+	0.994±0.004	{7/2+[633]⊗2+}	Decay scheme	h

[a] Thompson *et al.* (1976).
[b] Stephens *et al.* (1968).
[c] Friedman *et al.* (1974).
[d] Casten *et al.* (1976).
[e] Ahmad *et al.* (1976a).
[f] Yates *et al.* (1975b).
[g] Ahmad *et al.* (1976b).
[h] Ahmad *et al.* (1976c).
[s] This is the ratio of the rotational constant of the vibrational band to that of the base band K_0. The errors were calculated by us, using the errors in level energies given in original references.
[t] This band was also identified by Davies and Hollander (1965), and the value of rotational constant and decoupling parameter were found to be 5.043 keV and 0.48, respectively.

in the initial and final states. The phonon admixture in the $\frac{5}{2}+[622]$ state at 145 keV of ^{249}Cf was deduced from the $E3$ admixture in the predominantly $M2$ transition (Ahmad *et al.*, 1976b). This admixture (amplitude square = 0.29) was found to be in excellent agreement with the value (0.30) extracted from the (d,d') reaction cross section (Yates *et al.*, 1975b). A large phonon admixture in this $\frac{5}{2}+[622]$ state was predicted by Gareev *et al.* (1971).

G. Moment of inertia and decoupling parameter

From the known level energies of a band the rotational constant $\hbar^2/2\mathcal{I}$ and the decoupling parameter **a** can be determined. Rotational constants for single-particle states in the actinide region are ~6.0 keV. For bands having strong Coriolis interaction these values may change considerably, e.g., the $\frac{5}{2}+[642]$ band in ^{245}Am has $\hbar^2/2\mathcal{I}$ of 2.8 keV (Ahmad, 1966). For two interacting bands the rotational constant increases for the upper band and decreases for the lower one.

The sign and magnitude of the decoupling parameter can be used to characterize a $K=\frac{1}{2}$ band. The experimental and theoretical values of **a** for $K=\frac{1}{2}$ bands are given in Table IV.

There are sufficient data to study the systematic behavior of the $\frac{1}{2}+[631]$ neutron orbital throughout the actinides. The value of **a** for that orbital changes by a factor of 5 as the neutron number is increased from 143 to 149. The pure single-particle values are in good agreement with the measurements except for the nuclide ^{233}Th. It should be noted that the value of **a** for this band is rather sensitive to the magnitude of both the $P_4^0(\cos\theta)$ and $P_6^0(\cos\theta)$ deformation of the potential. The set of deformation parameters ($\nu_2=0.19, \nu_4=-0.04, \nu_6=-0.02$) gives a wave function with a decoupling parameter of −0.31. The set of deformation parameters ($\nu_2=0.19, \nu_4=-0.06, \nu_6=0.00$) gives a decoupling parameter of −0.27 for this band. It is also noteworthy in this regard that the choice ($\nu_2=0.19, \nu_4=-0.04, \nu_6=-0.02$) gives a decoupling parameter of −1.50 for the proton orbital $\frac{1}{2}-[530]$ and the choice ($\nu_2=0.19, \nu_4=-0.06, \nu_6=0.00$) gives −1.54 for this proton orbital.

H. Effects of Coriolis interaction on level energies and transition probabilities

The Coriolis interaction was discussed by Bohr (1952) in his original paper on nuclear rotation, and it was first used by Kerman (1956) to explain the anomalous level spacings of the $K\pi=\frac{1}{2}-$ and $\frac{3}{2}-$ bands in ^{183}W (see Sec. II.A and Appendix C). Clear manifestations of this interaction in the actinide region occur in the α decays of ^{235}U (Pilger *et al.*, 1957), ^{235}Np (Browne and Asaro, 1973), and ^{249}Bk (Ahmad, 1966). In these studies the low hindrance factors, observed for bands

TABLE IV. Values of decoupling parameter a.

State	Nuclide	Exptl.[s]	References	Decoupling parameter a calculated value $\nu_2 = 0.19$, $\nu_4 = -0.04$, $A = 232$	$\nu_2 = 0.22$, $\nu_4 = -0.02$, $A = 238$	$\nu_2 = 0.25$, $\nu_4 = 0.0$, $A = 244$
1/2 + [631]	^{233}Th	−0.145 0 ± 0.000 9	a			
	^{235}U	−0.285 4 ± 0.000 9	b			
	^{237}U	−0.403 ± 0.005	c			
	^{239}U	−0.421 ± 0.005	d			
	^{237}Pu	−0.469 5 ± 0.000 3	e	−0.39	−0.57	−0.70
	^{239}Pu	−0.580 88 ± 0.000 04	f			
	^{243}Pu	−0.581 ± 0.005	g			
	^{245}Cm	−0.724 ± 0.001	h, i			
1/2 + [620]	^{243}Pu	0.34 ± 0.02	g			
	^{245}Cm	0.36 ± 0.11	h, i			
	^{247}Cm	0.52 ± 0.17	j			
	^{249}Cm	0.29 ± 0.10	i	0.09	0.21	0.29
	^{249}Cf	0.32 ± 0.11	k			
	^{251}Cf	0.285 4 ± 0.000 8	l			
1/2 − [501]	^{231}Th	~0.8	m			
	^{237}U	~0.8	m	0.87	0.81	0.76
	^{243}Pu	1.4	g			
1/2 − [750]	^{243}Pu	−5.6[t]	g	−3.3	−3.3	−3.4
1/2 − [530]	^{231}Pa	−1.498 ± 0.000 7	n			
	^{233}Pa	−1.38[t]	o			
	^{237}Np	−1.692 ± 0.002	p	−1.8	−2.0	−2.2
	^{241}Am	−1.8[t]	q			
1/2 + [400]	^{237}Np	1.08 ± 0.05	p			
	^{241}Am	0.7[t]	q	1.16	0.60	0.59

[a] Von Egidy *et al.* (1972).
[b] Cline (1968).
[c] Ahmad *et al.* (1968).
[d] Bollinger and Thomas (1972).
[e] Ahmad *et al.* (1975b).
[f] Porter *et al.* (1972).
[g] Casten *et al.* (1976).
[h] Ahmad *et al.* (1976a).
[i] Braid *et al.* (1971).
[j] Browne and Asaro (1968).
[k] Ahmad *et al* (1967).
[l] Ahmad *et al.* (1971).
[m] Boyno *et al.* (1970).
[n] Browne and Asaro (1973).
[o] Hoekstra and Wapstra (1969).
[p] Yamazaki and Hollander (1966); Lederer *et al.* (1966).
[q] Porter *et al.* (1974).
[s] The errors were calculated by us, using the errors in level energies given in original references.
[t] These values were calculated from the energies of only 1/2 and 3/2 members, using a value of $\hbar^2/2\mathcal{I} = 6.0$ keV.

other than the favored bands, were explained in terms of Coriolis mixing. The Coriolis mixing also has strong effects on level energies (Stephens, 1975), gamma transition probabilities (Brockmeier *et al.*, 1965; Stephens *et al.*, 1968; Friedman *et al.*, 1969), and nuclear reaction cross sections (Erskine, 1965).

Expressions to calculate level energies and admixture coefficients for the two band interaction are given in Appendix C. In these calculations the bandhead energies, the values of $\hbar^2/2\mathcal{I}$ and the Coriolis matrix elements are varied to obtain a best fit between the experimental and calculated level energies. The values of the rotational constant $\hbar^2/2\mathcal{I}$ in the actinide region lie between 6.0 and 6.6, with the typical value being 6.2 keV. The Coriolis matrix elements determined from the fitting procedures are found to be smaller than the values calculated from single-particle wave functions including pair correlation effects. Recently Ring *et al.* (1974) have calculated the attenuation of Coriolis matrix elements using the cranking model within the framework of the Hartree–Fock–Bogoliubov theory. Also, part of the reduction could arise from large admixtures in the states involved (Gareev *et al.*, 1971).

I. Data tables on individual nuclides

We present the experimental data on the intrinsic states of odd-mass actinide nuclei in Tables V–XXXVII in the order of increasing A and Z. The data on odd-

TABLE V. Intrinsic states of $^{229}_{90}Th_{139}$.

$^{233}U \xrightarrow{\alpha}, 5/2+[633]$ $^{230}Th(d,t)$ Bandhead energy (keV)	I	$K\pi$	Assigned character [d]	$^{229}_{90}Th_{139}$ $\hbar^2/2\mathcal{I}$ (keV)	a	Empirical data used to deduce assignment	References
0		5/2+	5/2+[633]	6.0		I, μ, Fav.α	a,b
<0.1		3/2+	3/2+[631]	5.8		$\alpha, \gamma, (d,t)$	b,c
146.4		5/2−	5/2−[752]	0.3		α, γ	b
164.5		3/2−	3/2−[761]	10.5		α, γ	b
261.7		1/2+	1/2+[631] A			(d,t)	c
535.5		1/2−	1/2−[501] A			(d,t)	c

[a] Gerstenkorn *et al.* (1974); I, μ.
[b] Kroger and Reich (1976); ^{233}U α decay.
[c] Braid *et al.* (1976); $^{230}Th(d,t)$ reaction.
[d] Comment: There is strong Coriolis mixing between the 3/2−[761] and 5/2−[752] bands. Also the $K\pi = 3/2-$ band at 164.5 keV contains a large admixture of $\{3/2+[631] \otimes 0^-\}_{3/2-}$ vibrational component.

neutron nuclei are given first, followed by data on odd-proton nuclei. The single-particle orbital assignments followed by no letter represent well established assignments. The meanings of the notations employed in the tables are as follows:

A Letter *A* after an orbital assignment suggests a less certain assignment supported by some experimental evidence
B Letter *B* after an orbital assignment indicates an assignment made on the basis of systematics
I Measured spin
μ Measured magnetic moment
τ Measured half-life of the state
γ Indicates that the γ-ray intensity pattern was used to deduce the spin and parity of the state
γ-mult Indicates that the γ-ray multipolarities were used to deduce the spin and parity of the state. It is used only when the spin and parity of the other state involved in the transition is known.
Fav. α Indicates that the state is populated by favored α transition. Hence this state in the daughter has the same single-particle configuration as the parent ground state.

TABLE VI. Intrinsic states of $^{231}_{90}Th_{141}$.

$^{235}U \xrightarrow{\alpha}, 7/2-[743]$ $^{232}Th(d,t), ^{232}Th(^3He,\alpha), ^{230}Th(d,p)$ Bandhead energy (keV)	I	$K\pi$	Assigned character [d]	$^{231}_{90}Th_{141}$ $\hbar^2/2\mathcal{I}$ (keV)	a	Empirical data used to deduce assignment	References
0		5/2+	5/2+[633]	6.0		$\alpha, (d,t), (^3He,\alpha)$	a,b,c
185.7		5/2−	5/2−[752]	2.8		$\alpha, \gamma, (^3He,\alpha), (d,t)$	a,b,c
221.4		3/2+	3/2+[631]	3.9		$\alpha, \gamma, (d,t)$	a,b
253.0		1/2+	1/2+[631]	7.7	−0.14	$\alpha, \gamma, (d,t), (d,p)$	a,b,d
387.8		7/2−	7/2−[743]	7.2		Fav.$\alpha, \gamma, (^3He,\alpha)$	a,c
558		1/2−	1/2−[501] A	6.7	~0.8	(d,t)	b
871	7/2	3/2+	3/2+[642] A	5.0		$(^3He,\alpha)$	c
876		5/2−	5/2−[503] A			(d,t)	b

[a] Vaño *et al.* (1975); ^{235}U α decay.
[b] Boyno *et al.* (1970); $^{232}Th(d,t)$.
[c] Elze *et al.* (1969); $^{232}Th(^3He,\alpha)$.
[d] Braid *et al.* (1965); $^{230}Th(d,p)$.
[e] Comment: The 5/2− band at 185.7 keV and 7/2− band at 387.8 keV are strongly Coriolis-mixed, and so are the 1/2+[631] and 3/2+[631] bands.

TABLE VII. Intrinsic states of $^{233}_{92}Th_{143}$.

$^{232}Th(d,p)$, $^{232}Th(n,\gamma)$ Bandhead energy (keV)	I	$K\pi$	$^{233}_{92}Th_{143}$ Assigned character	$\hbar^2/2\mathcal{I}$ (keV)	a	Empirical data used to deduce assignment	References
0		1/2 +	1/2 + [631]	6.6	−0.145	$^{233}Th\ \beta^-$ decay, (d,p)	a–c
6.0		5/2 +	5/2 + [622]			(d,p), (n,γ)	b,c
252.3	15/2	7/2 −	7/2 − [743]			(d,p)	b
262.1		5/2 +	5/2 + [633]			(d,p), (n,γ)	b,c
278		7/2 +	7/2 + [624]			(d,p)	b
335.9		3/2 +	3/2 + [631]			(d,p), (n,γ)	b,c
539.5		1/2 −	1/2 − [501]			(d,p), (n,γ)	b,c

[a] Hoekstra and Wapstra (1969); $^{233}Th\ \beta^-$ decay.
[b] Von Egidy *et al.* (1972); $^{232}Th(d,p)$, $^{232}Th(n,\gamma)$ reactions.
[c] Kern and Due (1974); $^{232}Th(n,\gamma)$ reaction.

α Indicates that the α intensity pattern and hindrance factors were used to make the assignment

EC, β^- Indicates that the state is fed by electron capture or β^- decay. The number in parentheses denotes the logft value of the transition.

(d,p), (d,t), $(^3He,\alpha)$, $(^3He,d)$, (α,t), (d,d') Denote the particular reaction used to excite that state and indicate that the observed signature of the reaction cross section was employed in the level assignment.

Coul Denotes Coulomb excitation, indicates vibrational component

(n,γ) Denotes (n,γ) reaction, indicates low spin

In Tables V–XXXVII we have compiled all data published before 1 December 1976. In a few cases we have also included unpublished work. We have listed only the latest references on each nucleus; earlier references can be found in the Table of Isotopes (Lederer *et al.*, 1967) and the data tables compiled by the Nuclear Data Group at Oak Ridge.

TABLE VIII. Intrinsic states of $^{233}_{92}U_{141}$.

$^{233}Pa \overset{\beta^-}{\Rightarrow}$, 3/2, 1/2 − [530] $^{235}U(p,t)$ Bandhead energy (keV)	I	$K\pi$	$^{233}_{92}U_{141}$ Assigned character [e]	$\hbar^2/2\mathcal{I}$ (keV)	a	Empirical data used to deduce assignment	References
0		5/2 +	5/2 + [633]	5.8		I,μ,γ	a,b
311.9		3/2 +	3/2 + [631]	5.7		$\beta^-(7.3)$, γ-mult	b
318	7/2	5/2 −	5/2 − [752]			(p,t), (d,d')	c,d
398.6		1/2 +	1/2 + [631]			$\beta^-(6.6)$, γ-mult	b
502		7/2 −	7/2 − [743]			(p,t), (d,d')	c,d
748		5/2 −	{5/2 + [633] ⊗ 0−}			(d,d')	d
819	7/2	7/2 −	?			(p,t)	c
1824	7/2	7/2 −	?			(p,t)	c
2070	7/2	7/2 −	?			(p,t)	c

[a] Dorain *et al.* (1957); Vander Sluis (1956); I,μ.
[b] Albridge *et al.* (1961); Bisgård *et al.* (1963); $^{233}Pa\ \beta^-$ decay.
[c] Friedman *et al.* (1974); $^{235}U(p,t)$ reaction.
[d] Thompson *et al.* (1976); $^{233}U(d,d')$ reaction.
[e] Comment: The 819, 1824, and 2070 keV levels are populated in the (p,t) reaction with $L=0$ transitions. These could be {7/2 − [743] ⊗ 0+} vibrational states.

TABLE IX. Intrinsic states of $^{235}_{92}U_{143}$.

$^{239}Pu \xrightarrow{\alpha}$, 1/2 + [631]
$^{234}U(d,p)$, $^{236}U(d,t)$, $^{236}U(^3He,\alpha)$, $^{234}U(n,\gamma)$, $^{233}U(t,p)$, $^{235}U(d,d')$, ^{235}U–Coul
$^{235}_{92}U_{143}$
$\xleftarrow{EC}$ ^{235}Np, 5/2 + [642]

Bandhead energy (keV)	I	$K\pi$	Assigned character	$\hbar^2/2\mathcal{I}$ (keV)	a	Empirical data used to deduce assignment	References
0		7/2 –	7/2 – [743]	5.1		I,μ, (d,p), (d,t), $(^3He,\alpha)$	a–c
0.08		1/2 +	1/2 + [631]	6.0	–0.28	Fav.α, (d,p), (d,t), $(^3He,\alpha)$	b–d
129.3		5/2 +	5/2 + [622]	6.0		α,γ, (d,p), (d,t), $(^3He,\alpha)$, (n,γ)	b–g
332.7		5/2 +	5/2 + [633]	4.9		α,γ, (d,p), (d,t), $(^3He,\alpha)$, (n,γ), (t,p)	b–g
393.0		3/2 +	3/2 + [631]	6.7		α,γ, (d,p), (d,t), $(^3He,\alpha)$, (n,γ)	b,c,e, f,g
491.9		7/2 +	7/2 + [624]			(n,γ)	g
507.7		5/2 +	collective			(n,γ), (t,p)	g
633.1		5/2 –	5/2 – [752]	5.4		Coul, (d,p), (d,t), $(^3He,\alpha)$, (n,γ)	b,c,g,h
637.9		3/2 –	{7/2 – [743] ⊗ 2+}	5.3		Coul, (d,p), (n,γ), (d,d')	g–i
640.5		1/2 +	collective			(n,γ), (t,p)	g
659.0		1/2 –	1/2 – [501]			(d,p), (d,t), (n,γ)	b,g
760.9		1/2 +	{1/2 + [631] ⊗ 0+}			(n,γ)	g
821.6		9/2 –	9/2 – [734]	5.9		Coul, (d,d')	h,i
920.7		11/2 –	{7/2 – [743] ⊗ 2+}	5.1		Coul, (d,d')	h,i
1053		7/2 –	{7/2 – [743] ⊗ 0+}			Coul	h
1236		7/2 +	7/2 + [613]			(d,p), (d,t)	b
1255		1/2 +	1/2 + [620]			(d,p)	b
1392		3/2 +	3/2 + [622]			(d,p)	b
1438		9/2 +	9/2 + [615]			(d,p)	b

[a] Dorain *et al.* (1957); Vander Sluis (1956); I,μ.
[b] Braid *et al.* (1970); $^{234}U(d,p)$, $^{236}U(d,t)$ reactions.
[c] Elze and Huizenga (1969); $^{236}U(^3He,\alpha)$ reaction.
[d] Baranov *et al.* (1963); ^{239}Pu α decay.
[e] Ahmad (1966); ^{239}Pu α,γ decays.
[f] Cline, 1968; γ rays in ^{239}Pu α decay.
[g] Rickey *et al.* (1972); $^{233}U(t,p)$, $^{235}U(d,d')$, $^{234}U(d,p)$, $^{236}U(d,t)$, and $^{234}U(n,\gamma)$ reactions.
[h] Stephens *et al.* (1968); ^{235}U Coulombic excitation.
[i] Thompson *et al.* (1976); $^{235}U(d,d')$ reaction.

TABLE X. Intrinsic states of $^{237}_{92}U_{145}$.

$^{241}Pu \xrightarrow{\alpha}$, 5/2 + [622]
$^{236}U(d,p)$, $^{238}U(d,t)$, $^{238}U(^3He,\alpha)$
$^{237}_{92}U_{145}$

Bandhead energy (keV)	I	$K\pi$	Assigned character	$\hbar^2/2\mathcal{I}$ (keV)	a	Empirical data used to deduce assignment	References
0		1/2 +	1/2 + [631]	6.4	–0.40	α,γ, (d,p), (d,t), $(^3He,\alpha)$	a–d
160.0		5/2 +	5/2 + [622]	6.3		Fav.α,γ,τ, (d,p) (d,t), $(^3He,\alpha)$	a–d
274		7/2 –	7/2 – [743]	4.7		α,γ,τ, (d,t), $(^3He,\alpha)$	a,c,d
551	11/2	7/2 +	7/2 + [624]			(d,p), $(^3He,\alpha)$	b,d
668		3/2 +	3/2 + [631]			(d,t), $(^3He,\alpha)$	c,d
865		1/2 –	1/2 – [501]	~7	~0.8	(d,t), $(^3He,\alpha)$	c,d
946	9/2	5/2 +	5/2 + [633]			(d,t), $(^3He,\alpha)$	c,d
1110		1/2 +	1/2 + [620]			(d,p)	b
1126	9/2	7/2 +	7/2 + [613]			(d,p)	b
1259	15/2	5/2 –	5/2 – [752]			$(^3He,\alpha)$	d

[a] Ahmad *et al.* (1968); ^{241}Pu α decay.
[b] Braid *et al.* (1965); $^{236}U(d,p)$ reaction.
[c] Boyno *et al.* (1970); $^{238}U(d,t)$ reaction.
[d] Von Egidy *et al.* (1970); $^{238}U(^3He,\alpha)$ reaction.

TABLE XI. Intrinsic states of $^{239}_{92}U_{147}$.

$^{238}U(n,\gamma)$, $^{238}U(d,p)$ Bandhead energy (keV)	I	$K\pi$	$^{239}_{92}U_{147}$ Assigned character	$\hbar^2/2\mathcal{I}$ (keV)	a	Empirical data used to deduce assignment	References
0		5/2+	5/2 + [622]	6.1		(d,p), (n,γ)	a,b
133.7		1/2+	1/2 + [631]	6.8	−0.42	(d,p), (n,γ), $(d,p\gamma)$, τ	a–c
173		7/2+	7/2 + [624]	6.2		(d,p)	a
688		1/2+	1/2 + [620]	8.8	+0.07	(d,p), (n,γ)	a,b
726		3/2+	3/2 + [631]			(n,γ)	b
746		1/2−	1/2 − [750] [d]			(d,p), (n,γ)	a,b
815		1/2−	1/2 − [501]			(d,p), (n,γ)	a,b
853		3/2+	3/2 + [622]	7.0		(n,γ)	b

[a] Sheline *et al.* (1966); $^{238}U(d,p)$ reaction.
[b] Bollinger and Thomas (1972); $^{238}U(n,\gamma)$ reaction.
[c] Yates *et al.* (1975a); $^{238}U(d,p\gamma)$, τ.
[d] The 1/2 − [750] state is sometimes labeled as 1/2 − [761].

TABLE XII. Intrinsic states of $^{237}_{94}Pu_{143}$.

$^{241}Cm \xrightarrow{\alpha}$, 1/2+ [631] $^{238}Pu(d,t)$ $^{239}Pu(p,t)$ Bandhead energy (keV)	I	$K\pi$	$^{237}_{94}Pu_{143}$ Assigned character [d]	$\hbar^2/2\mathcal{I}$ (keV)	a	$\xleftarrow{EC}{}^{237}Am$, 5/2 − [523] Empirical data used to deduce assignment	References
0		7/2−	7/2 − [743]	5.3		γ-mult., (d,t)	a,b
145.6		1/2+	1/2 + [631]	6.2	−0.47	Fav. α, (d,t), (p,t)	a–c
280.2		5/2+	5/2 + [622]	5.8		γ-mult., EC(6.0), (d,t)	a,b
370.4		3/2+	3/2 + [631]	6.7		γ-mult., EC(7.3), (d,t)	a,b
407.8		5/2+	5/2 + [633]	4.4		γ-mult., EC(6.8), (d,t)	a,b
473.5		7/2+	7/2 + [624]			γ-mult., EC(6.7)	a
545		1/2−	1/2 − [501]			(d,t)	b
655.3		5/2−	5/2 − [752]	5.8		γ-mult., EC(7.2)	a
800		1/2+	{1/2 + [631] ⊗ 0+}			(p,t)	c
908.8		7/2+	7/2 + [613]A			γ-mult., EC(6.4)	a
1014		3/2−	3/2 − [501]B			(d,t)	b

[a] Ahmad *et al.* (1975b); ^{237}Am EC decay and ^{241}Cm α decay.
[b] Grotdal *et al.* (1973); $^{238}Pu(d,t)$ reaction.
[c] Friedman *et al.* (1974); $^{239}Pu(p,t)$ reaction.
[d] Comment: The 852 keV level observed by Grotdal *et al.* (1973) is most likely the 5/2+ member of the 1/2+ band at 800 keV.

TABLE XIII. Intrinsic states of $^{239}_{94}Pu_{145}$.

$^{243}Cm \xrightarrow{\alpha}$, 5/2 + [622] $^{239}Np \xrightarrow{\beta^-}$ 5/2 + [642] $^{238}Pu(d,p)$, $^{239}Pu(d,d')$ Bandhead energy (keV)	I	$K\pi$	$^{239}_{94}Pu_{145}$ Assigned character	$\hbar^2/2\mathcal{I}$ (keV)	a	$\xleftarrow{EC}{}^{239}Am$, 5/2 − [523] Empirical data used to deduce assignment	References
0		1/2+	1/2 + [631]	6.3	−0.58	I, μ, α, (d,p)	a–c
285.5		5/2+	5/2 + [622]	6.4		Fav. α, γ-mult., τ, β^-(7.1), EC(6.0), (d,p)	b–e
391.6		7/2−	7/2 − [743]			α, γ-mult., τ, β^-(6.3), EC(8.6), (d,p)	b–e
469.8		1/2−	1/2 − [501] + {1/2[631] ⊗ 0−}	5.0	+0.48	γ, (d,d')	c,f
511.8		7/2+	7/2 + [624]			γ-mult., EC(5.8)	e
1017		1/2−	1/2 − [750]B			(d,p)	c
1214		1/2+	1/2 + [620]B			(d,p)	c
1233	9/2	7/2+	7/2 + [613]B			(d,p)	c
1261		3/2+	3/2 + [622]B			(d,p)	c

[a] Faust *et al.* 1965; I,μ.
[b] Baranov *et al.* 1966; ^{243}Cm α decay.
[c] Grotdal *et al.* 1973; $^{238}Pu(d,p)$ and $^{239}Pu(d,d')$ reactions.
[d] Ewan *et al* (1959); $^{239}Np\beta^-$ decay.
[e] Porter *et al.* (1972); ^{239}Am EC decay.
[f] Davies and Hollander (1965); $^{239}Np\beta^-$ decay.
[g] Thompson *et al.* (1976); $^{239}Pu(d,d')$ reaction.

TABLE XIV. Intrinsic states of $^{241}_{94}Pu_{147}$.

$^{245}Cm \overset{\alpha}{\Rightarrow}$, 7/2 + [624]
$^{240}Pu(d,p)$, $^{242}Pu(d,t)$, $^{242}Pu(^3He,\alpha)$ $^{241}_{94}Pu_{147}$

Bandhead energy (keV)	I	$K\pi$	Assigned character	$\hbar^2/2\mathcal{I}$ (keV)	a	Empirical data used to deduce assignment	References
0		5/2+	5/2 + [622]	6.0		$I, \mu, \gamma, (d,p), (d,t), (^3He,\alpha)$	a–d,g
161.4		1/2+	1/2 + [631]			$(d,t\gamma), \tau, (d,p), (d,t), (^3He,\alpha)$	c–e
175.0		7/2+	7/2 + [624]	6.3		Fav. $\alpha, \gamma, (d,p), (d,t)$	b,f,g
570	15/2	7/2–	7/2 – [743]			$(d,p), (d,t), (^3He,\alpha)$	c,d
752		1/2+	1/2 + [620]*A*			$(d,p), (d,t)$	c
770	5/2	3/2+	3/2 + [631]*B*			$(d,p), (d,t)$	c
800	9/2	7/2+	7/2 + [613]*B*			$(d,p), (d,t)$	c
844		1/2–	1/2 – [501] +1/2 – [750]*B*			$(d,p), (d,t)$	c
936		3/2+	3/2 + [622]*B*			$(d,p), (d,t)$	c
967		1/2–	1/2 – [501]			$(d,p), (d,t)$	c,d

[a] Edelstein (1970); I, μ.
[b] Ahmad *et al.* (1976d); $^{245}Cm\ \alpha, \gamma$.
[c] Braid *et al.* (1972); $^{240}Pu(d,p)$ and $^{242}Pu(d,t)$ reactions.
[d] Elze and Huizenga (1971); $^{242}Pu(d,t)$ and $^{242}Pu(^3He,\alpha)$ reactions.
[e] Yates *et al.* (1975a); $^{242}Pu(d,t\gamma), \tau$.
[f] Friedman and Milsted (1966); $^{245}Cm\ \alpha$ decay.
[g] Baranov and Shatinskii (1975); $^{245}Cm\ \alpha$ decay.

TABLE XV. Intrinsic states of $^{243}_{94}Pu_{149}$.

$^{247}Cm \overset{\alpha}{\Rightarrow}$, 9/2 – [734]
$^{244}Pu(d,t)$, $^{242}Pu(d,p)$, $^{242}Pu(n,\gamma)$ $^{243}_{94}Pu_{149}$

Bandhead energy (keV)	I	$K\pi$	Assigned character	$\hbar^2/2\mathcal{I}$ (keV)	a	Empirical data used to deduce assignment	References
0		7/2+	7/2 + [624]	6.4		$^{243}Pu\beta^-$, $^{247}Cm\alpha$, (d,t)	a–c
287.4		5/2+	5/2 + [622]	6.5		α, γ-mult., $(n,\gamma), (d,p), (d,t)$	b,c
383.6		1/2+	1/2 + [631]	6.9	–0.58	$(d,t\gamma), \tau, (d,p), (d,t)$	c,d
402.4		9/2–	9/2 – [734]	4.6		Fav. $\alpha, (d,p), (d,t)$	b,c
625.6		1/2+	1/2 + [620]	7.0	+0.34	$(d,p), (d,t), (n,\gamma)$	c
626	9/2	7/2+	7/2 + [613]			(d,p)	c
703.9		3/2–	$\{7/2 + [624] \otimes 2^+\}_{3/2^-}$			(n,γ)	c
790.7		3/2–	1/2 – [750][e]	8.1	~–5.6	$(d,p), (n,\gamma)$	c
813.8		3/2+	3/2 + [622]	6.3		(d,p)	c
905.9		1/2–	1/2 – [501]	6.0 (assumed)	+1.4	(d,t)	c
981.1	5/2	3/2+	3/2 + [631]			$(d,p), (d,t)$	c
1044	11/2	9/2+	9/2 + [615]			(d,p)	c
1212.8		5/2–	5/2 – [503]			(d,t)	c

[a] Friedman *et al.* (1969); $^{243}Pu\beta^-$ decay.
[b] Fields *et al.* (1971); $^{247}Cm\ \alpha$ decay.
[c] Casten *et al.* (1976); $(d,p)(d,t), (n,\gamma)$.
[d] Yates *et al.* (1975a); $(d,t\gamma), \tau$.
[e] The 1/2 – [750] state is sometimes labeled as 1/2 – [761].

TABLE XVI. Intrinsic states of $^{245}_{94}Pu_{151}$.

$^{244}Pu(d,p)$ $^{245}_{94}Pu_{151}$

Bandhead energy (keV)	I	$K\pi$	Assigned character	$\hbar^2/2\mathcal{I}$ (keV)	a	Empirical data used to deduce assignment	References
220[a]	15/2	9/2–	9/2 – [734]			(d,p)	b
249	9/2	5/2+	5/2 + [622]*B*			(d,p)	b
309	1/2	1/2+	1/2 + [620]*A*			(d,p)	b
328	9/2	7/2+	7/2 + [613]*A*			(d,p)	b
578	3/2	3/2+	3/2 + [622]*A*			(d,p)	b
640[c]	3/2	1/2–	1/2 – [750]*A*			(d,p)	b
805	11/2	9/2+	9/2 + [615]*A*			(d,p)	b

[a] The energy of the 15/2 member of 9/2 – [734] band was assumed at 220 keV, from analogy to levels of ^{249}Cf (Ahmad *et al.*, 1976b). All other energies were measured relative to this energy.
[b] Erskine *et al.* (1976); $^{244}Pu(d,p)$ reaction.
[c] The 1/2 – [750] state is sometimes labeled as 1/2 – [761].

TABLE XVII. Intrinsic states of $^{243}_{96}Cm_{147}$.

$^{244}Cm(d,t)$ Bandhead energy (keV)	I	$K\pi$	$^{243}_{96}Cm_{147}$ Assigned character	$\hbar^2/2\mathcal{I}$ (keV)	a	$\xleftarrow{EC}{}^{243}Bk, 3/2-[521]$ Empirical data used to deduce assignment	References
0		5/2+	5/2 + [622]	6.0		$I, \mu, (d,t)$	a,b
87.4		1/2+	1/2 + [631]			γ-mult., τ, (d,t)	b,c
133		7/2+	7/2 + [624]B			(d,t)	b
530	15/2	7/2−	7/2 − [743]B			(d,t)	b
729		1/2−	1/2 − [501]			(d,t)	b
798	5/2	3/2+	3/2 + [631]B			(d,t)	b
1136		5/2−	5/2 − [503]B			(d,t)	b

[a] Abraham *et al.* (1973); I, μ.
[b] Braid *et al.* (1971); (d,t) reaction.
[c] Yates *et al.* (1975a); γ-mult. and τ measurement.

TABLE XVIII. Intrinsic states of $^{245}_{96}Cm_{149}$.

$^{249}Cf \xRightarrow{\alpha}$, 9/2 − [734] $^{244}Cm(d,p)$, $^{246}Cm(d,t)$ $^{245}Am \xrightarrow{\beta^-}$, 5/2 + [642] Bandhead energy (keV)	I	$K\pi$	$^{245}_{96}Cm_{149}$ Assigned character	$\hbar^2/2\mathcal{I}$ (keV)	a	$\xleftarrow{EC}{}^{245}Bk, 3/2-[521]$ Empirical data used to deduce assignment	References
0		7/2+	7/2 + [624]	6.1		$I, \mu, (d,t), \beta^-(6.3)$	a–d
252.9		5/2+	5/2 + [622]	6.1		α, γ-mult., EC(6.9), $\beta^-(6.5)(d,p)$, (d,t)	b–f
356.0		1/2+	1/2 + [631]	6.6	−0.72	γ-mult., τ, EC(8.0), (d,p), (d,t)	e–g
388.2		9/2−	9/2 − [734]	5.0		α, γ-mult., (d,p), (d,t)	b,c,e
633.7		3/2−	$\{7/2 + [624] \otimes 2^-\}$	5.6		γ-mult., EC(6.9),	f
643.5		7/2−	7/2 − [743]	6.5		α, γ-mult., (d,t)	b,c,e
741.0		1/2+	1/2 + [620]	6.9	+0.36	γ-mult., EC(6.0), (d,p), (d,t)	e,f
782	9/2	7/2+	7/2 + [613]A			(d,p), (d,t)	c,e
908		3/2+	3/2 + [622]B			(d,p), (d,t)	e
913		1/2−	1/2 − [501]			(d,p), (d,t)	e
980[h]	3/2	1/2−	1/2 − [750]B			(d,p), (d,t)	e
995	5/2	3/2+	3/2 + [631]B			(d,p), (d,t)	e
1271		5/2−	5/2 − [503]B			(d,p), (d,t)	e

[a] Abraham *et al.* (1970); I, μ.
[b] Ahmad (1966); ^{249}Cf α decay.
[c] Baranov *et al.* (1973); ^{249}Cf α decay.
[d] Bunker *et al.* (1967); $^{245}Am\beta^-$ decay.
[e] Braid *et al.* (1971); (d,p), (d,t) reactions.
[f] Ahmad *et al.* (1976a); ^{245}Bk EC decay.
[g] Yates *et al.* (1975a); τ measurement.
[h] The 1/2 − [750] state is sometimes labeled as 1/2 − [761].

TABLE XIX. Intrinsic states of $^{247}_{96}Cm_{151}$.

$^{251}Cf \xRightarrow{\alpha}$, 1/2 + [620] $^{246}Cm(d,p)$, $^{248}Cm(d,t)$ Bandhead energy (keV)	I	$K\pi$	$^{247}_{96}Cm_{151}$ Assigned character	$\hbar^2/2\mathcal{I}$ (keV)	a	Empirical data used to deduce assignment	References
0		9/2−	9/2 − [734]	5.6		$I, \mu, (d,t), \gamma$	a–d
227		5/2+	5/2 + [622]	6.2		α, γ-mult., τ, (d,p), (d,t)	b–d
285.0		7/2+	7/2 + [624]	6.3		α, γ, (d,t)	b–d
403.6		1/2+	1/2 + [620]	6.6	+0.52	Fav. α, γ-mult., (d,p), (d,t)	b–d
439	9/2	7/2+	7/2 + [613]B			(d,p), (d,t)	b
506		1/2+	1/2 + [631]A			(d,t)	b
668		3/2+	3/2 + [622]B	6.2		(d,p), (d,t)	b
687	11/2	9/2+	9/2 + [615]B			(d,p), (d,t)	b
784	3/2	1/2−	1/2 − [750]B			(d,p)	b
958		1/2−	1/2 − [501]A			(d,t)	b
1079	5/2	3/2+	3/2 + [631]B			(d,t)	b
1283		5/2−	5/2 − [503]B			(d,t)	b

[a] Abraham *et al.* (1973); I, μ.
[b] Braid *et al.* (1971); (d,p), (d,t) reactions.
[c] Chetham-Strode *et al.* (1968); ^{251}Cf α decay.
[d] Browne and Asaro (1969); ^{251}Cf α decay.

TABLE XX. Intrinsic states of $^{249}_{96}Cm_{153}$.

$^{248}Cm(d,p)$ Bandhead energy (keV)	I	$K\pi$	$^{249}_{96}Cm_{153}$ Assigned character	$\hbar^2/2\mathcal{I}$ (keV)	a	Empirical data used to deduce assignment	References
0		1/2+	1/2 + [620]	6.5	+0.29	(d,p)	a
110	9/2	7/2+	7/2 + [613]			(d,p)	a
208		3/2+	3/2 + [622]A	6.8		(d,p)	a
220		9/2+	9/2 + [615]B			(d,p)	a
469 [b]	3/2	1/2−	1/2 − [750]A			(d,p)	a

[a] Braid *et al.* (1971); $^{248}Cm(d,p)$.
[b] The 1/2 − [750] state is sometimes labeled as 1/2 − [761].

TABLE XXI. Intrinsic states of $^{247}_{98}Cf_{149}$.

$^{251}Fm \xrightarrow{\alpha}$, 9/2 − [734] Bandhead energy (keV)	I	$K\pi$	$^{247}_{98}Cf_{149}$ Assigned character	$\hbar^2/2\mathcal{I}$ (keV)	a	Empirical data used to deduce assignment	References
0		7/2+	7/2 + [624]	6.1		α,γ-mult.	a
383.2		5/2+	5/2 + [622]	6.3		α,γ-mult.	a
480.4		9/2−	9/2 − [734]	4.7		Fav. α,γ-mult.	a
678.0		7/2−	7/2 − [743]	6.7		α,γ	a

[a] Ahmad *et al.* (1973a); ^{251}Fm α decay.

TABLE XXII. Intrinsic states of $^{249}_{98}Cf_{151}$.

$^{253}Fm \xrightarrow{\alpha}$, 1/2 + [620]
$^{249}Cf(d,d')$, 9/2 − [734]
$^{249}Bk \xrightarrow{\beta^-}$, 7/2 + [633]

Bandhead energy (keV)	I	$K\pi$	$^{249}_{98}Cf_{151}$ Assigned character	$\hbar^2/2\mathcal{I}$ (keV)	a	$\xleftarrow{EC}\ ^{249}Es$, 7/2 + [633] Empirical data used to deduce assignment	References
0		9/2−	9/2 − [734]	5.7		Fav. α, EC(6.7), α	a–c
145.0		5/2+	5/2 + [622] [e]	6.1		γ-mult., τ, EC(7.3), (d,d')	b–d
379.5		7/2+	7/2 + [624]	6.5		γ-mult., EC(6.2)	b
416.6		1/2+	1/2 + [620]	5.9	+0.32	Fav. α,γ-mult.	c
443.0		7/2+	7/2 + [613]			γ-mult., EC(7.2)	b
551		1/2+	1/2 + [631]A			α	c
668		13/2−	{9/2 − [734] ⊗ 2+}	5.5		(d,d')	d
813.2		5/2−	{9/2 − [734] ⊗ 2+}	5.6		γ-mult., EC(6.3), (d,d')	b,d
920		11/2+	{9/2 − [734] ⊗ 1−}	5.5		(d,d')	d
1007.9		9/2+	9/2 + [615]			γ-mult., EC(6.6)	b
1063		13/2+	{9/2 − [734] ⊗ 2−}	5.4		(d,d')	d
1078		15/2+	{9/2 − [734] ⊗ 3−}	5.9		(d,d')	d
1218.5		7/2−	{3/2 + [622] ⊗ 2−} [f]			γ-mult., EC(5.5)	b
1415		7/2+	{9/2 − [734] ⊗ 1−}	5.7		(d,d')	d

[a] Ahmad (1966); ^{249}Cf α decay.
[b] Ahmad *et al.* (1976b); ^{249}Es EC decay.
[c] Ahmad *et al.* (1967); ^{253}Fm α decay.
[d] Yates *et al.* (1975b); $^{249}Cf(d,d')$.
[e] Large vibrational admixture.
[f] In the ^{249}Es EC decay the three-quasiparticle component {p[633] 7/2+; p[521] 3/2−; n[622] 3/2+} of this particle-plus-phonon state was identified.

TABLE XXIII. Intrinsic states of $^{251}_{98}Cf_{153}$.

$^{255}Fm \xrightarrow{\alpha}$, 7/2 + [613] Bandhead energy (keV)	I	$K\pi$	$^{251}_{98}Cf_{153}$ Assigned character	$\hbar^2/2\mathcal{I}$ (keV)	a	$\xleftarrow{EC}\ ^{251}Es, 3/2-[521]$ Empirical data used to deduce assignment	References
0		1/2+	1/2 + [620]	6.4	+0.285	γ-mult., EC(6.2)	a
106.3		7/2+	7/2 + [613]	6.7		Fav. α, γ-mult., τ	b
177.6		3/2+	3/2 + [622]	6.8		α, γ-mult., EC(~5.7)	a,b
370.4		11/2−	11/2 − [725]			α, γ-mult., τ	b,c
434.2		9/2−	9/2 − [734]			α, γ-mult.	b,c
544.1		5/2+	5/2 + [622]	6.6		α, γ-mult.	b,c

[a] Ahmad *et al.* (1970); ^{251}Es EC decay.
[b] Ahmad *et al.* (1971); ^{255}Fm α decay and γ.
[c] Ahmad and Milsted (1975a); ^{255}Fm α decay.

TABLE XXIV. Intrinsic states of $^{253}_{98}Cf_{155}$.

$^{257}Fm \xrightarrow{\alpha}$, 9/2 + [615] Bandhead energy (keV)	I	$K\pi$	$^{253}_{98}Cf_{155}$ Assigned character	$\hbar^2/2\mathcal{I}$ (keV)	a	Empirical data used to deduce assignment	References
0		7/2+	7/2 + [613]	6.8		γ-mult.	a,b
241.0		9/2+	9/2 + [615]	7.6		Fav. α	a,b

[a] Asaro and Perlman (1967); ^{257}Fm α decay.
[b] Ahmad *et al.* (1976d); ^{257}Fm α decay.

TABLE XXV. Intrinsic states of $^{251}_{100}Fm_{151}$.

$^{255}No \xrightarrow{\alpha}$, 1/2 + [620] Bandhead energy (keV)	I	$K\pi$	$^{251}_{100}Fm_{151}$ Assigned character	$\hbar^2/2\mathcal{I}$ (keV)	a	Empirical data used to deduce assignment	References
0		9/2−	9/2 − [734]				a–c
190		5/2+	5/2 + [622]B				b,c
550		1/2+	1/2 + [620]B				b,c

[a] Ahmad *et al.* (1973a); ^{251}Fm α decay.
[b] Eskola *et al.* (1970); ^{255}No α decay.
[c] Dittner *et al.* (1971); ^{255}No α decay.

TABLE XXVI. Intrinsic states of $^{231}_{91}Pa_{140}$.

$^{235}Np \xrightarrow{\alpha}$, 5/2 + [642]
$^{231}Th \xrightarrow{\beta^-}$, 5/2 + [633]
$^{230}Th(\alpha, t)$

Bandhead energy (keV)	I	$K\pi$	$^{231}_{91}Pa_{140}$ Assigned character	$\hbar^2/2\mathcal{I}$ (keV)	a	Empirical data used to deduce assignment	References
0	3/2	1/2−	1/2 − [530]	6.2	−1.5	$I, \mu, (\alpha, t)$	a–d
102.3		3/2+	3/2 + [651]			$\alpha, \beta^-(5.6), \gamma$-mult., (α, t)	b–d
174.1		5/2−	5/2 − [523]	6.3		$\beta^-(6.8), \gamma$-mult., (α, t)	b–d
183.5		5/2+	5/2 + [642]			Fav. $\alpha, \beta^-(5.7), \gamma$-mult.	c,d
287		1/2+	1/2 + [400]A			(α, t)	b
320.2		3/2−	3/2 − [532]A			$\beta^-(6.8)$	d
604		3/2−	3/2 − [521]B			(α, t)	b

[a] Axe *et al.* (1961); I, μ.
[b] Erskine *et al.* (1975); ^{230}Th(α, t) reaction.
[c] Browne and Asaro (1973); ^{235}Np α decay and ^{231}Th β^- decay.
[d] Hornshøj *et al.* (1975); ^{231}Th β^- decay.

TABLE XXVII. Intrinsic states of $^{233}_{91}Pa_{142}$.

$^{237}Np \xrightarrow{\alpha}, 5/2+[642]$
$^{233}Th \xrightarrow{\beta^-}, 1/2+[631]$
$^{232}Th(^3He,d), ^{232}Th(\alpha,t)$

Bandhead energy (keV)	I	$K\pi$	$^{233}_{91}Pa_{142}$ Assigned character	$\hbar^2/2\mathcal{I}$ (keV)	a	Empirical data used to deduce assignment	References
0	3/2	1/2−	1/2−[530]	5.9	−1.38	$I,\mu,\beta^-(5.9),(^3He,d),(\alpha,t)$	a–c
94.7		3/2+	3/2+[651]			$\alpha,\beta^-(6.5),\gamma$-mult., $(^3He,d),(\alpha,t)$	b–d
169.4		1/2+	1/2+[400][e]			$\alpha,\beta^-(\sim 7),\gamma$-mult., $(^3He,d),(\alpha,t)$	b–d
238.0		5/2+	5/2+[642]			Fav. α,γ-mult., $(^3He,d),(\alpha,t)$	c,d
298		5/2−	5/2−[523]A			$(^3He,d),(\alpha,t)$	c
670		3/2−	3/2−[521]			$(^3He,d),(\alpha,t)$	c

[a] Marrus *et al.* (1961); I,μ.
[b] Hoekstra and Wapstra (1969); $^{233}Th\ \beta^-$ decay.
[c] Elze and Huizenga (1975); $^{232}Th(^3He,d)$, $^{232}Th(\alpha,t)$ reactions.
[d] Browne and Asaro (1968); $^{237}Np\ \alpha$ decay.
[e] In Refs. b and c this state has been assigned to the 1/2+[660] orbital.

TABLE XXVIII. Intrinsic states of $^{235}_{93}Np_{142}$.

$^{239}Am \xrightarrow{\alpha}, 5/2-[523]$
$^{237}Np(p,t)$

Bandhead energy (keV)	I	$K\pi$	$^{235}_{93}Np_{142}$ Assigned character	$\hbar^2/2\mathcal{I}$ (keV)	a	$\xleftarrow{EC}\ ^{235}Pu, 5/2+[633]$ Empirical data used to deduce assignment	References
0		5/2+	5/2+[642]	4.9		$(p,t),\alpha$	a–c
49.0		5/2−	5/2−[523]	6.1		Fav. α,γ-mult., τ	a,b
756.4		3/2−	3/2−[521]B	4.6		EC	b
834	5/2	5/2+	$\{5/2+[642]\otimes 0+\}A$			(p,t)	c
260	5/2	5/2+				(p,t)	c

[a] Gorman and Asaro (1971); $^{239}Am\ \alpha$ decay and ^{235}Pu EC decay.
[b] Jäger *et al.* (1973); ^{235}Pu EC decay.
[c] Friedman *et al.* (1974); $^{237}Np(p,t)$ reaction.

TABLE XXIX. Intrinsic states of $^{237}_{93}Np_{144}$.

$^{241}Am \xrightarrow{\alpha}, 5/2-[523]$
$^{237}U \xrightarrow{\beta^-}, 1/2+[631]$
$^{237}Np(d,d')$

Bandhead energy (keV)	I	$K\pi$	$^{237}_{93}Np_{144}$ Assigned character	$\hbar^2/2\mathcal{I}$ (keV)	a	$\xleftarrow{EC}\ ^{237}Pu,\ 7/2-[743]$ Empirical data used to deduce assignment	References
0		5/2+	5/2+[642]	4.7		I,μ,α, EC(~6.8)	a–f
59.5		5/2−	5/2−[523]	6.2		Fav. α,γ-mult., τ, EC(~6.8)	b–f
281.4		1/2−	1/2−[530]	6.7	−1.69	$\beta^-(6.5),\gamma$-mult.	e,f
332.4		1/2+	1/2+[400]	6.2	+1.08	$\beta^-(7.3),\gamma$-mult.	e
516		3/2−	3/2−[521]	5.8		(d,d')	f,g
721.9		5/2−	$\{5/2-[523]\otimes 0+\}$ $+\{5/2+[642]\otimes 0-\}$	4.9		α,γ-mult., (d,d')	d,g

[a] Hutchison and Weinstock (1960); Lewis *et al.* (1970); I,μ.
[b] Baranov *et al.* (1964); $^{241}Am\ \alpha$ decay.
[c] Hoffman and Dropesky (1958); ^{237}Pu EC decay.
[d] Lederer *et al.* (1966); $^{241}Am\ \alpha$ and γ decays.
[e] Yamazaki and Hollander (1966); $^{237}U\ \beta^-$ decay.
[f] Elze and Huizenga (1970b); $^{236}U(\alpha,t)$ and $^{236}U(^3He,d)$ reactions.
[g] Thompson *et al.* (1976); $^{237}Np(d,d')$ reaction.

TABLE XXX. Intrinsic states of $^{239}_{93}Np_{146}$.

$^{243}Am \xrightarrow{\alpha}, 5/2-[523]$
$^{239}U \xrightarrow{\beta^-}, 5/2+[622]$
$^{238}U(^3He,d), ^{238}U(\alpha,t)$

$^{239}_{93}Np_{146}$

Bandhead energy (keV)	I	$K\pi$	Assigned character	$\hbar^2/2\mathcal{I}$ (keV)	a	Empirical data used to deduce assignment	References
0		5/2+	5/2+[642]	4.4		$I,\alpha,\gamma,\beta^-(6.7),(\alpha,t)$	a–g
74.6		5/2−	5/2−[523]	6.2		Fav. α,γ-mult., τ, $(^3He,d),(\alpha,t)$	b–g
271		1/2−	1/2−[530]			$\alpha,(^3He,d),(\alpha,t)$	b,e,f
450		3/2−	3/2−[521]			$(^3He,d),(\alpha,t)$	e

[a] Hubs and Marrus (1958); I.
[b] Baranov *et al.* (1964); ^{243}Am α decay.
[c] Van Hise and Engelkemeir (1968); ^{243}Am α,γ decays.
[d] Engelkemeir (1969); ^{243}Am α, ce^- decays.
[e] Von Egidy *et al.* (1975); $^{238}U(^3He,d)$, $^{238}U(\alpha,t)$ reactions.
[f] Lederer *et al.* (1966); ^{243}Am α,γ decays.
[g] Blinowska *et al.* (1964); ^{239}U β^- decay.

TABLE XXXI. Intrinsic states of $^{239}_{95}Am_{144}$.

$^{243}Bk \xrightarrow{\alpha}, 3/2-[521]$

$^{239}_{95}Am_{144}$

Bandhead energy (keV)	I	$K\pi$	Assigned character	$\hbar^2/2\mathcal{I}$ (keV)	a	Empirical data used to deduce assignment	References
0		5/2−	5/2−[523]	5.8		^{239}Am EC decay, α	a,b
187		5/2+	5/2+[642]	4.7		α,γ-mult.	b
558		3/2−	3/2−[521]	5.8		Fav. α,γ-mult.	b

[a] Porter *et al.* (1972); ^{239}Am EC decay.
[b] Ahmad (1966); ^{243}Bk α decay.

TABLE XXXII. Intrinsic states of $^{241}_{95}Am_{146}$.

$^{245}Bk \xrightarrow{\alpha}, 3/2-[521]$
$^{240}Pu(\alpha,t)$
$^{241}Pu \xrightarrow{\beta^-}, 5/2+[622]$

$^{241}_{95}Am_{146}$

$\xleftarrow{EC}{}^{241}Cm, 1/2+[631]$

Bandhead energy (keV)	I	$K\pi$	Assigned character	$\hbar^2/2\mathcal{I}$ (keV)	a	Empirical data used to deduce assignment	References
0		5/2−	5/2−[523]	5.9		$I,\mu,(\alpha,t),(p,t),\beta^-(5.8)$	a–d
205.9		5/2+	5/2+[642]	4.3		γ-mult., (α,t)	b,c
471.8		3/2−	3/2−[521]	6.5		Fav. α,γ-mult., EC(7.7), (α,t)	b,c
623.1		1/2+	1/2+[400]	6.0 (assumed)	+0.7	γ-mult., EC(8.0), (α,t)	b,c
652.1		1/2−	1/2−[530]	6.0 (assumed)	−1.8	γ-mult., EC(6.2), (α,t)	b,c
670.2		3/2+	3/2+[651]A			γ-mult., EC(7.7)	b
822	13/2	7/2+	7/2+[633]A			(α,t)	c
952		5/2−	$\{5/2-[523]\otimes 0+\}A$			(p,t)	d
1163	9/2	7/2−	7/2−[514]B			(α,t)	c

[a] Armstrong and Marrus (1966); I,μ.
[b] Porter *et al.* (1974); ^{245}Bk α decay and ^{241}Cm EC decay.
[c] Erskine *et al.* (1975); (α,t) reaction.
[d] Friedman *et al.* (1974); $^{243}Am(p,t)$ reaction.

TABLE XXXIII. Intrinsic states of $^{243}_{95}Am_{148}$.

$^{247}Bk \xrightarrow{\alpha}, 3/2-[521]$
$^{243}Pu \xrightarrow{\beta^-}, 7/2+[624]$
$^{242}Pu(^3He,d), ^{242}Pu(\alpha,t)$

Bandhead energy (keV)	I	$K\pi$	$^{243}_{95}Am_{148}$ Assigned character	$\hbar^2/2\mathcal{I}$ (keV)	a	Empirical data used to deduce assignment	References
0		5/2−	5/2−[523]	6.0		$I,\mu,\beta^-(6.1)$, $(^3He,d),(\alpha,t)$	a–d
84.0		5/2+	5/2+[642]	3.6		γ-mult., $\tau,\beta^-(6.1),(^3He,$, (α,t)	b–d
267.0		3/2−	3/2−[521]	6.2		Fav. $\alpha,(^3He,d),(\alpha,t)$	b,d
465.7		7/2+	7/2+[633]	7.4		γ-mult., $\beta^-(5.5)(^3He,d),(\alpha,t)$	b–d
977	9/2	7/2−	7/2−[514]			$(^3He,d),(\alpha,t)$	d

[a] Armstrong and Marrus (1966); Manning *et al.* (1956); I,μ.
[b] Friedman *et al.* (1969); $^{243}Pu\ \beta^-$ decay.
[c] Hoffman *et al.* (1969); $^{243}Pu\ \beta^-$ decay.
[d] Elze and Huizenga (1970a); $(^3He,d)$, (α,t) reactions.

TABLE XXXIV. Intrinsic states of $^{245}_{95}Am_{150}$.

$^{249}Bk \xrightarrow{\alpha}, 7/2+[633]$
$^{245}Pu \xrightarrow{\beta^-}, 9/2-[734]$

Bandhead energy (keV)	I	$K\pi$	$^{245}_{95}Am_{150}$ Assigned character [d]	$\hbar^2/2\mathcal{I}$ (keV)	a	Empirical data used to deduce assignment	References
0		5/2+	5/2+[642]	2.8		α,γ-mult.	a–c
28		5/2−	5/2−[523]	6.0		γ-mult.	b
154		3/2−	3/2−[521]	6.6		α	c
327.2		7/2+	7/2+[633]	7.6		Fav. $\alpha,\beta^-(7.3)$	a–c

[a] Ahmad (1966); $^{249}Bk\ \alpha$ decay.
[b] Daniels *et al.* (1968); $^{245}Pu\ \beta^-$ decay.
[c] Ahmad *et al.* (1976d); $^{249}Bk\ \alpha$ decay.
[d] Comment: There is strong Coriolis mixing between the 5/2+[642] and 7/2+[633] bands.

TABLE XXXV. Intrinsic states of $^{247}_{97}Bk_{150}$.

$^{246}Cm(\alpha,t)$
$^{251}Es \xrightarrow{\alpha}, 3/2-[521]$
$\xleftarrow{EC}\ ^{247}Cf, 7/2+[624]$

Bandhead energy (keV)	I	$K\pi$	$^{247}_{97}Bk_{150}$ Assigned character	$\hbar^2/2\mathcal{I}$ (keV)	a	Empirical data used to deduce assignment	References
0		3/2−	3/2−[521]	6.0		Fav. $\alpha,(\alpha,t)$	a
40.8		7/2+	7/2+[633]	4.7		$\alpha,(\alpha,t)$	a
334.9		5/2+	5/2+[642]			EC, γ-mult.	a
447.8		5/2−	5/2−[523]	5.8		EC, (α,t)	a,b
487		1/2+	1/2+[400]*A*	6.0 (assumed)	+0.7	(α,t)	b
704		1/2−	1/2−[521]	6.0	+0.7	(α,t)	b
904	9/2	7/2−	7/2−[514]*A*			(α,t)	b

[a] Ahmad *et al.* (1976c); ^{247}Cf EC decay and $^{251}Es\ \alpha$ decay.
[b] Ahmad *et al.* (1977); $^{246}Cm(\alpha,t)$ reaction.

TABLE XXXVI. Intrinsic states of $^{249}_{97}Bk_{152}$.

$^{253}Es \xrightarrow{\alpha}$, 7/2 + [633]
$^{249}Cm \xrightarrow{\beta^-}$, 1/2 + [620]
$^{248}Cm(^3He,d)$, $^{248}Cm(\alpha,t)$

Bandhead energy (keV)	I	$K\pi$	Assigned character	$\hbar^2/2\mathcal{I}$ (keV)	a	Empirical data used to deduce assignment	References
0		7/2+	7/2 + [633]	4.6		I,μ, Fav. α, $(^3He,d)$, (α,t)	a–d
8.8		3/2–	3/2 – [521]	6.2		$\alpha,\gamma,\beta^-(5.9)(^3He,d),(\alpha,t)$	b–f
377.6		1/2+	1/2 + [400]A	6.6	+0.67	β^-,γ-mult., $(^3He,d)$, (α,t)	c,e,f
389.2		5/2+	5/2 + [642]	5.7		α,γ-mult., (α,t)	b–d
569.2		1/2–	1/2 – [530]A	6.0 (assumed)	–1.6	$\beta^-(\sim 7),\gamma$-mult., $(^3He,d)$, (α,t)	c,e,f
621.9	9/2	5/2–	5/2 – [523]A			$(\alpha,t),(^3He,d),\alpha,\gamma$	c,f
643.2		1/2–	1/2 – [521]A [g]	6.0 (assumed)	+0.02	$\beta^-(5.9),\gamma$-mult.	e,f
750.7	9/2	7/2–	7/2 – [514]A			$(^3He,d),(\alpha,t),\alpha,\gamma$	e,f
1229	13/2	9/2+	9/2 + [624]A			$(^3He,d),(\alpha,t)$	c

[a] Boatner *et al.* (1972); I,μ.
[b] Ahmad and Milsted (1975a); ^{253}Es α decay.
[c] Erskine *et al.* (1975); $^{248}Cm(^3He,d)$, $^{248}Cm(\alpha,t)$ reaction.
[d] Holtz and Hollander (1970); γ ray with ^{253}Es α decay.
[e] Hoff *et al.* (1971); ^{249}Cm β^- decay.
[f] Hoff (1975); ^{249}Cm β^- decay.
[g] Anomalous decoupling parameter.

IV. DISCUSSION

A. Extracted single-particle level spacings and occupation probabilities

Within the context of the pairing force model, we can deduce the true single-particle level spacings from the experimentally observed single-particle excitations. The method we use is as follows: (1) assume a single-particle spectrum; (2) calculate the excitation spectrum, with blocking taken into account for each configuration; (3) compare the calculated spectrum with the experimentally determined level spacings; (4) change the single-particle spectrum as suggested by this comparison. Steps 2, 3, and 4 are repeated until the calculated spectrum agrees with the observed one. The extracted level spacings obtained in this way do not include the effects of particle–hole interactions on the single-particle energy level shifts. As we have shown in Sec. II.B.2.b., these effects are smaller than suggested by the calculations of Gareev *et al.* (1971).

Calculations of the extracted level spacings, with constant pairing matrix elements, have been carried out for most of the actinides (Braid *et al.*, 1965, 1970, 1971, 1972; Erskine *et al.*, 1975). These calculations give some large and sudden shifts of the single-particle level spacings that are not consistent with smooth changes in the nuclear deformation. This is particularly noticeable for the neutron orbitals that arise from $j_{15/2}$ in the spherical limit. In Figs. 15 and 16, we present the extracted single-particle level spacings for a representative set

TABLE XXXVII. Intrinsic states of $^{251}_{99}Es_{152}$.

$^{255}Md \xrightarrow{\alpha}$, 7/2 – [514]
$^{250}Cf(\alpha,t)$
$\xleftarrow{EC}$ ^{251}Fm, 9/2 – [734]

Bandhead energy (keV)	I	$K\pi$	Assigned character [e]	$\hbar^2/2\mathcal{I}$ (keV)	a	Empirical data used to deduce assignment	References
0		3/2–	3/2 – [521]	6.3		^{251}Es EC decay, (α,t)	a,d
8.3		7/2+	7/2 + [633]	5.3		EC(6.7), (α,t)	b,d
411		1/2–	1/2 – [521]	6.8	+1.0	(α,t)	d
461.4		7/2–	7/2 – [514]			Fav. α, EC(7.7), γ-mult.	b,c,d
777.9		9/2+	9/2 + [624]A			EC(8.0), γ-mult.	b
889.1		11/2+	{7/2 + [633] ⊗ 2+}	5.2		EC(7.9), γ-mult.	b
1238.9		11/2+	{n9/2 – [734]; n1/2 + [620]; p3/2 – [521]}			EC(6.0), γ-mult.	b
1264.9		11/2+	three-quasiparticle state			EC(6.1), γ-mult.	b

[a] Ahmad *et al.* (1970); ^{251}Es EC decay.
[b] Ahmad *et al.* (1973b); ^{251}Fm EC decay.
[c] Ahmad *et al.* (1976c); ^{255}Md α decay.
[d] Ahmad *et al.* (1977); $^{250}Cf(\alpha,t)$ reaction.
[e] The 1265 keV level has not been given a definite assignment.

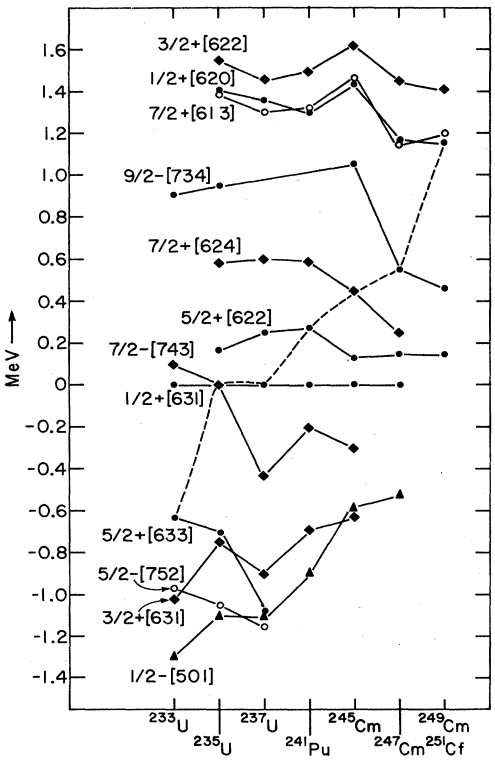

FIG. 15. Extracted neutron single-particle energies as determined with constant pairing matrix elements. The dashed line connects ground states.

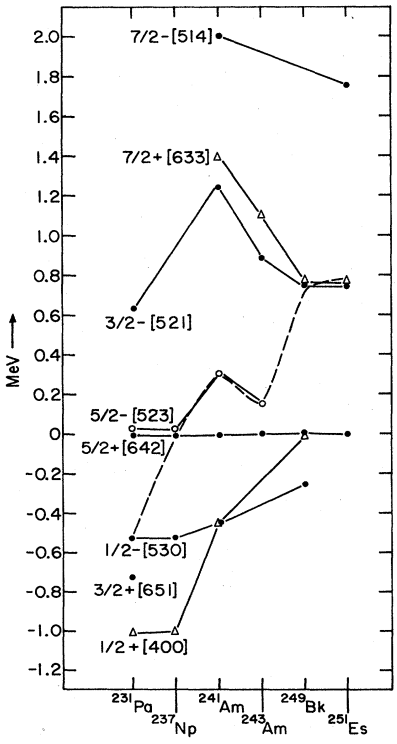

FIG. 16. Extracted proton single-particle energies as determined with constant pairing matrix elements. The dashed line connects ground states.

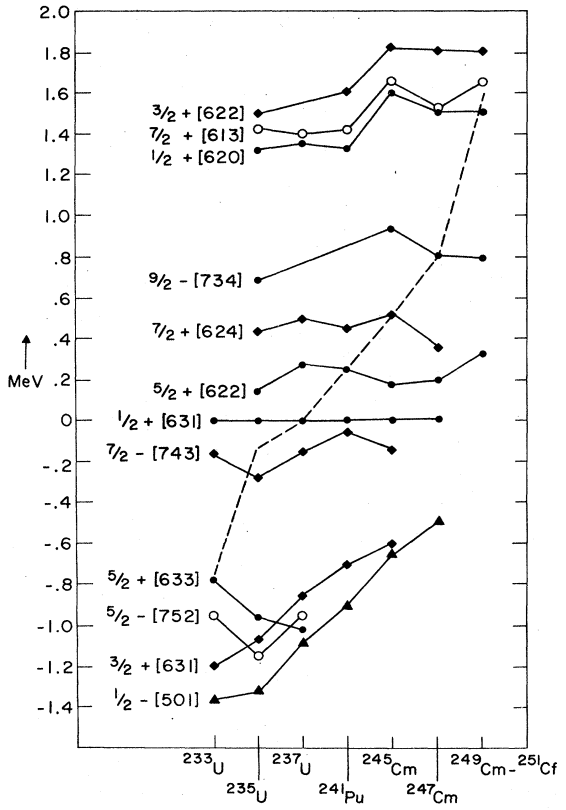

FIG. 17. Extracted neutron single-particle energies as determined with pairing matrix elements obtained from density-dependent delta interaction. The dashed line connects ground states.

of odd-neutron and odd-proton actinides, as calculated with the pairing constants of Eq. (2.32). This set includes the best studied nuclide for each odd value of N and Z.

We have also determined the extracted single-particle spectra for the same nuclides, using pairing matrix elements calculated with a density-dependent delta interaction (Chasman, 1976). These extracted level spacings are shown in Figs. 17 and 18. In contrast to the spacings obtained with constant pairing matrix elements, the level spacings obtained with this set of pairing interaction matrix elements can, on the whole, be well explained in terms of reasonable shifts in the deformation parameters of the central potential.

In Appendix B, we have tabulated the occupation probabilities $\langle N_K \rangle (V_K^2$ in the BCS theory) for all of the single-particle configurations indicated in the figures, using both types of matrix elements discussed above. The interesting feature is the similarity of the two sets of occupation probabilities, with the exception of the $j_{15/2}$ orbitals mentioned above.

We have explicitly taken into account the energy shifts of the $\frac{5}{2}+[622]$ and the $\frac{9}{2}-[734]$ orbitals in ^{247}Cm and ^{249}Cm due to mutual interaction via the 2^- phonon. The magnitude of these shifts was estimated using experimentally observed configuration mixing coefficients (Yates *et al.*, 1975b).

The calculations of Gareev *et al.* (1971) suggest sev-

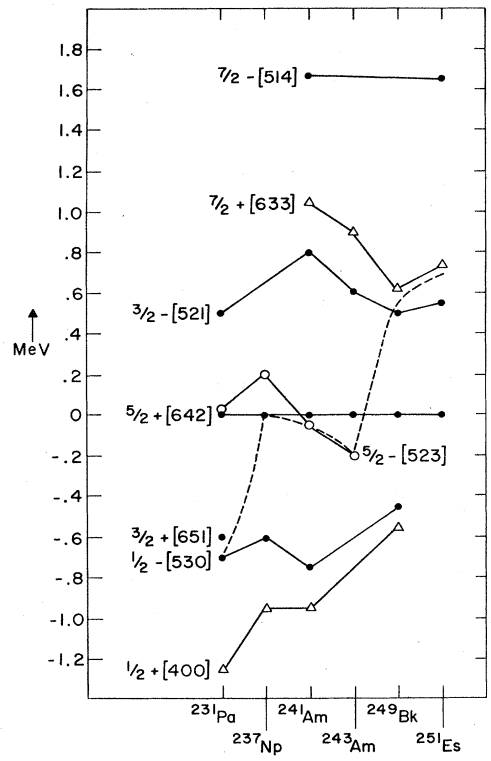

FIG. 18. Extracted proton single-particle energies as determined with pairing matrix elements obtained from density-dependent delta interaction. The dashed line connects ground states.

eral other instances, as well, where anomalies in the level spacings may be due to particle–hole interactions. Specifically, the low extracted energies of the neutron orbitals $\frac{1}{2}+[620]$ and $\frac{3}{2}+[622]$ in the light actinides (Fig. 17) are explained in terms of interactions with the configurations $\frac{5}{2}+[622]\otimes 2^+$ and $\frac{7}{2}+[624]\otimes 2^+$, respectively.

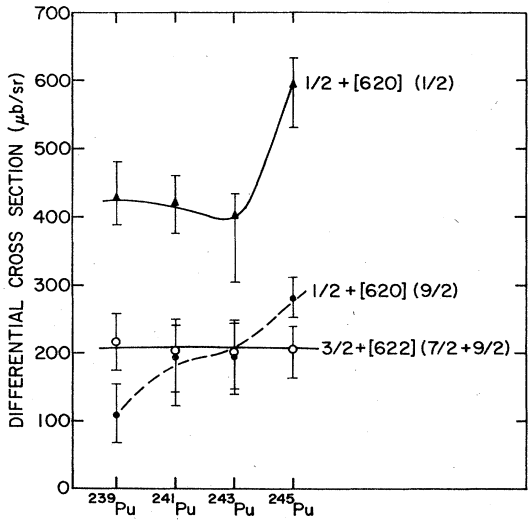

FIG. 19. Summed differential cross sections at 90° and 140° for (d,p) reactions populating levels of the 1/2 +[620] and 3/2 +[622] bands in ^{239}Pu, ^{241}Pu, ^{243}Pu, and ^{245}Pu.

This configuration interaction is expected to cause a decrease in the single-neutron transfer reaction cross section (Soloviev and Vogel, 1967). In Fig. 19, we have plotted the sum of differential cross sections at 90° and 140° for (d,p) reactions populating levels of the $\frac{1}{2}+[620]$ and $\frac{3}{2}+[622]$ bands in ^{239}Pu (Grotdal *et al.*, 1973), ^{241}Pu (Braid *et al.*, 1972), ^{243}Pu (Casten *et al.*, 1976), and ^{245}Pu (Erskine *et al.*, 1975). These summed cross sections to members of the $\frac{1}{2}+[620]$ band are roughly constant for ^{239}Pu–^{243}Pu and increase dramatically for ^{245}Pu. The sum of cross sections to the levels of the $\frac{3}{2}+[622]$ band is almost constant for all of the Pu isotopes. Since the Q value for these (d,p) reactions is essentially constant, we have not corrected for reaction mechanism effects. These results are at variance with the calculations of Gareev *et al.* (1971) and Komov *et al.* (1971); these calculations suggest a large increase in the cross sections of both the $\frac{1}{2}+[620]$ and $\frac{3}{2}+[622]$ orbital in going from ^{241}Pu to ^{243}Pu. The variations of the extracted single-particle level spacings in Fig. 17 also suggest that there is a marked increase in the purity of these two orbitals for the Pu isotopes heavier than ^{241}Pu. On this basis, we again expect the increase in (d,p) cross sections to occur in going from ^{241}Pu to ^{243}Pu, rather than between ^{243}Pu and ^{245}Pu. The situation in the Cm isotopes agrees better with our expectations, but the experimental data are rather fragmentary because many of the relevant peaks are unresolved doublets. The data of Braid *et al.* (1971) indicate that the $\frac{1}{2}+[620]$ orbital is equally pure in ^{245}Cm and ^{247}Cm. A measurement of the differential cross section for populating this orbital in the reaction ^{242}Cm$(d,p)^{243}$Cm would be of particular interest.

The low extracted energy of the neutron orbital $\frac{3}{2}+[631]$ in the heavy actinides (Fig. 17) can be explained (Gareev *et al.*, 1971) in terms of interaction with the configuration $\frac{1}{2}+[631]\otimes 2^+$. Their calculations also suggest reasonable explanations for the low-lying $\frac{1}{2}-$ bands in ^{249}Bk, that are hard to characterize in terms of single-particle states.

On the whole, the particle–hole interaction calculations of the Dubna group give reasonable qualitative explanations for the energy shifts when the extracted level spacings obtained with the density-dependent pairing matrix elements are anomalous, but should not be considered quantitative.

B. Nuclear shapes

Many calculations and experiments have been done to determine the magnitudes of the deformations appropriate to actinide nuclides.

In the earliest calculations, sums of single-particle eigenvalues without the inclusion of pairing energies (Bohr, 1952; Hill and Wheeler, 1953; Moszkowski, 1955; Mottelson and Nilsson, 1959) or with pairing energies (Bès and Szymanski, 1961) were used to estimate the equilibrium quadrupole deformation. A condition of self-consistency between the potential shape and the density distribution at equilibrium was used by Kjallquist (1958) to deduce hexadecapole deformations. Harada (1964) used a minimization condition to estimate hexadecapole deformations.

In recent years, the equilibrium deformations of the

actinides have been calculated using the liquid drop model with shell corrections (Strutinsky, 1967). In this procedure, the liquid drop energy is calculated as a function of deformation for the value of Z and A of interest. In addition, a shell correction term which depends on the single-particle level density at the Fermi level for each deformation is added to the liquid drop energy. This shell correction term is the difference between the sum of the actual single-particle eigenvalues and the single-particle energy of an appropriately smoothed level density. The equilibrium deformation is determined by the minimum in the total energy. Early calculations were carried out with this technique, using both the modified oscillator potential (Arseniev *et al.*, 1968; Nilsson *et al.*, 1969) and the Woods–Saxon potential (Gareev *et al.*, 1969). Recent calculations done with this method (Pauli, 1973; Møller *et al.*, 1974; Brack *et al.*, 1974; Seeger and Howard, 1975), using both modified oscillator and Woods–Saxon potentials, are in good agreement with each other. An interesting feature of the calculation of Møller *et al.* (1974) is the study of the sensitivity of the calculated equilibrium deformation to the details of the liquid drop model. They find that β_2 is relatively insensitive to these assumptions, but β_4 shows variations of ~0.02. The equilibrium deformations have also been calculated using a many-body interaction in a self-consistent calculation (Quentin, 1973; Kolb *et al.*, 1974), as well as with wave functions that are not self-consistent (Ko *et al.*, 1974).

Another way of obtaining information about the deformation of the potential is by comparing the experimental single-particle level spacings with those calculated at various deformations. However, residual interaction effects must first be taken into account before such comparisons can be made. Calculations by Chasman (1976), discussed in Sec. IV.A, have been used to deduce deformation parameters in this way.

An experimental approach to the problem is through Coulomb excitation or inelastic scattering experiments. Measurements of the Coulomb excitation probability (Bemis *et al.*, 1973) may be related to the multipole moments of the nuclear charge distribution through the rigid rotor relation [Bohr and Mottelson, 1975 (Chap. 4)],

$$B(E, 0 \rightarrow \lambda) = [(2\lambda + 1)/16\pi]\, Q_{\lambda 0}^2 . \tag{4.1}$$

In practice, the analysis of these experiments is complicated by competing modes of level population; e.g., it is sometimes hard to determine $B(E4, 0 \rightarrow 4)$ because of the competing process of double $E2$ excitation. The information obtained in this way on the moments $Q_{\lambda 0}$ can in turn be used to infer the shape of the nuclear charge density. There is a serious caveat here (Bemis *et al.*, 1973): the shape of the radial density distribution must be specified, since changes in the radial distribution give large changes in the inferred deformations.

A few measurements involving light ion scattering (Hendrie, 1973; Moss *et al.*, 1971) and μ mesonic x-ray shifts (Davidson *et al.*, 1974) have been done in the actinides to determine deformations. In the case of light ion scattering, the interactions are nuclear and take place at the nuclear surface. Coulomb effects are secondary. The results obtained in these experiments are related to the moments of the mass distribution at the nuclear surface. The mesonic x-ray experiments are sensitive to the nuclear charge distribution in two different ways. There is a level shift due to the extended charge distribution and a level splitting due to the fact that the quadrupole and hexadecapole moments of the nuclear charge distribution destroy the spherical symmetry of the central field. In the case of the mesonic x-ray experiments, one must also make assumptions about the radial density distribution of the charge, in order to make inferences about the deformation parameters. There are some large discrepancies between the various "measured" deformations that are not understood. A part of these discrepancies may arise from inadequacies in the coupled-channel analysis used to derive deformation parameters, or from higher-order effects not explicitly considered.

Brack *et al.* (1974) have used the experimentally determined multipole moments directly as a test of their calculated equilibrium deformations. The parameter r_0 in the potential is adjusted to get a best overall fit to the measured quadrupole moments. Fixing this single parameter also tests the calculated β_4 equilibrium deformation, if the measured hexadecapole moments are available. Brack *et al.* (1974) found excellent agreement between all the measured values of the quadrupole moments and the values calculated with their wave functions. They also found good agreement with the measured hexadecapole moments, from mass 230 to mass 242. For higher masses, the experimental errors are extremely large. They noted that the proton density in the nuclear surface region is increased by Coulomb repulsion effects. Accordingly the magnitudes of the deformation parameters that they obtain are somewhat smaller than the values obtained with the Fermi distribution used by Bemis *et al.* (1973). Milner, Bemis, and McGowan (1976) have recently calculated β_2 and β_4 deformation parameters for ^{234}U using their measured transition moments (Bemis *et al.*, 1973) and a radial distribution of the proton density similar in shape to that given by Chasman (1976). They find that this modification of the radial distribution

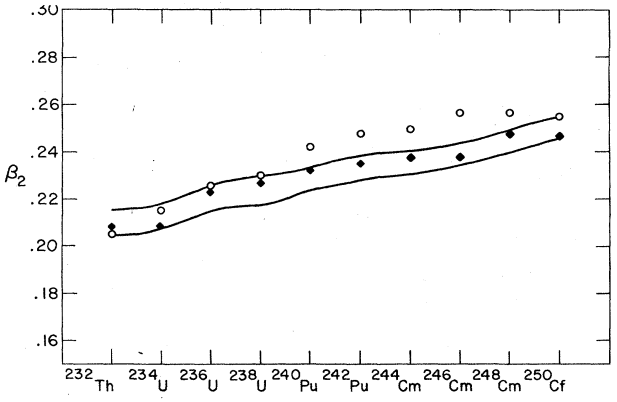

FIG. 20. Calculated values of β_2 in the actinides. The solid lines indicate the range of values of the equilibrium quadrupole deformations obtained in recent Strutinsky-type calculations. The diamonds indicate the values obtained by Brack *et al.* (1974) using the Strutinsky prescription, which give moments in agreement with the measured values of Bemis *et al.* (1973). The open circles indicate deformations inferred from extracted level spacings by Chasman (1976).

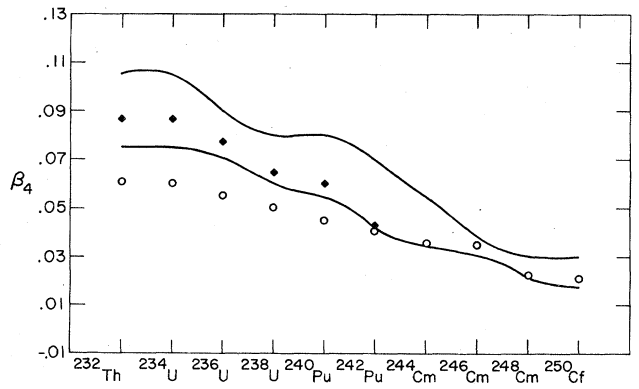

FIG. 21. Calculated values of β_4 in the actinides. See caption for Fig. 20 for details.

function reduces the calculated value of β_2 by ~10% and β_4 by ~15% from the values estimated with a deformed Fermi distribution. A small increase of their radial scale (changing r_0 from 1.10 fm to 1.15 fm) decreases the inferred β_4 deformation parameter by roughly an additional 10%.

In Fig. 20, we present several calculations of the equilibrium value of β_2, and in Fig. 21 we present a similar figure for the β_4 equilibrium deformation. The solid diamonds represent the values of β_2 obtained by Brack *et al.* (1974), which are in good agreement with the measured values of the multipole moments. The solid lines indicate the range of values found in the recent Strutinsky-type calculations (Pauli, 1973; Møller *et al.*, 1974; Brack *et al.*, 1974) mentioned above. The open circles represent the values of the deformation parameters we have inferred from the extracted single-particle level spacings (Chasman, 1976). The various deformation parameters used in the original calculations are converted to β_2 and β_4 with the relations of Appendix A. There is good agreement in the overall trends of the deformation parameters obtained in these ways. We believe that the remaining differences between the deformation parameters deduced from the electric moments and those deduced from extracted level spacings indicate that there are some interesting features yet to be found in the effective nuclear interaction.

There is some weak evidence for nonzero values of the magnitudes of the $P_6(\cos\theta)$ deformation mode in the actinides. The values of the decoupling parameters of the $\frac{1}{2}+[631]$ neutron orbital and the $\frac{1}{2}-[530]$ proton orbital discussed in Sec. III.G suggest a possibility $\nu_6 \approx -0.02$ in the mass 230 region. The stability calculations of Møller *et al.* (1974) and the extracted level spacings of Chasman (1976) suggest values of $\nu_6 \approx 0.01$ in the mass 250 region.

V. CONCLUSIONS AND SUMMARY

There is a remarkable parallel in the present status of theory and experiment as regards the description of the actinides.

The single-particle model, utilizing a deformed potential, provides an extremely good description of level orderings, spins, and measured single-particle matrix elements in the region that we have surveyed. The experimental data on single-particle structure in odd-neutron nuclides is quite extensive. Our knowledge of the single-particle structure of the odd-proton actinides, particularly the hole states, is less extensive. Recent improvements in accelerator beam quality and increases in bombarding energy should make it possible to learn about these states. Calculations of single-particle wave functions have been carried out using a modified oscillator potential and Woods–Saxon potentials, both momentum independent and momentum dependent. In spite of the apparent large differences in these potentials, there is a good overall agreement in the wave functions one obtains with these potentials. For more detailed agreement with the experimental data, the Woods–Saxon wave functions are superior.

The pairing force is the most important residual interaction in the actinides. The effects of a pairing force can be calculated with very high accuracy for all magnitudes of the interaction strength, for both constant and nonconstant pairing matrix elements. The effect of the pairing force is to modify the occupation probabilities of nucleon orbitals and change the level spacings relative to those of the simple single-particle model. These occupation probabilities are tested in one-nucleon transfer reactions by comparing cross sections for reactions such as the (d,p) and (d,t) reaction. We find that the pairing interaction gives reasonably good explanations of the occupation probabilities observed in this way. We have also found that the energy level spacing shifts observed in the actinides can be explained with pairing matrix elements obtained from a density-dependent delta interaction and cannot be easily understood with constant pairing matrix elements. It is possible to distinguish between these alternatives only because of the large amount of experimental data obtained in one-nucleon transfer studies.

Calculations of actinide equilibrium deformations can be carried out with the Strutinsky prescription. Such calculations depend on both the single-particle potential and the pairing interaction. After correcting for the different parametrizations of the potential deformation used by different authors, we find that the deformations calculated in this way with the Strutinsky procedure are fairly consistent with each other. We also find that the deformations deduced from extracted single-particle level spacings are in moderately good agreement with these calculations. There is also good agreement between measured quadrupole and hexadecapole moments and those obtained from wave functions calculated at the equilibrium deformations deduced in the Strutinsky-type calculations. This agreement is somewhat dependent on the value of the nuclear radius assumed for the single-particle potential. There is little evidence for higher deformation modes in the actinides, but there are some suggestions of $\nu_6 < 0$ in the mass 230 region and $\nu_6 > 0$ in the mass 250 region.

Residual interactions other than the pairing force can be treated accurately only in the regime of relatively weak interaction strengths, and even in this regime the calculations must be done with care. The calculations that have so far been done for the actinides are qualitative and provide only an indication of those configurations that are strongly mixed. The experimental information

on particle-plus-phonon admixtures in actinide single-particle states is also quite fragmentary at present. Admixtures involving the ground-state orbital can be seen in excited states with reactions such as (d,d') inelastic scattering. Other admixtures in excited states have not been systematically studied. There is much to be done in understanding the role of particle–hole interactions in the actinides from both an experimental and theoretical point of view.

Another area that merits attention is that of understanding the magnitudes of absolute and relative differential cross sections in one-nucleon transfer reactions. Recent developments in the understanding of the transfer mechanism together with the recent availability of coupled-channel codes suggest the possibility of detailed understanding of the transfer process in the actinides.

ACKNOWLEDGMENTS

We acknowledge with pleasure the help of our many colleagues, those who have collaborated with us in the studies that form the basis for this review and those who have made critical comments on this manuscript. We thank F. Asaro, T. H. Braid, C. E. Bemis, Jr., E. Browne, R. F. Casten, J. W. Durso, P. R. Fields, M. S. Freedman, D. Gale, R. W. Hoff, J. R. Huizenga, K. Katori, G. Kyle, P. Møller, S. G. Nilsson, F. T. Porter, J. O. Rasmussen, G. L. Struble, S. Wahlborn, and S. W. Yates. Special thanks are due M. E. Bunker and W. Ogle for their comments and corrections of this manuscript and Y. A. Ellis of the Nuclear Data Project for providing us references to the experimental literature on the actinides.

We thank Professor A. Bohr for the hospitality of the Niels Bohr Institute, where some of the work on this paper was done by one of us (R.R.C.).

We thank R. Straz for assistance in plotting the figures of single-particle energy levels, and C. Carbaugh for typing the manuscript.

APPENDIX A: RELATION BETWEEN DEFORMATION PARAMETERS

There is a considerable amount of confusion in the literature concerning the relations between different ways of describing the nuclear deformation (Gareev *et al.*, 1969; Ogle *et al.*, 1971; Nilsson *et al.*, 1969) to which we have made a major contribution (Braid *et al.*, 1971; Erskine *et al.*, 1975). In this appendix, we discuss these relations in extensive detail in the hopes of clarifying the situation.

We relate the different descriptions by equating equipotential surfaces at the half-density point for the Woods–Saxon potential. We also compare these Woods–Saxon equipotentials with the modified oscillator equipotential surface. As noted in the text, deformations are introduced in the Woods–Saxon potential either via the substitution

$$r^2 \to r^2\left(1+\sum_{K=2,4,6}\lambda_K P_K(\cos\theta)\right) \tag{A1}$$

or the substitution

$$R_0 \to R_0\left(1+\sum_{K=2,4,6}\beta_K Y_K^0(\cos\theta)\right). \tag{A2}$$

The other parametrizations of nuclear deformations can be related easily to one of these forms. Equating the surfaces given by Eqs. (A1) and (A2) at the Woods–Saxon half-density gives

$$\left(1+\sum_K \beta_K Y_K^0(\cos\theta)\right) = \frac{1}{\left[1+\sum_K \lambda_K P_K(\cos\theta)\right]^{1/2}}. \tag{A3}$$

Using the Taylor series expansion of $(1+x)^{-1/2}$, we get

$$1-\frac{1}{2}\sum_K \lambda_K P_K(\cos\theta)+\tfrac{3}{8}\left[\lambda_2^2 P_2^2(\cos\theta)+2\lambda_2\lambda_4 P_2(\cos\theta)P_4(\cos\theta)+2\lambda_2\lambda_6 P_2(\cos\theta)P_6(\cos\theta)+\lambda_4^2 P_4^2(\cos\theta)\right]-\tfrac{5}{16}\lambda_2^3 P_2^3(\cos\theta)$$
$$=1+\beta_2 Y_2^0(\cos\theta)+\beta_4 Y_4^0(\cos\theta)+\beta_6 Y_6^0(\cos\theta) \tag{A4}$$

including the terms that might be important for the actinides. Equation (A4) is simplified by making use of the relations

$$P_K(\cos\theta)P_{K'}(\cos\theta)=\sum_{K''}\langle K,0,K',0|K'',0\rangle^2 P_{K''}(\cos\theta) \tag{A5}$$

and

$$Y_K^0(\cos\theta)=\left[(2K+1)/4\pi\right]^{1/2}P_K(\cos\theta). \tag{A6}$$

Equating coefficients of $P_K(\cos\theta)$, we obtain

$$N_0\sqrt{5/4\pi}\,\beta_2=-0.5\lambda_2+0.106\lambda_2^2+0.214\lambda_2\lambda_4+0.055\lambda_4^2-0.134\lambda_2^3, \tag{A7}$$

$$N_0\sqrt{9/4\pi}\,\beta_4=-0.5\lambda_4+0.193\lambda_2^2+0.195\lambda_2\lambda_4+0.236\lambda_2\lambda_6+0.061\lambda_4^2-0.087\lambda_2^3, \tag{A8}$$

$$N_0\sqrt{13/4\pi}\,\beta_6=-0.5\lambda_6+0.34\lambda_2\lambda_4+0.190\lambda_2\lambda_6+0.075\lambda_4^2-0.073\lambda_2^3, \tag{A9}$$

with

$$N_0=1+0.075\lambda_2^2+0.0416\lambda_4^2-0.018\lambda_2^3. \tag{A10}$$

Strictly speaking, the relations (A7)–(A10) hold when the equipotential surface in Eq. (A1) is defined as $[r^2/(1+N_0)^2]$.

The η coefficients of Ogle *et al.* (1971) are equivalent to the λ coefficients defined above. The relations are

$$\eta_2=-\lambda_2,\quad \eta_4=\lambda_4,\quad \eta_6=\lambda_6. \tag{A11}$$

The equipotential surface used by Chasman (Braid *et al.*,

1971; Erskine *et al.*, 1975) is

$$r^2\left[\exp(\tfrac{2}{3}\nu_2)\sin^2\theta+\exp(-\tfrac{4}{3}\nu_2)\cos^2\theta + \sum_{K=4,6}\nu_K\sqrt{K+\tfrac{1}{2}}P_K(\cos\theta)\right]. \quad \text{(A12)}$$

The ν coefficients can be directly related to the λ coefficients, giving

$$\lambda_2=(-\tfrac{4}{3}\nu_2+\tfrac{4}{9}\nu_2^2-\tfrac{8}{27}\nu_2^3)/N_1,$$
$$\lambda_4=2.12\nu_4/N_1,$$
$$\lambda_6=2.55\nu_6/N_1, \quad \text{(A13)}$$

with

$$N_1=1+\tfrac{4}{9}\nu_2^2-\tfrac{8}{81}\nu_2^3.$$

The situation is slightly more complicated with the modified oscillator deformation parameters (Nilsson *et al.*, 1969). The modified oscillator equipotential surface is

$$r^2\left[(1+\tfrac{1}{3}\epsilon)^2\sin^2\theta+(1-\tfrac{2}{3}\epsilon)^2\cos^2\theta + 2(r')^2\sum_{K=4,6}\epsilon_K P_K(\cos\theta')\right], \quad \text{(A14)}$$

where θ' and r' are the stretched coordinates;

$$(r')^2=r^2[1-\tfrac{2}{3}\epsilon P_2(\cos\theta)], \quad \text{(A15)}$$

$$\cos^2\theta'=\frac{(1-\tfrac{2}{3}\epsilon)\cos^2\theta}{[1-\tfrac{2}{3}\epsilon P_2(\cos\theta)]}. \quad \text{(A16)}$$

Substituting the relations (A15) and (A16), (A14) becomes

$$r^2\left[\begin{array}{c}1+\tfrac{2}{9}\epsilon^2+P_2(\cos\theta)[-\tfrac{4}{3}\epsilon+\tfrac{2}{9}\epsilon^2]\\+2\epsilon_4P_4(\cos\theta)+2\epsilon_6P_6(\cos\theta)\\+2\epsilon\,\epsilon_4[0.303P_6(\cos\theta)-0.303P_4(\cos\theta)\\-0.667P_2(\cos\theta)]\end{array}\right] \quad \text{(A17)}$$

neglecting the term proportional to $\epsilon\epsilon_6$. The relations between the λ coefficients and the ϵ coefficients are

TABLE A.1. Relation of deformation parameters.

$\nu_2=0.19$	$\nu_4=-0.04$	
$\eta_2=0.234$	$\eta_4=-0.083$	
$\epsilon=0.191$	$\epsilon_4=-0.044$	
$\beta_2=0.203$	$\beta_4=0.067$	$\beta_6=0.008$
$\nu_2=0.22$	$\nu_4=-0.02$	
$\eta_2=0.269$	$\eta_4=-0.0415$	
$\epsilon=0.215$	$\epsilon_4=-0.022$	
$\beta_2=0.232$	$\beta_4=0.0453$	$\beta_6=0.005$
$\nu_2=0.25$	$\nu_4=0.00$	
$\eta_2=0.301$	$\eta_4=0.00$	
$\epsilon_2=0.239$	$\epsilon_4=0.00$	
$\beta_2=0.258$	$\beta_4=0.023$	$\beta_6=0.002$

$$\lambda_2=[-\tfrac{4}{3}\epsilon+\tfrac{2}{9}\epsilon^2-\tfrac{4}{3}\epsilon\epsilon_4]/N_2,$$
$$\lambda_4=[2\epsilon_4-0.606\epsilon\epsilon_4]/N_2, \quad \text{(A18)}$$
$$\lambda_6=[2\epsilon_6+0.606\epsilon\epsilon_4]/N_2,$$
$$N_2=(1+\tfrac{2}{9}\epsilon^2).$$

In Table A.1, we relate these sets of deformation coordinates to each other for the values of the deformation parameters that are used in the other appendixes.

APPENDIX B: PAIR OCCUPATION PROBABILITIES

In Tables B.1–B.7 (neutron system) and B.8–B.13 (proton system), we present values of occupation probabilities $\langle N_K\rangle$ (called V_K^2 in BCS theory) for different orbitals. The values are read across a row for the configuration in which the state denoted by X is blocked. The numbers in the first row for each configuration were calculated with the constant pairing matrix elements (given in Sec. II) and the values in the second row were computed with density-dependent pairing matrix elements (Chasman, 1976). Both sets of calculations were done using the method of correlated quasiparticles (Chasman, 1972). The emptiness factor U^2 is given by the expression $U^2=1-V^2$.

The pairing factors for various one-body matrix elements between two one-quasiparticle states are given as follows (Kisslinger and Sorensen, 1963; Soloviev, 1963; Wahlborn, 1966)

TABLE B.1. Values of pair occupation probability, V^2, in ^{233}U.

V^2 \ State	5/2+[633]	3/2+[631]	1/2+[631]	5/2−[752]	7/2−[743]	1/2−[501]
	0.82	0.92	0.12	0.92	0.10	X
	0.80	0.92	0.11	0.84	0.23	X
	0.83	X	0.11	0.92	0.09	0.95
	0.81	X	0.10	0.85	0.19	0.97
	0.83	0.93	0.11	X	0.09	0.95
	0.83	0.94	0.07	X	0.14	0.97
	X	0.93	0.07	0.93	0.06	0.97
	X	0.94	0.07	0.86	0.13	0.97
	0.36	0.84	X	0.83	0.07	0.91
	0.42	0.87	X	0.69	0.14	0.95
	0.36	0.84	0.08	0.82	X	0.91
	0.42	0.88	0.06	0.73	X	0.95

TABLE B.2. Values of pair occupation probability, V^2, in ^{235}U.

V^2 \ State	7/2 − [743]	1/2 + [631]	5/2 + [633]	3/2 + [631]	5/2 + [622]	7/2 + [624]	5/2 − [752]	1/2 − [501]
	0.43	0.43	0.89	0.90	0.24	0.10	0.94	X
	0.66	0.24	0.91	0.94	0.16	0.10	0.92	X
	0.42	0.42	0.90	X	0.23	0.10	0.94	0.95
	0.65	0.22	0.92	X	0.15	0.09	0.93	0.97
	0.42	0.42	X	0.91	0.23	0.10	0.94	0.95
	0.64	0.22	X	0.94	0.15	0.08	0.93	0.97
	X	0.16	0.90	0.91	0.11	0.05	0.95	0.95
	X	0.07	0.95	0.96	0.05	0.04	0.95	0.98
	0.16	X	0.90	0.91	0.11	0.05	0.95	0.95
	0.25	X	0.89	0.92	0.07	0.05	0.90	0.97
	0.16	0.16	0.88	0.89	X	0.05	0.94	0.94
	0.26	0.10	0.88	0.91	X	0.05	0.89	0.97
	0.17	0.17	0.86	0.87	0.12	X	0.93	0.93
	0.26	0.10	0.88	0.91	0.07	X	0.89	0.96

TABLE B.3. Values of pair occupation probability, V^2, in ^{237}U.

V^2 \ State	1/2 + [631]	5/2 + [622]	7/2 − [743]	7/2 + [624]	3/2 + [631]	5/2 + [633]	1/2 − [501]
	0.70	0.26	0.90	0.11	X	0.96	0.96
	0.70	0.30	0.75	0.17	X	0.95	0.97
	0.70	0.27	0.90	0.12	0.95	0.96	X
	0.69	0.30	0.75	0.18	0.94	0.95	X
	0.70	0.27	0.90	0.12	0.95	X	0.96
	0.70	0.30	0.74	0.16	0.95	X	0.97
	0.70	0.23	X	0.10	0.96	0.96	0.97
	0.70	0.20	X	0.11	0.96	0.96	0.98
	X	0.11	0.91	0.06	0.96	0.97	0.97
	X	0.19	0.74	0.11	0.95	0.95	0.97
	0.22	X	0.86	0.06	0.95	0.96	0.96
	0.37	X	0.64	0.11	0.93	0.94	0.97
	0.23	0.13	0.82	X	0.94	0.95	0.95
	0.35	0.17	0.63	X	0.93	0.94	0.97

TABLE B.4. Values of pair occupation probability, V^2, in ^{241}Pu.

V^2 \ State	5/2 + [622]	1/2 + [631]	7/2 + [624]	7/2 − [743]	1/2 + [620]	3/2 + [622]	3/2 + [631]	7/2 + [613]
	0.73	0.86	0.27	0.91	0.06	0.05	X	0.06
	0.67	0.82	0.39	0.77	0.07	0.05	X	0.06
	0.73	0.87	0.25	X	0.06	0.04	0.96	0.06
	0.67	0.84	0.30	X	0.05	0.04	0.96	0.05
	0.73	X	0.22	0.91	0.05	0.04	0.96	0.05
	0.67	X	0.34	0.77	0.06	0.05	0.95	0.06
	X	0.87	0.15	0.92	0.04	0.03	0.96	0.04
	X	0.82	0.27	0.76	0.05	0.04	0.95	0.04
	0.34	0.78	X	0.87	0.05	0.04	0.95	0.05
	0.44	0.76	X	0.71	0.05	0.04	0.94	0.04
	0.34	0.73	0.16	0.84	X	0.04	0.94	0.05
	0.42	0.72	0.25	0.64	X	0.04	0.93	0.05
	0.34	0.73	0.16	0.84	0.05	0.04	0.94	X
	0.42	0.69	0.25	0.64	0.05	0.04	0.93	X
	0.34	0.73	0.16	0.84	0.05	X	0.94	0.05
	0.42	0.70	0.25	0.64	0.05	X	0.93	0.05

TABLE B.5. Values of pair occupation probability, V^2, in ^{245}Cm.

V^2 \ State	7/2 + [624]	5/2 + [622]	1/2 + [631]	9/2 − [734]	7/2 − [743]	1/2 + [620]	3/2 + [622]	7/2 + [613]
	0.87	0.94	0.95	0.12	X	0.06	0.04	0.06
	0.76	0.91	0.94	0.25	X	0.05	0.04	0.05
	0.87	0.94	X	0.11	0.97	0.05	0.04	0.05
	0.76	0.91	X	0.28	0.93	0.05	0.04	0.05
	0.87	X	0.95	0.10	0.97	0.05	0.04	0.05
	0.76	X	0.94	0.26	0.93	0.04	0.03	0.04
	X	0.94	0.96	0.07	0.97	0.04	0.03	0.04
	X	0.92	0.95	0.15	0.94	0.03	0.02	0.03
	0.35	0.83	0.88	X	0.94	0.05	0.04	0.05
	0.28	0.87	0.92	X	0.92	0.03	0.02	0.03
	0.32	0.82	0.87	0.09	0.93	X	0.04	0.05
	0.36	0.82	0.88	0.18	0.87	X	0.03	0.04
	0.36	0.82	0.87	0.09	0.93	0.05	0.04	X
	0.33	0.82	0.87	0.18	0.87	0.04	0.03	X
	0.36	0.81	0.87	0.09	0.93	0.05	X	0.05
	0.32	0.82	0.87	0.18	0.87	0.04	X	0.04

TABLE B.6. Values of pair occupation probability, V^2, in ^{247}Cm.

V^2 \ State	9/2 − [734]	5/2 + [622]	7/2 + [624]	1/2 + [620]	3/2 + [622]	7/2 + [613]	1/2 + [631]
	0.79	0.91	0.90	0.15	0.08	0.15	X
	0.77	0.95	0.91	0.09	0.06	0.10	X
	0.79	X	0.90	0.14	0.08	0.14	0.94
	0.79	X	0.91	0.09	0.05	0.09	0.97
	0.79	0.92	X	0.13	0.08	0.13	0.94
	0.79	0.95	X	0.08	0.05	0.08	0.97
	X	0.92	0.90	0.10	0.06	0.10	0.94
	X	0.96	0.94	0.04	0.03	0.04	0.98
	0.42	0.84	0.80	X	0.07	0.11	0.89
	0.34	0.90	0.79	X	0.04	0.06	0.94
	0.42	0.84	0.80	0.11	0.07	X	0.89
	0.34	0.89	0.79	0.06	0.04	X	0.94
	0.41	0.83	0.79	0.11	X	0.11	0.88
	0.34	0.89	0.79	0.06	X	0.06	0.94

TABLE B.7. Values of pair occupation probability, V^2, in ^{249}Cm–^{251}Cf.

V^2 \ State	1/2 + [620]	7/2 + [613]	3/2 + [622]	9/2 + [615]	9/2 − [734]	11/2 − [725]	5/2 + [622]	1/2 − [750]
	0.43	0.23	0.17	0.17	0.94	0.12	X	0.10
	0.41	0.23	0.16	0.21	0.87	0.24	X	0.06
	0.43	0.22	0.17	0.17	X	0.12	0.96	0.10
	0.40	0.21	0.14	0.17	X	0.21	0.96	0.05
	X	0.06	0.05	0.05	0.95	0.04	0.96	0.03
	X	0.08	0.06	0.08	0.85	0.11	0.96	0.03
	0.08	X	0.05	0.05	0.94	0.04	0.96	0.03
	0.12	X	0.07	0.09	0.83	0.12	0.95	0.03
	0.08	0.07	X	0.05	0.94	0.04	0.96	0.04
	0.12	0.09	X	0.08	0.83	0.12	0.95	0.03
	0.08	0.06	0.05	X	0.94	0.04	0.96	0.04
	0.11	0.08	0.07	X	0.84	0.12	0.95	0.03
	0.08	0.06	0.05	0.05	0.93	X	0.95	0.04
	0.09	0.07	0.05	0.07	0.88	X	0.97	0.03

TABLE B.8. Values of pair occupation probability, V^2, in ^{231}Pa.

V^2 State	1/2 − [530]	3/2 + [651]	5/2 − [523]	5/2 + [642]	1/2 + [400]	3/2 − [521]
	0.71	X	0.22	0.23	0.87	0.09
	0.71	X	0.13	0.22	0.90	0.06
	X	0.79	0.20	0.20	0.87	0.08
	X	0.80	0.14	0.24	0.89	0.06
	0.48	0.69	0.18	X	0.82	0.08
	0.61	0.68	0.11	X	0.81	0.06
	0.48	0.69	X	0.18	0.82	0.08
	0.58	0.65	X	0.20	0.80	0.06
	0.46	0.66	0.18	0.18	0.80	X
	0.59	0.62	0.12	0.20	0.79	X

TABLE B.9. Values of pair occupation probability, V^2, in ^{237}Np.

V^2 State	5/2 + [642]	5/2 − [523]	1/2 − [530]	1/2 + [400]
	0.65	0.42	0.85	X
	0.72	0.33	0.88	X
	0.65	0.42	X	0.87
	0.72	0.32	X	0.91
	X	0.32	0.85	0.87
	X	0.20	0.90	0.91
	0.43	X	0.82	0.85
	0.46	X	0.83	0.86

TABLE B.11. Values of pair occupation probability, V^2, in ^{243}Am.

V^2 State	5/2 − [523]	5/2 + [642]	3/2 − [521]	7/2 + [633]
	0.80	X	0.18	0.12
	0.85	X	0.16	0.14
	X	0.85	0.16	0.11
	X	0.83	0.17	0.15
	0.52	0.71	X	0.10
	0.70	0.60	X	0.14
	0.52	0.69	0.15	X
	0.70	0.63	0.14	X

TABLE B.10. Values of pair occupation probability, V^2, in ^{241}Am.

V^2 State	5/2 − [523]	5/2 + [642]	3/2 − [521]	7/2 + [633]	1/2 + [400]	1/2 − [530]
	0.86	0.91	0.14	0.11	X	0.94
	0.86	0.87	0.15	0.13	X	0.94
	0.86	0.91	0.14	0.11	0.94	X
	0.87	0.88	0.13	0.12	0.95	X
	0.86	X	0.12	0.09	0.95	0.95
	0.88	X	0.11	0.09	0.96	0.95
	X	0.92	0.09	0.08	0.95	0.95
	X	0.89	0.10	0.09	0.96	0.95
	0.49	0.78	X	0.08	0.89	0.89
	0.58	0.67	X	0.09	0.90	0.90
	0.49	0.78	0.10	X	0.89	0.89
	0.58	0.69	0.09	X	0.89	0.89

$$P_{i,f} = (U_i U_f \pm V_i V_f) R_{i,f} , \tag{B1}$$

where V_i^2 denotes the occupation probability of level i in the configuration in which level f is blocked. $R_{i,f}$ is an overlap factor and is defined as

$$R_{i,f} = \sum_{s \neq i,f} (U_s^i U_s^f + V_s^i V_s^f) . \tag{B2}$$

In the above equation $(V_s^i)^2$ represents the occupation probability of level s in the configuration in which level i is blocked. In Eq. (B1) the plus sign applies to matrix elements that are odd under time reversal, such as Coriolis and magnetic transition matrix elements. The negative sign applies to electric transitions which are even under time reversal.

For β transitions the pairing factor $P_{i,f}$ is given by (Kisslinger and Sorensen, 1963; Soloviev, 1963; Wahlborn, 1966)

$$P_{i,f} = (U_i U_f) R_{i,f} , \tag{B3}$$

for β^- decay of odd-neutron nuclides and electron capture decay of odd-proton nuclides, and

$$P_{i,f} = (V_i V_f) R_{i,f} , \tag{B4}$$

for β^- decay of odd-proton nuclides and EC decay of odd-neutron nuclides.

TABLE B.12. Values of pair occupation probability, V^2, in ^{249}Bk.

V^2 \ State	7/2 + [633]	3/2 − [521]	5/2 + [642]	5/2 − [523]	1/2 + [400]	7/2 − [514]
	0.50	0.60	0.88	0.90	X	0.10
	0.51	0.61	0.87	0.90	X	0.08
	0.51	0.60	0.88	X	0.88	0.11
	0.50	0.62	0.87	X	0.91	0.08
	0.50	0.60	X	0.90	0.88	0.10
	0.48	0.62	X	0.90	0.91	0.07
	0.35	X	0.87	0.89	0.87	0.08
	0.34	X	0.86	0.90	0.90	0.06
	X	0.36	0.87	0.89	0.87	0.08
	X	0.33	0.87	0.90	0.90	0.05
	0.32	0.33	0.82	0.85	0.82	X
	0.33	0.32	0.80	0.85	0.85	X

The overlap factor $R_{i,f}$ is defined here as in Eq. (B2) but extends over both proton and neutron orbitals. In the above equations i and f refer to the initial and final systems; V_i^2 denotes occupation probability in the appropriate even-nucleon system. The values of U_s and V_s can be estimated from Tables B.1–B.13 using a configuration in which a highly excited orbital is blocked.

For one-nucleon transfer reactions the pairing factor P_K is defined as

$$P_K = U_K R_K , \tag{B5}$$

for one-particle stripping reactions; and

$$P_K = V_K R_K , \tag{B6}$$

for one-particle pickup reactions. The term R_K is the same as given in Eq. (B2) except that only level K is excluded from the product.

In many calculations the overlap factors $R_{i,f}$ and R_K are taken as unity. This is usually a good approximation.

APPENDIX C: SINGLE-PARTICLE MATRIX ELEMENTS

In Tables C.1–C.6 we list the matrix elements $\langle j_+ \rangle$, $\langle l_+ \rangle$, $\langle s_+ \rangle$, $\langle l_3 \rangle$, $\langle s_3 \rangle$, $\langle r^2 \rangle$, $\langle r^2 Y_2^0(\cos\theta) \rangle$, and $E1$ matrix elements calculated with our wave functions (Chasman, 1971). These values are given for three deformations that are representative of the actinide region: $\nu_2 = 0.19$, $\nu_4 = -0.04, A = 232$; $\nu_2 = 0.22$, $\nu_4 = -0.02, A = 238$; $\nu_2 = 0.25$, $\nu_4 = 0.0, A = 244$. We have chosen the phases of our wave functions to reproduce the signs of large $\langle j_+ \rangle$, $\langle l_3 \rangle$ and $E1$ matrix elements calculated with Nilsson (1955) wave functions.

TABLE B.13. Values of pair occupation probability, V^2, in ^{251}Es.

V^2 \ State	7/2 + [633]	3/2 − [521]	5/2 + [642]	7/2 − [514]
	0.82	0.83	X	0.15
	0.86	0.88	X	0.11
	0.83	X	0.95	0.11
	0.88	X	0.95	0.08
	X	0.84	0.95	0.11
	X	0.89	0.96	0.07
	0.51	0.62	0.91	X
	0.55	0.65	0.90	X

1. Coriolis matrix elements

The Coriolis matrix element between states K and $K \pm 1$ is given by (Kerman, 1956; Brockmeir *et al.*, 1965)

$$A_K = -\frac{\hbar^2}{2\mathcal{I}} [(I - K_<)(I + K_>)]^{1/2} \langle K \pm 1 | j_\mp | K \rangle P_{K,K\pm1} , \tag{C1}$$

where $P_{K,K\pm1}$ is the pairing factor. The decoupling parameter a is (Nilsson, 1955)

$$\mathbf{a} = -\langle \chi_{1/2} | j_+ | \chi_{-1/2} \rangle . \tag{C2}$$

In the case of Coriolis mixing between two bands, if we denote the energies of the unperturbed bands by E_K and $E_{K\pm1}$ and the observed energies by E_H and E_L, then

$$E_{H,L} = \tfrac{1}{2}(E_K + E_{K\pm1}) \pm [(E_K - E_{K\pm1})^2 + 4A_K^2]^{1/2} . \tag{C3}$$

The admixture coefficients a_K and $a_{K\pm1}$ in the lower (L) and higher (H) states are (Kerman, 1956)

$$\frac{a_K(L,H)}{a_{K\pm1}(L,H)} = \frac{-A_K}{E_K - E_{L,H}} = \frac{E_{K\pm1} - E_{L,H}}{-A_K} \tag{C4}$$

and

$$a_K^2(L,H) + a_{K\pm1}^2(L,H) = 1 . \tag{C5}$$

In calculations involving more than two bands the secular equations are solved with a computer. Several computer codes are available for such calculations, for example, BANDMIX (Erskine, 1966).

Equations for the calculation of $\langle j_+ \rangle$ matrix elements from Nilsson (1955) wave functions are given by Brockmeir *et al.* (1965).

2. Matrix elements for $M1$ transitions

$M1$ matrix elements can be calculated with the expectation values $\langle l_+ \rangle$ and $\langle s_+ \rangle$ for $|\Delta K| = 1$ transitions. Magnetic moments and $M1$ matrix elements for $\Delta K = 0$ transitions can be calculated from $\langle l_3 \rangle$ and $\langle s_3 \rangle$. Our $\langle l_3 \rangle$, $\langle s_3 \rangle$, $\langle l_+ \rangle$, and $\langle s_+ \rangle$ values are related to the G_{ML} and G_{MS} values of Browne and Femenia (1971) as follows:

$$G_{ML} = 2\langle l_3 \rangle \text{ and } G_{MS} = 2\langle s_3 \rangle \text{ for } \Delta K = 0$$
$$G_{ML} = 2\langle l_+ \rangle \text{ and } G_{MS} = 2\langle s_+ \rangle \text{ for } |\Delta K| = 1 . \tag{C6}$$

The magnetic moment μ in nuclear magnetons can be calculated using the expression (Nilsson, 1955)

$$\mu = [\Omega K/(I+1)](g_\Omega - g_R) + g_R I , \tag{C7}$$

TABLE C.1. Neutron matrix elements $\langle j_+ \rangle$, $\langle l_+ \rangle$[a], and $\langle s_+ \rangle$.

		$\langle j_+ \rangle$			$\langle s_+ \rangle$		
		$A = 232$	238	244	$A = 232$	238	244
		$\nu_2 = 0.19$	0.22	0.25	$\nu_2 = 0.19$	0.22	0.25
Initial state	Final state	$\nu_4 = -0.04$	−0.02	0.0	$\nu_4 = -0.04$	−0.02	0.0
1/2 + [651]	1/2 + [651]			2.06			−0.60
	1/2 + [640]			4.04			0.22
	1/2 + [631]			0.03			0.15
	1/2 + [620]			0.37			0.07
	3/2 + [642]			4.47			−0.29
	3/2 + [631]			−0.02			−0.19
	3/2 + [622]			0.37			−0.07
1/2 + [640]	1/2 + [640]	−0.16	−0.58	−1.03	−0.55	−0.58	−0.60
	1/2 + [631]	2.81	2.72	2.61	−0.28	−0.30	−0.32
	1/2 + [620]	0.16	0.06	−0.03	−0.16	−0.15	−0.14
	3/2 + [642]	0.83	1.00	1.03	−0.46	−0.43	−0.41
	3/2 + [631]	4.83	4.69	4.57	0.25	0.29	0.32
	3/2 + [622]	8.3(−3)	−0.03	−0.08	0.14	0.14	0.14
1/2 + [631]	1/2 + [631]	0.39	0.57	0.70	−0.41	−0.39	−0.37
	1/2 + [620]	3.44	3.36	3.29	0.30	0.29	0.29
	3/2 + [642]	2.74	2.56	2.39	0.30	0.27	0.24
	3/2 + [631]	−0.39	−0.55	−0.64	−0.61	−0.65	−0.67
	3/2 + [622]	3.33	3.33	3.32	−0.25	−0.27	−0.28
1/2 + [620]	1/2 + [620]	−0.09	−0.21	−0.29	−0.65	−0.70	−0.74
	3/2 + [642]	0.02	0.06	0.09	0.17	0.14	0.11
	3/2 + [631]	2.12	2.12	2.13	−0.32	−0.31	−0.31
	3/2 + [622]	0.33	0.54	0.66	−0.36	−0.31	−0.27
3/2 + [642]	5/2 + [633]	4.82	4.85	4.85	−0.24	−0.29	−0.32
	5/2 + [622]	0.35	0.15	0.07	−0.24	−0.19	−0.14
3/2 + [631]	5/2 + [633]	0.46	0.67	0.74	−0.38	−0.32	−0.29
	5/2 + [622]	4.82	4.67	4.57	0.23	0.29	0.31
3/2 + [622]	5/2 + [633]	2.05	1.98	1.94	0.33	0.28	0.24
	5/2 + [622]	−0.27	−0.42	−0.49	−0.63	−0.71	−0.76
5/2 + [633]	7/2 + [624]	4.56	4.71	4.73	−0.18	−0.27	−0.30
	7/2 + [613]	0.99	0.35	0.15	−0.26	−0.17	−0.11
5/2 + [622]	7/2 + [624]	4.5(−3)	0.52	0.63	−0.35	−0.26	−0.20
	7/2 + [613]	4.42	4.25	4.17	0.15	0.25	0.27
7/2 + [624]	9/2 + [615]	3.00	4.09	4.22	0.03	−0.22	−0.26
	9/2 + [604]	2.46	0.67	0.18	−0.27	−0.16	−0.08
7/2 + [613]	9/2 + [615]	−1.15	0.47	0.67	−0.29	−0.21	−0.13
	9/2 + [604]	3.53	3.37	3.25	−0.08	0.17	0.20
9/2 + [615]	11/2 + [615]	−0.43	−0.45	−0.41	−0.33	−0.80	−0.87
	11/2 + [606]	1.13	2.92		−0.09	−0.20	
9/2 + [604]	11/2 + [615]	−0.03	0.45	0.70	−0.81	−0.39	−0.21
	11/2 + [606]	3.12	1.60		−0.22	−0.10	
11/2 + [615]	13/2 + [606]	3.61	3.62	3.63	0.25	0.23	0.22
11/2 + [606]	13/2 + [606]	−0.09	−0.15		−0.93	−0.94	
1/2 − [510]	1/2 − [510]	0.56		0.61	0.86		0.91
	1/2 − [770]	−0.33		−8.7(−3)	0.03		−6.1(−3)
	1/2 − [501]	−1.46		−1.82	0.24		0.18
	1/2 − [750]	0.18		6.0(−3)	−5.9(−3)		6.6(−3)
	3/2 − [512]	0.72		0.70	−0.15		−0.10
	3/2 − [501]	2.09		2.24	0.24		0.18
	3/2 − [761]	−0.36		−0.01	−0.02		6.8(−3)
	3/2 − [752]			8.4(−3)			−7.8(−3)
1/2 − [770]	1/2 − [770]	7.28	7.36	7.42	0.58	0.57	0.56
	1/2 − [501]	−0.15	−0.13	−8.5(−4)	0.01	9.6(−4)	−2.4(−3)
	1/2 − [750]	−1.33	−1.23	−1.12	0.17	0.16	0.15
	3/2 − [512]	0.23		5.8(−4)	0.02		−7.6(−3)
	3/2 − [501]	−0.08	−3.39	0.01	−5.9(−3)	−0.25	−1.1(−3)
	3/2 − [761]	7.31	6.55	7.41	0.53	0.47	0.54
	3/2 − [752]		−0.68	−0.74		0.14	0.15
1/2 − [501]	1/2 − [501]	−0.87	−0.81	−0.76	0.07	0.05	0.04
	1/2 − [750]	−9.2(−3)	−0.01	−2.8(−3)	−5.7(−3)	−2.9(−3)	2.9(−3)
	3/2 − [512]	1.37		1.66	0.20		0.14
	3/2 − [501]	−0.20	−0.20	−0.33	−0.94	−0.84	−0.97
	3/2 − [761]	−0.11	−0.21	1.7(−3)	−0.04	−0.45	4.7(−3)
	3/2 − [752]		−0.03	−3.8(−3)		−1.9(−3)	−3.8(−3)

TABLE C.1. (*Continued*)

		$\langle j_+ \rangle$				$\langle s_+ \rangle$	
		$A=232$	238	244	$A=232$	238	244
		$\nu_2=0.19$	0.22	0.25	$\nu_2=0.19$	0.22	0.25
Initial state	Final state	$\nu_4=-0.04$	−0.02	0.0	$\nu_4=-0.04$	−0.02	0.0
1/2 − [750]	1/2 − [750]	3.26	3.25	3.36	0.81	0.82	0.81
	3/2 − [512]	−0.14		−7.0(−3)	−2.4(−3)		7.9(−3)
	3/2 − [501]	0.06	0.69	7.7(−4)	1.9(−3)	0.09	2.2(−3)
	3/2 − [761]	−1.60	−1.26	−1.28	−0.22	−0.18	−0.18
	3/2 − [752]		4.63	4.62		0.24	0.26
3/2 − [512]	5/2 − [503]	−2.20		−2.39	0.24		0.19
	5/2 − [752]	0.25		6.6(−3)	−6.1(−3)		0.01
3/2 − [501]	5/2 − [503]	−0.80	−0.62	−0.69	0.06	0.04	0.03
	5/2 − [752]	−0.18	3.43	0.01	−0.02	0.23	4.2(−3)
3/2 − [761]	5/2 − [503]	−0.03	−0.42	0.02	−0.02	9.1(−3)	4.6(−3)
	5/2 − [752]	7.32	6.48	7.33	0.49	0.44	0.50
3/2 − [752]	5/2 − [503]		0.05	1.3(−4)		2.2(−3)	−4.7(−3)
	5/2 − [752]		−1.49	−1.37		−0.26	−0.27
5/2 − [503]	7/2 − [503]			−0.36			−0.97
	7/2 − [743]	−0.09	−0.13	0.02	0.01	9.6(−4)	−4.4(−3)
5/2 − [752]	7/2 − [503]			6.9(−3)			5.9(−3)
	7/2 − [743]	7.16	7.15	7.12	0.45	0.46	0.46
7/2 − [503]	9/2 − [734]			0.01			−6.5(−3)
7/2 − [743]	9/2 − [734]	6.81	6.78	6.74	0.42	0.41	0.41
9/2 − [734]	11/2 − [725]	6.21	6.18	6.15	0.37	0.37	0.36
11/2 − [725]	13/2 − [716]	5.29	5.28	5.27	0.32	0.31	0.30

[a] The matrix element $\langle l_+ \rangle$ can be obtained from the relation $\langle l_+ \rangle = \langle j_+ \rangle - \langle s_+ \rangle$.

TABLE C.2. Neutron matrix elements $\langle l_3 \rangle$,[a] $\langle s_3 \rangle$, $\langle r^2 \rangle$, $\langle r^2 Y_2^0(\cos\theta) \rangle$.

			$\langle s_3 \rangle$			$\langle r^2 \rangle$			$\langle r^2 Y_2^0(\cos\theta) \rangle$	
		$A=232$	238	244	232	238	244	232	238	244
		$\nu_2=0.19$	0.22	0.25	0.19	0.22	0.25	0.19	0.22	0.25
Initial state	Final state	$\nu_4=-0.04$	−0.02	0.0	−0.04	−0.02	0.0	−0.04	−0.02	0.0
1/2 + [651]	1/2 + [651]			0.10			8.65			3.47
	1/2 + [640]			−0.22			0.08			
	1/2 + [631]			−0.15			0.08			
	1/2 + [620]			−0.07			0.03			
1/2 + [640]	1/2 + [640]	0.05	0.08	0.10	8.22	8.33	8.43	2.58	2.68	2.78
	1/2 + [631]	0.28	0.30	0.32	0.12	0.11	0.09			
	1/2 + [620]	0.16	0.15	0.14	3.8(−3)	0.04	0.07			
1/2 + [631]	1/2 + [631]	−0.09	−0.11	−0.13	7.73	7.81	7.90	1.95	2.04	2.11
	1/2 + [620]	−0.30	−0.29	−0.29	0.15	0.15	0.13			
1/2 + [620]	1/2 + [620]	0.15	0.20	0.24	7.28	7.34	7.42	1.00	1.03	1.06
3/2 + [642]	3/2 + [642]	−0.03	−0.06	−0.08	8.15	8.31	8.47	2.29	2.37	2.44
	3/2 + [631]	−0.26	−0.25	−0.24	0.11	0.12	0.11			
	3/2 + [622]	−0.15	−0.13	−0.11	−0.01	0.03	0.07			
3/2 + [631]	3/2 + [631]	0.15	0.19	0.22	7.86	7.96	8.08	1.69	1.77	1.84
	3/2 + [622]	0.27	0.29	0.30	0.14	0.12	0.10			
3/2 + [622]	3/2 + [622]	−0.11	−0.18	−0.23	7.23	7.33	7.44	0.79	0.88	0.94
5/2 + [633]	5/2 + [633]	−0.09	−0.16	−0.19	7.78	7.99	8.18	1.26	1.38	1.46
	5/2 + [622]	−0.30	−0.26	−0.24	0.17	0.15	0.14			
5/2 + [622]	5/2 + [622]	0.19	0.26	0.31	7.44	7.53	7.65	0.73	0.76	0.82
7/2 + [624]	7/2 + [624]	−0.045	−0.21	−0.28	7.31	7.57	7.79	0.14	0.36	0.46
	7/2 + [613]	−0.37	−0.29	−0.23	0.21	0.18	0.15			
7/2 + [613]	7/2 + [613]	0.13	0.31	0.38	7.10	7.10	7.17	−0.20	−0.28	−0.25
9/2 + [615]	9/2 + [615]	0.38	−0.22	−0.35	6.75	7.11	7.33	−1.35	−0.73	−0.56
	9/2 + [604]	−0.31	−0.35	−0.21	0.15	0.21	0.15			
9/2 + [604]	9/2 + [604]	−0.26	0.33	0.45	6.99	6.73	6.64	−0.78	−1.31	−1.36
11/2 + [615]	11/2 + [615]	0.44	0.44	0.45	8.11	8.23	8.36	−0.90	−0.81	−0.71
	11/2 + [606]	0.23	0.22		0.03	0.04				
11/2 + [606]	11/2 + [606]	−0.44	−0.45		6.82	6.81		−1.62	−1.58	
13/2 + [606]	13/2 + [606]	0.50	0.50	0.50	7.92	7.88	7.86	−1.95	−1.89	−1.82
1/2 − [510]	1/2 − [510]	0.36		0.41	6.69		6.87	0.13		0.16
	1/2 − [770]	0.025		−6.1(−3)	−0.23		−7.4(−3)			

TABLE C.2. (*Continued*)

		$\langle s_3 \rangle$			$\langle r^2 \rangle$			$\langle r^2 Y_2^0(\cos\theta) \rangle$		
		232	238	244	232	238	244	232	238	244
		0.19	0.22	0.25	0.19	0.22	0.25	0.19	0.22	0.25
Initial state	Final state	−0.04	−0.02	0.0	−0.04	−0.02	0.0	−0.04	−0.02	0.0
	1/2 − [501]	0.24		0.18	0.048		0.07			
	1/2 − [750]	−5.9(−3)		6.6(−3)	0.31		0.08			
1/2 − [770]	1/2 − [770]	0.08	0.07	0.06	9.77	9.98	10.15	3.30	3.33	3.34
	1/2 − [501]	0.011	9.6(−4)	−2.4(−3)	−0.03	−0.03	2.5(−4)			
	1/2 − [750]	0.17	0.16	0.15	−0.14	−0.14	−0.13			
1/2 − [501]	1/2 − [501]	−0.43	−0.45	−0.46	6.37	6.36	6.37	−1.18	−1.20	−1.18
	1/2 − [750]	−5.7(−3)	−2.9(−3)	2.9(−3)	−0.01	−0.02	−4.8(−3)			
1/2 − [750]	1/2 − [750]	0.31	0.32	0.31	8.71	8.81	8.91	3.71	3.79	3.84
3/2 − [512]	3/2 − [512]	−0.35		−0.39	6.70		6.92	0.058		0.096
	3/2 − [501]	−0.20		−0.15	0.03		0.06			
	3/2 − [761]	0.018		−8.7(−3)	0.17		−2.5(−4)			
	3/2 − [752]			8.8(−3)			−0.05			
3/2 − [501]	3/2 − [501]	0.45	0.40	0.48	6.37	7.14	6.37	−1.20	−0.30	−1.20
	3/2 − [761]	0.017	0.13	−3.1(−3)	−0.09	−1.46	4.3(−3)			
	3/2 − [752]		−0.08	3.5(−3)		0.17	0.05			
3/2 − [761]	3/2 − [761]	0.17	0.23	0.16	9.66	9.10	10.05	2.89	2.03	3.00
	3/2 − [752]		0.15	0.18		−0.064	−0.14			
3/2 − [752]	3/2 − [752]		0.29	0.30		8.47	8.60		2.66	2.75
5/2 − [503]	5/2 − [503]	−0.43	−0.45	−0.46	6.38	6.39	6.40	−1.26	−1.26	−1.24
	5/2 − [752]	−0.017	−0.013	6.3(−3)	−0.05	−0.068	0.012			
5/2 − [752]	5/2 − [752]	0.24	0.24	0.23	9.45	9.67	9.86	2.29	2.38	2.45
7/2 − [503]	7/2 − [503]			0.49			6.57			−1.32
	7/2 − [743]			3.6(−3)			0.019			
7/2 − [743]	7/2 − [743]	0.29	0.30	0.30	9.15	9.38	9.59	1.57	1.67	1.75
9/2 − [734]	9/2 − [734]	0.34	0.35	0.35	8.78	9.02	9.24	0.74	0.85	0.94
11/2 − [725]	11/2 − [725]	0.39	0.40	0.40	8.40	8.61	8.82	−0.16	−0.051	0.052
13/2 − [716]	13/2 − [716]	0.44	0.45	0.45	8.07	8.20	8.33	−1.08	−0.99	−0.89

[a] $\langle l_3 \rangle + \langle s_3 \rangle = 0$ for non-diagonal elements and $\langle l_3 \rangle + \langle s_3 \rangle = \Omega$ for diagonal elements.

where

$$g_\Omega = (1/\Omega)[g_s \langle s_3 \rangle + g_l \langle l_3 \rangle] . \quad \text{(C8)}$$

For cases where $I = K = \Omega$ the above equations reduce to

$$\mu = [K^2/(K+1)](g_K - g_R) + g_R K , \quad \text{(C9)}$$

where

$$g_K = (1/K)[g_s \langle s_3 \rangle + g_l \langle l_3 \rangle] . \quad \text{(C10)}$$

The values of g_s for free nucleons are −3.8263 for neutrons and 5.5856 for protons. However, because of core polarization effects, lower values of g_s are usually used. The most commonly used values are

$$g_s^{\text{eff}} = 0.6\, g_s^{\text{free}} . \quad \text{(C11)}$$

Thus for the odd-neutron case $g_s^{\text{eff}} = -2.296$, $g_l = 0$ and for the odd-proton case $g_s^{\text{eff}} = 3.351$ and $g_l = 1$. For g_R, which is roughly Z/A, a value of 0.39 (Browne and Femenia, 1971) is commonly used in the actinides. Using the above values of g_s and g_R, we have calculated the magnetic moments for the single-particle states for which magnetic moments have been experimentally measured. These are included in Table I of the text.

The $M1$ matrix elements can be calculated with the expression (Nilsson, 1955; Browne and Femenia, 1971)

$$G_{M1} = (g_s - g_R)\langle s_3 \rangle + (g_l - g_R)\langle l_3 \rangle, \quad \text{for } \Delta K = 0 \quad \text{(C12)}$$

and

$$G_{M1} = (g_s - g_R)\langle s_+ \rangle + (g_l - g_R)\langle l_+ \rangle, \quad \text{for } |\Delta K| = 1 . \quad \text{(C13)}$$

The reduced transition probability $B(M1)$ between states $K_i I_i$ and $K_f I_f$ is given by

$$B(M1, I_i \to I_f) = (3/4\pi)\mu_0^2 |\langle I_i 1 K_i (K_f - K_i) | I_i 1 I_f K_f \rangle G_{M1}(K_i \to K_f) + (-)^{I_f + K_f} \langle I_i 1 K_i (-K_f - K_i) | I_i 1 I_f - K_f \rangle \times G_{M1}(K_i \to -K_f)|^2 . \quad \text{(C14)}$$

In the above equation $\mu_0 = e\hbar/2Mc$ is the nuclear magneton and the second term has nonzero value only for states $K_i = K_f = \frac{1}{2}$. Note that the $\langle l_+ \rangle$ and $\langle s_+ \rangle$ values between two $K = \frac{1}{2}$ states give the matrix element $G_{M1}(\frac{1}{2} \to -\frac{1}{2})$, and $\langle l_3 \rangle$ and $\langle s_3 \rangle$ give $G_{M1}(\frac{1}{2} \to \frac{1}{2})$. Also note that in our expression we have used $3/4\pi$ instead of $3/16\pi$ used by Browne and Femenia (1971). This is because our $\langle l_3 \rangle$, $\langle s_3 \rangle$, $\langle l_+ \rangle$, and $\langle s_+ \rangle$ are one-half of their respective G_{ML} and G_{MS} values. With respect to interchange of K_i and K_f the $M1$ matrix elements have the following properties (Brockmeier *et al.*, 1965):

$$\left.\begin{aligned} G_{M1}(K_i \to K_f) &= G_{M1}(K_f \to K_i) \\ G_{M1}(K_i \to -K_f) &= G_{M1}(K_f \to -K_i) \end{aligned}\right\} \text{when } K_i = K_f$$
$$\left.\begin{aligned} G_{M1}(K_i \to K_f) &= -G_{M1}(K_f \to K_i) \\ G_{M1}(K_i \to -K_f) &= -G_{M1}(K_f \to -K_i) \end{aligned}\right\} \text{when } K_i \neq K_f . \quad \text{(C15)}$$

3. $\langle r^2 \rangle$, $\langle r^2 Y_2^0(\cos\theta) \rangle$, and $E1$ matrix elements

The matrix element $\langle r^2 \rangle$ given in Tables C.2 and C.5 can be used to calculate $E0$ transition matrix elements.

TABLE C.3. Neutron matrix elements for $E1$ transitions.

		$A = 232$ $\nu_2 = 0.19$ $\nu_4 = -0.04$		$A = 238$ $\nu_2 = 0.22$ $\nu_4 = -0.02$		$A = 244$ $\nu_2 = 0.25$ $\nu_4 = 0.0$	
Initial state	Final state	$K_i \rightarrow K_f$	$K_i \rightarrow -K_f$	$K_i \rightarrow K_f$	$K_i \rightarrow -K_f$	$K_i \rightarrow K_f$	$K_i \rightarrow -K_f$
1/2 + [651]	1/2 − [510]					−0.019	4.7(−3)
	1/2 − [770]					−0.046	−0.073
	1/2 − [501]					−4.1(−3)	−2.2(−3)
	1/2 − [750]					1.43	0.12
	3/2 − [512]					7.7(−3)	
	3/2 − [501]					−1.3(−3)	
	3/2 − [761]					0.040	
	3/2 − [752]					−0.71	
1/2 + [640]	1/2 − [510]	−0.13	−0.028			−0.028	−0.014
	1/2 − [770]	−0.053	0.039	−0.020	0.037	0.014	0.028
	1/2 − [501]	0.016	−0.021	4.8(−3)	−6.6(−3)	−7.5(−3)	3.7(−3)
	1/2 − [750]	−0.82	−0.37	−0.95	−0.38	−1.07	−0.38
	3/2 − [512]	−0.039				−0.020	
	3/2 − [501]	−0.018		0.040		2.0(−3)	
	3/2 − [761]	−0.12		−0.091		−0.069	
	3/2 − [752]			0.46		0.49	
1/2 + [631]	1/2 − [510]	−0.23	0.15			−0.20	0.09
	1/2 − [770]	0.045	−0.020	0.018	−0.021	−6.5(−3)	−0.019
	1/2 − [501]	−0.13	−0.018	−0.078	−0.012	−0.033	−8.2(−3)
	1/2 − [750]	−0.12	0.11	−0.080	0.096	−0.035	0.08
	3/2 − [512]	0.14				0.11	
	3/2 − [501]	−0.021		−0.019		−7.4(−3)	
	3/2 − [761]	0.020		7.5(−3)		7.7(−3)	
	3/2 − [752]			−0.13		−0.11	
1/2 + [620]	1/2 − [510]	1.13	−0.19			1.19	−0.16
	1/2 − [770]	−0.073	1.9(−3)	−0.036	5.8(−3)	1.6(−3)	1.5(−3)
	1/2 − [501]	−0.11	0.034	−0.096	0.022	−0.09	0.016
	1/2 − [750]	0.085	5.3(−3)	0.054	−1.0(−3)	0.024	−4.7(−3)
	3/2 − [512]	2.3(−3)				0.015	
	3/2 − [501]	0.091		0.061		0.045	
	3/2 − [761]	−5.4(−3)		0.017		−0.011	
	3/2 − [752]			0.045		0.034	
3/2 + [642]	1/2 − [510]	0.040				0.017	
	1/2 − [770]	−0.074		−0.066		−0.054	
	1/2 − [501]	0.017		6.9(−3)		−9.0(−4)	
	1/2 − [750]	0.28		0.25		0.24	
	3/2 − [512]	−0.13				−0.043	
	3/2 − [501]	0.025		0.021		−8.2(−3)	
	3/2 − [761]	−0.010		−0.030		−0.055	
	3/2 − [752]			1.24		1.22	
	5/2 − [503]	0.024		8.2(−3)		−2.5(−3)	
	5/2 − [752]	0.097		0.069		0.044	
3/2 + [631]	1/2 − [510]	−0.085				−0.05	
	1/2 − [770]	4.6(−3)		0.011		0.012	
	1/2 − [501]	8.2(−3)		6.5(−3)		4.2(−3)	
	1/2 − [750]	−0.17		−0.18		−0.19	
	3/2 − [512]	−0.092				−0.11	
	3/2 − [501]	−0.11		−0.033		−0.019	
	3/2 − [761]	−0.086		−0.068		−5.2(−3)	
	3/2 − [752]			−0.99		−1.05	
	5/2 − [503]	0.020		0.014		8.2(−3)	
	5/2 − [752]	−0.10		−0.078		−0.051	
3/2 + [622]	1/2 − [510]	0.24				0.11	
	1/2 − [770]	5.7(−3)		−5.9(−3)		−8.2(−3)	
	1/2 − [501]	−0.043		−0.020		−8.2(−3)	
	1/2 − [750]	4.2(−3)		0.012		0.017	
	3/2 − [512]	1.09				1.18	
	3/2 − [501]	−0.23		−0.18		−0.15	
	3/2 − [761]	0.078		−0.051		−6.5(−3)	
	3/2 − [752]			−0.078		−0.036	
	5/2 − [503]	−0.085		−0.066		−0.054	
	5/2 − [752]	0.016		0.013		3.8(−3)	

TABLE C.3. (*Continued*)

Initial state	Final state	$A=232$, $\nu_2=0.19$, $\nu_4=-0.04$		$A=238$, $\nu_2=0.22$, $\nu_4=-0.02$		$A=244$, $\nu_2=0.25$, $\nu_4=0.0$	
		$K_i \to K_f$	$K_i \to -K_f$	$K_i \to K_f$	$K_i \to -K_f$	$K_i \to K_f$	$K_i \to -K_f$
5/2 + [633]	3/2 − [512]	−0.082				−0.022	
	3/2 − [501]	0.016		0.029		7.3(−3)	
	3/2 − [761]	−0.039		−0.031		−0.038	
	3/2 − [752]			0.22		0.20	
	5/2 − [503]	0.097		0.060		0.029	
	5/2 − [752]	0.016		−0.024		−0.052	
	7/2 − [503]					0.016	
	7/2 − [743]	0.090		0.064		0.044	
5/2 + [622]	3/2 − [512]	0.096				0.098	
	3/2 − [501]	−0.024		−0.013		−0.012	
	3/2 − [761]	−0.021		−0.012		4.5(−3)	
	3/2 − [752]			−0.16		−0.15	
	5/2 − [503]	0.040		0.042		0.052	
	5/2 − [752]	−0.10		−0.058		−0.013	
	7/2 − [503]					−0.098	
	7/2 − [743]	−0.067		−0.052		−0.031	
7/2 + [624]	5/2 − [503]	0.036		0.011		−2.5(−3)	
	5/2 − [752]	−0.010		−0.023		−0.024	
	7/2 − [503]					0.17	
	7/2 − [743]	0.053		−7.3(−3)		−0.045	
	9/2 − [734]	0.077		0.055		0.041	
7/2 + [613]	5/2 − [503]	−0.052		−0.066		−0.068	
	5/2 − [752]	−0.037		−0.016		5.1(−4)	
	7/2 − [503]					−0.83	
	7/2 − [743]	−0.087		−0.058		−0.013	
	9/2 − [734]	−0.023		−0.025		−0.016	
9/2 + [615]	7/2 − [503]					−0.24	
	7/2 − [743]	0.015		−0.011		−0.015	
	9/2 − [734]	0.071		7.1(−3)		−0.034	
	11/2 − [725]	0.040		0.041		0.035	
9/2 + [604]	7/2 − [503]					1.54	
	7/2 − [743]	−0.024		−0.016		−1.5(−3)	
	9/2 − [734]	−0.014		−0.039		−0.011	
	11/2 − [725]	0.025		−1.7(−3)		−3.9(−3)	
11/2 + [615]	9/2 − [734]	0.28		0.26		0.24	
	11/2 − [725]	1.05		1.09		1.13	
	13/2 − [716]	−1.76		−1.76		−1.76	
11/2 + [606]	9/2 − [734]	−5.8(−3)		−8.1(−3)			
	11/2 − [725]	0.021		1.6(−3)			
	13/2 − [716]	0.020		0.024			
13/2 + [606]	11/2 − [725]	0.16		0.15		0.13	
	13/2 − [716]	0.73		0.77		0.80	

So far no $E0$ transition has been observed in odd-mass actinides.

The diagonal $\langle r^2 Y_2^0 \rangle$ matrix elements are included in Table C.2 and C.5 in order to further characterize the single-particle state, and can be used to calculate nuclear quadrupole moments. The $\langle r^2 Y_2^0 \rangle$ matrix element is related to the asymptotic quantum numbers n_z and $n_\perp$ as follows:

$$\langle r^2 Y_2^0 \rangle \simeq \sqrt{5/4\pi}\,[\langle n_z + \tfrac{1}{2} \rangle - \tfrac{1}{2}\langle n_\perp + 1 \rangle]\,, \tag{C16a}$$

where

$$\langle n_\perp \rangle = \langle N - n_z \rangle\,. \tag{C16b}$$

The electric quadrupole moment of a nucleus can be calculated with the following equation:

$$Q = \sum_i 2V_i^2 \langle r^2 Y_2^0 \rangle_i\,. \tag{C17}$$

The $E1$ matrix elements G_{E1} are listed in Tables C.2 and C.6. The $B(E1)$ value from state $K_i I_i$ to $K_f I_f$ is given by the expression (Nilsson, 1955)

$$\begin{aligned} B(E1) = e^2 \left(1 - \frac{Z}{A}\right)^2 \left(\frac{\hbar}{M\omega_0}\right) \frac{3}{4\pi} \\ \times [\langle I_i 1 K_i (K_f - K_i) | I_i 1 I_f K_f \rangle G_{E1}(K_i \to K_f) \\ + (-)^{I_f + K_f} \langle I_i 1 K_i (-K_f - K_i) | I_i 1 I_f - K_f \rangle \\ \times G_{E1}(K_i \to -K_f)]^2\,. \end{aligned} \tag{C18}$$

TABLE C.4. Proton matrix elements $\langle j_+ \rangle$, $\langle l_+ \rangle$,[a] and $\langle s_+ \rangle$.

		$\langle j_+ \rangle$			$\langle s_+ \rangle$		
		$A=232$	238	244	$A=232$	238	244
		$Z=92$	94	96	$Z=92$	94	96
		$\nu_2=0.19$	0.22	0.25	$\nu_2=0.19$	0.22	0.25
Initial state	Final state	$\nu_4=-0.04$	−0.02	0.0	$\nu_4=-0.04$	−0.02	0.0
1/2 + [660]	1/2 + [660]	−5.87	−6.52	−6.59	−0.62	−0.58	−0.57
	1/2 + [400]	1.79	0.43	−0.02	−0.10	−0.02	4.9(−3)
	1/2 + [651]	1.11	1.02	0.87	−0.29	−0.33	−0.36
	3/2 + [402]	0.04	0.43	0.34	0.05	0.05	0.03
	3/2 + [651]	6.17	6.51	6.56	0.51	0.53	0.54
1/2 + [400]	1/2 + [400]	−1.16	−0.60	−0.59	−0.94	−0.98	−0.98
	1/2 + [651]	−0.25	−6.3(−3)	−5.8(−3)	0.09	0.03	−5.2(−3)
	3/2 + [402]	−0.65	−0.61	−0.55	0.03	0.03	0.02
	3/2 + [651]	−1.98	−0.40	−0.05	−0.16	−0.04	−5.0(−3)
1/2 + [651]	1/2 + [651]	−0.53	0.34	1.23	−0.68	−0.66	−0.64
	3/2 + [402]	−0.15	−0.13	−0.03	−0.02	−0.03	−0.03
	3/2 + [651]	−1.12	−0.91	−0.72	−0.41	−0.44	−0.46
3/2 + [402]	5/2 + [642]	0.36	0.52	0.33	−0.01	0.02	0.02
3/2 + [651]	5/2 + [642]	6.42	6.42	6.42	0.48	0.49	0.50
5/2 + [642]	7/2 + [633]	6.20	6.17	6.14	0.43	0.44	0.45
7/2 + [633]	9/2 + [624]	5.70	5.68	5.65	0.39	0.39	0.39
9/2 + [624]	11/2 + [615]	4.89	4.88	4.87	0.34	0.33	0.32
11/2 + [615]	13/2 + [606]	3.60	3.61	3.62	0.26	0.25	0.23
1/2 − [541]	1/2 − [541]	−2.81	−3.16	−3.43	0.43	0.43	0.45
	1/2 − [530]	−3.02	−2.72	−2.40	−0.18	−0.17	−0.16
	1/2 − [521]	−0.23	−0.32	−0.42	−0.09	−0.07	−0.06
	1/2 − [770]	0.07	0.05	−4.8(−4)	−0.05	−0.05	−0.05
	3/2 − [532]	4.13	4.16	4.15	−0.35	−0.36	−0.38
	3/2 − [521]	0.01	0.10	0.22	−0.10	−0.08	−0.06
	3/2 − [761]	8.7(−3)	−6.1(−4)	−0.03	0.05	0.05	0.05
1/2 − [530]	1/2 − [530]	1.80	2.01	2.22	0.78	0.80	0.80
	1/2 − [521]	−2.42	−2.34	−2.25	0.31	0.31	0.32
	1/2 − [770]	−0.09	−0.06	0.01	−0.06	−0.04	−0.02
	3/2 − [532]	0.91	0.82	0.69	−0.21	−0.19	−0.18
	3/2 − [521]	3.86	3.74	3.63	0.34	0.36	0.34
	3/2 − [761]	−0.24	−0.13	0.01	0.05	0.04	0.02
1/2 − [521]	1/2 − [521]	−0.80	−0.96	−1.02	0.23	0.21	0.21
	1/2 − [770]	1.33	0.67	0.03	0.07	0.03	−0.01
	3/2 − [532]	1.98	1.87	1.78	0.14	0.13	0.12
	3/2 − [521]	−0.91	−0.86	−0.83	−0.80	−0.82	−0.83
	3/2 − [761]	1.47	0.74	0.02	−0.04	−0.01	0.02
1/2 − [770]	1/2 − [770]	7.29	7.51	7.60	0.56	0.56	0.55
	3/2 − [532]	−0.06	−0.04	−0.02	−0.07	−0.05	−0.04
	3/2 − [521]	−0.64	−0.36	−0.02	0.08	0.04	−0.01
	3/2 − [761]	7.23	7.49	7.57	0.54	0.53	0.53
3/2 − [532]	5/2 − [523]	4.30	4.28	4.24	−0.34	−0.35	−0.35
	5/2 − [512]	−0.01	0.03	0.08	−0.08	−0.06	−0.04
	5/2 − [752]	0.03	−0.01	−0.06	0.06	0.06	0.06
3/2 − [521]	5/2 − [523]	0.63	0.58	0.53	−0.13	−0.11	−0.11
	5/2 − [512]	3.61	3.55	3.52	0.33	0.30	0.29
	5/2 − [752]	−0.56	−0.25	3.1(−3)	8.1(−3)	0.02	0.02
3/2 − [761]	5/2 − [523]	0.45	0.23	−6.3(−3)	−3.7(−3)	−0.02	−0.03
	5/2 − [512]	−0.61	−0.38	−0.03	−0.17	−0.11	−0.01
	5/2 − [752]	7.33	7.45	7.48	0.47	0.49	0.51
5/2 − [523]	7/2 − [514]	3.91	3.87	3.88	−0.31	−0.31	−0.29
5/2 − [512]	7/2 − [514]	0.55	0.49	0.47	−0.08	−0.07	−0.06
5/2 − [752]	7/2 − [514]	0.20	0.11	−0.01	−5.3(−3)	−0.01	−0.02
7/2 − [514]	9/2 − [505]	2.97	2.98	3.00	−0.25	−0.23	−0.21
9/2 − [505]	11/2 − [505]	−0.12	−0.19	−0.25	−0.93	−0.94	−0.95

[a] The matrix element $\langle l_+ \rangle$ can be obtained from the relation $\langle l_+ \rangle = \langle j_+ \rangle - \langle s_+ \rangle$.

TABLE C.5. Proton matrix elements $\langle l_3 \rangle$,[a] $\langle s_3 \rangle$, $\langle r^2 \rangle$, and $\langle r^2 Y_2^0(\cos\theta) \rangle$.

		$\langle s_3 \rangle$			$\langle r^2 \rangle$			$\langle r^2 Y_2^0(\cos\theta) \rangle$		
		$A=232$	238	244	$A=232$	238	244	$A=232$	238	244
		$Z=92$	94	96	$Z=92$	94	96	$Z=92$	94	96
		$\nu_2=0.19$	0.22	0.25	$\nu_2=0.19$	0.22	0.25	$\nu_2=0.19$	0.22	0.25
Initial state	Final state	$\nu_4=-0.04$	−0.02	0.0	$\nu_4=-0.04$	−0.02	0.0	$\nu_4=-0.04$	−0.02	0.0
1/2 + [660]	1/2 + [660]	0.12	0.08	0.07	8.34	8.87	9.05	2.57	2.91	2.93
	1/2 + [400]	0.10	0.02	−4.9(−3)	−1.06	−0.23	0.01			
	1/2 + [651]	0.29	0.33	0.36	−0.14	−0.11	−0.10			
1/2 + [400]	1/2 + [400]	0.44	0.48	0.48	5.26	4.97	5.00	−0.45	−0.76	−0.75
	1/2 + [651]	−0.09	−0.02	5.2(−3)	−0.11	−0.04	−0.02			
1/2 + [651]	1/2 + [651]	0.18	0.16	0.14	7.17	7.33	7.49	2.82	2.88	2.90
3/2 + [402]	3/2 + [402]	−0.42	−0.43	−0.46	5.15	5.15	5.21	−0.84	−0.85	−0.82
	3/2 + [651]	0.05	0.05	−0.04	0.23	0.31	−0.19			
3/2 + [651]	3/2 + [651]	0.19	0.18	0.18	8.49	8.72	8.87	2.46	2.51	2.57
5/2 + [642]	5/2 + [642]	0.26	0.26	0.26	8.29	8.50	8.70	1.86	1.94	2.00
7/2 + [633]	7/2 + [633]	0.33	0.33	0.33	7.94	8.16	8.38	1.10	1.19	1.27
9/2 + [624]	9/2 + [624]	0.37	0.38	0.39	7.51	7.71	7.97	0.20	0.31	0.41
11/2 + [615]	11/2 + [615]	0.43	0.44	0.45	7.13	7.27	7.46	−0.75	−0.65	−0.54
13/2 + [606]	13/2 + [606]	0.50	0.50	0.50	6.89	6.86	6.85	−1.69	−1.62	−1.55
1/2 − [541]	1/2 − [541]	−0.07	−0.07	−0.06	7.48	7.63	7.77	2.67	2.71	2.74
	1/2 − [530]	−0.18	−0.17	−0.16	0.07	0.07	0.08			
	1/2 − [521]	−0.09	−0.07	−0.06	0.04	0.07	0.10			
	1/2 − [770]	−0.05	−0.05	−0.05	0.02	−0.03	−0.07			
1/2 − [530]	1/2 − [530]	0.28	0.30	0.30	7.04	7.14	7.25	2.13	2.25	2.37
	1/2 − [521]	0.31	0.31	0.32	0.07	0.07	0.05			
	1/2 − [770]	−0.06	−0.04	−0.02	−0.34	−0.16	0.03			
1/2 − [521]	1/2 − [521]	−0.27	−0.29	−0.29	6.24	6.35	6.52	1.33	1.38	1.44
	1/2 − [770]	0.07	0.03	−0.01	0.47	0.23	6.9(−3)			
1/2 − [770]	1/2 − [770]	0.05	0.06	0.05	8.54	8.85	9.08	2.82	2.90	2.93
3/2 − [532]	3/2 − [532]	−0.22	−0.22	−0.20	7.15	7.34	7.53	1.69	1.76	1.83
	3/2 − [521]	−0.14	−0.14	−0.13	0.08	0.08	0.07			
	3/2 − [761]	−0.06	−0.06	−0.05	−0.07	−0.01	−0.08			
3/2 − [521]	3/2 − [521]	0.35	0.37	0.38	6.47	6.61	6.79	1.12	1.20	1.28
	3/2 − [761]	0.06	0.02	−0.01	−0.46	−0.24	−8.9(−3)			
3/2 − [761]	3/2 − [761]	0.15	0.15	0.14	8.39	8.73	8.97	2.51	2.62	2.68
5/2 − [523]	5/2 − [523]	−0.31	−0.31	−0.31	6.70	6.91	7.13	0.71	0.79	0.86
	5/2 − [512]	−0.12	−0.11	−0.11	0.08	0.08	0.08			
	5/2 − [752]	−0.04	−0.04	−0.04	0.10	0.01	−0.07			
5/2 − [512]	5/2 − [512]	0.40	0.42	0.44	5.89	6.02	6.20	0.04	0.08	0.16
	5/2 − [752]	0.02	7.8(−3)	−9.1(−3)	−0.49	−0.28	−0.03			
5/2 − [752]	5/2 − [752]	0.23	0.22	0.21	8.17	8.50	8.76	2.06	2.17	2.25
7/2 − [514]	7/2 − [514]	−0.37	−0.38	−0.38	6.26	6.44	6.62	−0.30	−0.24	−0.18
9/2 − [505]	9/2 − [505]	−0.43	−0.44	−0.45	5.96	6.00	6.02	−1.34	−1.32	−1.27
11/2 − [505]	11/2 − [505]	0.50	0.50	0.50	6.97	6.97	6.98	−1.64	−1.59	−1.52

[a] The matrix element $\langle l_3 \rangle$ can be obtained from the expressions $\langle l_3 \rangle + \langle s_3 \rangle = 0$ for nondiagonal elements and $\langle l_3 \rangle + \langle s_3 \rangle = \Omega$ for diagonal elements.

TABLE C.6. $E1$ matrix elements for proton states.

		$A=232$, $Z=92$, $\nu_2=0.19$, $\nu_4=-0.04$		$A=238$, $Z=94$, $\nu_2=0.22$, $\nu_4=-0.02$		$A=244$, $Z=96$, $\nu_2=0.25$, $\nu_4=0.0$	
Initial state	Final state	$K_i \to K_f$	$K_i \to -K_f$	$K_i \to K_f$	$K_i \to -K_f$	$K_i \to K_f$	$K_i \to -K_f$
1/2 + [660]	1/2 − [541]	0.07	−0.13	0.07	−0.12	0.07	−0.08
	1/2 − [530]	−7.2(−3)	0.09	−0.02	0.07	−0.05	0.05
	1/2 − [521]	−0.22	−0.12	−0.09	−0.06	5.3(−3)	−0.02
	1/2 − [770]	−1.61	−0.74	−1.70	−0.81	−1.71	−0.84
	3/2 − [532]	0.08		0.07		0.06	
	3/2 − [521]	−0.08		−0.05		−0.02	
	3/2 − [761]	0.87		0.95		0.98	

TABLE C.6. (*Continued*)

		$A=232$, $Z=92$, $\nu_2=0.19$, $\nu_4=-0.04$		$A=238$, $Z=94$, $\nu_2=0.22$, $\nu_4=-0.02$		$A=244$, $Z=96$, $\nu_2=0.25$, $\nu_4=0.0$	
Initial state	Final state	$K_i \to K_f$	$K_i \to -K_f$	$K_i \to K_f$	$K_i \to -K_f$	$K_i \to K_f$	$K_i \to -K_f$
1/2 + [400]	1/2 − [541]	−0.01	0.06	−9.6(−3)	0.014	0.01	1.5(−3)
	1/2 − [530]	−0.13	−4.6(−3)	−0.06	0.01	4.1(−4)	−0.01
	1/2 − [521]	−0.04	−0.10	−0.09	−0.09	0.09	0.08
	1/2 − [770]	0.46	0.24	0.07	0.05	−2.1(−3)	−2.8(−3)
	3/2 − [532]	−9.0(−3)		4.4(−3)		−4.3(−3)	
	3/2 − [521]	−0.07		−0.07		0.06	
	3/2 − [761]	−0.27		−0.05		3.2(−3)	
1/2 + [651]	1/2 − [541]	−1.44	−0.20	−1.48	−0.29	−1.52	−0.38
	1/2 − [530]	0.72	−0.40	0.69	−0.37	0.63	−0.33
	1/2 − [521]	0.05	0.12	0.02	0.08	−8.9(−3)	0.06
	1/2 − [770]	0.05	0.12	0.06	0.10	0.06	0.07
	3/2 − [532]	−0.36		−0.38		−0.40	
	3/2 − [521]	0.17		0.13		0.10	
	3/2 − [761]	−0.11		−0.07		−0.04	
3/2 + [402]	1/2 − [541]	0.02		4.4(−3)		1.5(−3)	
	1/2 − [530]	0.02		0.03		−0.01	
	1/2 − [521]	−0.16		−0.13		0.11	
	1/2 − [770]	−0.01		−0.05		−0.04	
	3/2 − [532]	0.11		0.06		−0.01	
	3/2 − [521]	0.02		0.05		−0.07	
	3/2 − [761]	−0.23		−0.21		−0.08	
	5/2 − [523]	0.06		0.04		−0.02	
	5/2 − [512]	−0.09		−0.09		0.08	
	5/2 − [752]	0.07		0.10		0.06	
3/2 + [651]	1/2 − [541]	−0.08		−0.05		−0.03	
	1/2 − [530]	0.17		0.13		0.09	
	1/2 − [521]	−0.08		−0.04		−0.01	
	1/2 − [770]	−0.65		−0.68		−0.70	
	3/2 − [532]	0.05		0.06		0.08	
	3/2 − [521]	0.12		0.05		−0.02	
	3/2 − [761]	−1.60		−1.63		−1.66	
	5/2 − [523]	0.05		0.04		0.04	
	5/2 − [512]	−0.03		−0.02		−0.02	
	5/2 − [752]	1.08		1.11		1.13	
5/2 + [642]	3/2 − [532]	−0.08		−0.06		−0.04	
	3/2 − [521]	0.15		0.11		0.06	
	3/2 − [761]	−0.56		−0.57		−0.57	
	5/2 − [523]	0.01		0.04		0.07	
	5/2 − [512]	0.20		0.10		8.8(−4)	
	5/2 − [752]	−1.53		−1.56		−1.58	
	7/2 − [514]	0.03		−0.02		0.02	
7/2 + [633]	5/2 − [523]	−0.08		−0.06		−0.05	
	5/2 − [512]	0.12		0.08		0.04	
	5/2 − [752]	−0.47		−0.46		−0.45	
	7/2 − [514]	−0.02		0.02		0.05	
	9/2 − [505]	8.6(−3)		0.01		8.2(−3)	
9/2 + [624]	7/2 − [514]	−0.06		−0.05		−0.04	
	9/2 − [505]	−0.03		−1.6(−3)		0.03	
	11/2 − [505]	−0.18		−0.17		−0.15	
11/2 + [615]	9/2 − [505]	−0.03		−0.03		−0.03	
	11/2 − [505]	−0.73		−0.78		−0.83	
13/2 + [606]	11/2 − [505]	1.76		1.75		1.73	

In the above equation the second term is nonzero only when $K_i = K_f = \frac{1}{2}$. The values of ω_0 in this equation are $\hbar\omega_0 = 7.5$ MeV for neutrons and 7.9 MeV for protons in our calculations. For $M = 244$, the above values of $\hbar\omega_0$ correspond to $\hbar/M\omega_0 = 5.26 \times 10^{-26}$ cm^2 for protons and 5.54×10^{-26} cm^2 for neutrons.

APPENDIX D: ANOMALOUS CONVERSION COEFFICIENTS

In the actinide region there are several $E1$ transitions known, for which the K, L_1, L_2, M_1, and M_2 experimental conversion coefficients are larger than the theoretical

TABLE D.1. Anomalous $E1$ conversion coefficients.

Nucleus	Initial state $(IK\pi)$	Final state $(IK\pi)$	Transition energy (keV)	Shell	$\frac{(ICC)_{exptl}}{(ICC)_{theo}}$ [s]	Ref.
^{231}Pa	5/2 3/2 + [651]	3/2 1/2 − [530]	84.17	L_1	20 ±3	a
				L_2	16 ±4	
				L_3	1.2 ±0.4	
				M_1	23	
				M_2	22	
				M_3	1.0	
^{233}Pa	5/2 3/2 + [651]	3/2 1/2 − [530]	86.3	L_1	5.7 ±2.4	a
				L_2	15 ±7	
				L_3	2.2 ±2.2	
^{237}Np	5/2 5/2 − [523]	5/2 5/2 + [642]	59.54	L_1	1.76 ±0.21	b
				L_2	3.1 ±0.3	
				L_3	1.1 ±0.1	
				M_1	1.9 ±0.3	
				M_2	4.6 ±0.6	
				M_3	1.1 ±0.2	
				M_4	1.4 ±0.5	
				M_5	1.5 ±0.5	
	5/2 5/2 − [523]	7/2 5/2 + [642]	26.35	L_3	1.00 ±0.13	
				M_1	2.4 ±0.4	
				M_2	3.2 ±0.5	
				M_3	1.2 ±0.2	
				M_4	0.8 ±0.2	
				M_5	1.3 ±0.2	
^{239}Pu	7/2 7/2 − [743]	5/2 5/2 + [622]	106.1	L_1	1.51 ±0.18	c
				L_2	2.86 ±0.29	
^{241}Am	3/2 3/2 − [521]	5/2 5/2 + [642]	265.92	K	98 ±14	d
				L_1	148 +11	
				L_2	195 ±40	
				M_1	220 ±35	
				M_2	122 ±80	
^{245}Cm	9/2 9/2 − [734]	7/2 7/2 + [624]	388.1	K	1.98 ±0.35	e
				L	2.3 ±0.5	
		9/2 7/2 + [624]	333.3	K	1.59 ±0.29	
				L	1.79 ±0.36	
		11/2 7/2 + [624]	266.6	K	2.26 ±0.45	
^{247}Cf	9/2 9/2 − [734]	7/2 7/2 + [624]	480.6	K	3.43 ±0.35	f
				L	4.3 ±1.4	

[a] Asaro *et al.* (1960).
[b] Yamazaki and Hollander (1966).
[c] Ewan *et al.* (1957).
[d] Porter *et al.* (1974).
[e] Ahmad (1966).
[f] Ahmad *et al.* (1973a).
[s] Theoretical values of ICC were taken from Hager and Seltzer (1968).

values (Hager and Seltzer, 1968), but the L_3 and M_3 conversion coefficients are in agreement with theory. In most of these cases the lifetimes of the γ transitions were measured and were found to be retarded relative to single-particle estimates (Moszkowski, 1965), the retardation factor being 10^3–10^7. The data on anomalous $E1$ conversion coefficients in L and M shells were reviewed by Asaro *et al.* (1960) who found a correlation between the anomaly factor and the γ-ray retardation factor. In their analysis they found a maximum anomaly for the 84.2 keV transition in ^{231}Pa, where the experimental L_1 conversion coefficient is 21 times larger than the theoretical value.

A theoretical explanation for anomalous $M1$ conversion was first given by Church and Weneser (1956), and the theory of anomalous $E1$ conversion coefficients was developed by Nilsson and Rasmussen (1958). According to these theories the anomalous conversion process occurs due to the penetration of the electron wave function into the nuclear volume. This introduces an additional term in the expression for the conversion electron transition. The magnitude of this "penetration" term is generally much smaller than the "normal" term and hence one does not see its effect on measured conversion coefficients. However, when the γ-transition lifetime is retarded, the "normal" term is also retarded, which in effect makes the contribution of the "penetration" term to the conversion coefficient significant. Because K, L_1, L_2, M_1, and M_2 electrons have larger probability distributions at the nucleus than do the L_3 and M_3 electrons, they exhibit anomalous conversion coefficients. From their analysis Nilsson and Rasmussen (1958) concluded that anomalous $E1$ conversion coefficients occur only for transitions retarded by a factor of greater than

10^5. However, if the transitions are retarded due to K-forbiddenness they have normal conversion coefficients. Selection rules in the asymptotic quantum numbers were also derived for anomalous $M1$ and $E1$ conversion coefficients.

Anomalies in K shell conversion coefficients have also been observed (Ahmad, 1966; Ahmad *et al.*, 1973; Porter *et al.*, 1974). The maximum anomaly occurs for the 266.6 keV transition in ^{241}Am, where the experimental conversion coefficient is 98 times the theoretical value. The data on anomalous conversion coefficients are summarized in Table D.1.

So far only one case of anomalous $M1$ conversion coefficients has been reported in the actinide region (Porter *et al.*, 1974). Penetration matrix elements for $M1$ transitions between various single-particle states are tabulated by Krpić *et al.* (1973).

REFERENCES

Abraham, M. M., L. A. Boatner, C. B. Finch, R. W. Reynolds, and H. Zeldes, 1970, Phys. Rev. B **1**, 3555.

Abraham, M. M., L. A. Boatner, C. B. Finch, R. W. Reynolds, and W. P. Unruh, 1973, Phys. Lett. A**44**, 527.

Ahmad, I., 1966, Lawrence Radiation Laboratory Report No. UCRL-16888.

Ahmad, I., A. M. Friedman, R. F. Barnes, R. K. Sjoblom, J. Milsted, and P. R. Fields, 1967, Phys. Rev. **164**, 1537.

Ahmad, I., A. M. Friedman, and J. P. Unik, 1968, Nucl. Phys. A **119**, 27.

Ahmad, I., R. K. Sjoblom, R. F. Barnes, E. P. Horwitz, and P. R. Fields, 1970, Nucl. Phys. A **140**, 141.

Ahmad, I., F. T. Porter, M. S. Freedman, R. F. Barnes, R. K. Sjoblom, F. Wagner, Jr., J. Milsted, and P. R. Fields, 1971, Phys. Rev. C **3**, 390.

Ahmad, I., J. Milsted, R. K. Sjoblom, J. Lerner, and P. R. Fields, 1973, Phys. Rev. C **8**, 737.

Ahmad, I., R. K. Sjoblom, F. Wagner, Jr., and P. R. Fields, 1973, Bull. Am. Phys. Soc. **18**, 1597.

Ahmad, I. and J. Milsted, 1975, Nucl. Phys. A **239**, 1.

Ahmad, I., F. T. Porter, M. S. Freedman, R. K. Sjoblom, J. Lerner, R. F. Barnes, J. Milsted, and P. R. Fields, 1975, Phys. Rev. C **12**, 541.

Ahmad, I., D. D. Sharma, and R. K. Sjoblom, 1976, Nucl. Phys. A **258**, 221.

Ahmad, I., R. K. Sjoblom, and P. R. Fields, 1976, Phys. Rev. C **14**, 218.

Ahmad, I., S. W. Yates, A. M. Friedman, and R. K. Sjoblom, 1976, to be published.

Ahmad, I., R. K. Sjoblom, and J. Milsted, 1976, unpublished data.

Ahmad, I., A. M. Friedman, R. R. Chasman, and S. W. Yates, 1977, Phys. Rev. Lett. **39**, 12.

Alaga, G., K. Alder, A. Bohr, and B. R. Mottelson, 1955, K. Dan. Vidensk. Selsk. Mat.-Fys. Medd. **29**, No. 9.

Alaga, G., 1957, Nucl. Phys. **4**, 625.

Albridge, R. G., J. M. Hollander, C. J. Gallagher, and J. H. Hamilton, 1961, Nucl. Phys. **27**, 529.

Anderson, B. L., B. B. Back, and J. M. Bang, 1970, Nucl. Phys. A **147**, 33.

Armstrong, L., Jr., and R. Marrus, 1966, Phys. Rev. **144**, 994.

Arseniev, D. A., L. A. Malov, U. V. Paskevitch, and V. G. Soloviev, 1968, Dubna preprint ER-3703.

Arvieu, R. and M. Veneroni, 1960, C. R. Acad. Sci. (Paris) **250**, 992, 2155.

Asaro, F., F. S. Stephens, J. M. Hollander, and I. Perlman, 1960, Phys. Rev. **117**, 492.

Asaro, F. and I. Perlman, 1967, Phys. Rev. **158**, 1073.

Ascuitto, R. J., N. K. Glendenning, and B. Sorenson, 1972, Nucl. Phys. A **183**, 60.

Axe, J. D., H. P. Stapleton, and C. D. Jeffries, 1961, Phys. Rev. **121**, 1630.

Bakke, F. H., 1958, Nucl. Phys. **9**, 670.

Bang, J. and F. A. Gareev, 1974, Nucl. Phys. A **232**, 45.

Baranger, M., 1960, Phys. Rev. **120**, 957.

Baranov, S. A., V. M. Kulakov, and S. N. Belenky, 1963, Nucl. Phys. **41**, 95.

Baranov, S. A., V. M. Kulakov, and V. M. Shatinsky, 1964, Nucl. Phys. **56**, 252.

Baranov, S. A., V. M. Shatinskii, V. M. Kulakov, and Yu. F. Rodionov, 1973, Zh. Eksp. Teor. Fiz. **64**, 1970–1973 [Sov. Phys.-JETP **37**, 993 (1973)].

Baranov, S. A. and V. M. Shatinskii, 1975, Yad. Fiz. **22**, 670–673 [Sov. J. Nucl. Phys. **22**, 346 (1975)].

Bardeen, J., L. N. Cooper, and J. R. Schrieffer, 1957a, Phys. Rev. **106**, 162.

Bardeen, J., L. N. Cooper, and J. R. Schrieffer, 1957b, Phys. Rev. **108**, 1175.

Bassel, R. H., R. M. Drisko, and G. R. Satchler, 1962, Oak Ridge National Laboratory Report No. ORNL-3240 (unpublished).

Belyaev, S. T., 1959, K. Dan. Vidensk. Selsk. Mat.-Fys. Medd. **31**, No. 11.

Belyaev, S. T. and V. G. Zelevinsky, 1962, Nucl. Phys. **39**, 582.

Bemis, C. E., F. K. McGowan, J. L. C. Ford, W. T. Milner, P. H. Stelson, and R. L. Robinson, 1973, Phys. Rev. C **8**, 1466.

Bengtson, R., 1975, Nucl. Phys. A **245**, 39.

Bès, D. R., 1961, K. Dan. Vidensk. Selsk. Mat.-Fys. Medd. **33**, No. 2.

Bès, D. R., 1966, private communication.

Bès, D. R. and Y. C. Cho, 1966, Nucl. Phys. **86**, 581.

Bès, D. R. and R. Sorenson, 1969, in *Advances in Nuclear Physics*, edited by M. Baranger and E. Vogt (Plenum, New York), Vol. III.

Bès, D. R. and Z. Szymanski, 1961, Nucl. Phys. **28**, 42.

Bès, D. R., R. A. Broglia, and B. Nilsson, 1972, Phys. Lett. B **40**, 338.

Bisgård, K. M., P. Dahl, P. Hornshøj, and A. B. Knutsen, 1963, Nucl. Phys. **41**, 21.

Blinowska, K. J., P. G. Hansen, H. L. Nielsen, G. Schult, and K. Wien, 1964, Nucl. Phys. **55**, 331.

Blomquist, J. and S. Wahlborn, 1960, Ark. Fys. **16**, 545.

Boatner, L. A., R. W. Reynolds, C. B. Finch, and M. M. Abraham, 1972, Phys. Lett. A**42**, 93.

Bogoliubov, N. N., 1958, JETP Lett. **7**, 41.

Bohr, A., 1951, Phys. Rev. **81**, 134.

Bohr, A., 1952, K. Dan. Vidensk. Selsk. Mat.-Fys. Medd. **26**, No. 14.

Bohr, A., 1976, Rev. Mod. Phys. **48**, 365.

Bohr, A. and B. R. Mottelson, 1953, K. Dan. Vidensk. Selsk. Mat.-Fys. Medd. **27**, No. 16.

Bohr, A., P. O. Froman, and B. R. Mottelson, 1955, Dan. Mat. Fys. Medd. **29**, No. 10.

Bohr, A. and B. R. Mottelson, 1955, in *Beta- and Gamma-ray Spectroscopy*, edited by K. Siegbahn (North-Holland, Amsterdam).

Bohr, A., B. R. Mottelson, and D. Pines, 1958, Phys. Rev. **110**, 936.

Bohr, A. and B. R. Mottelson, 1969, *Nuclear Structure* (Benjamin, New York), Vol. I.

Bohr, A. and B. R. Mottelson, 1975, *Nuclear Structure* (Benjamin, Reading, Mass.), Vol. II.

Boisson, J. P. and R. Peipenbring, 1971, Nucl. Phys. A **168**, 385.

Bollinger, L. M. and G. E. Thomas, 1972, Phys. Rev. C **6**, 1322.

Bolsterli, M., E. O. Fiset, J. R. Nix, and J. L. Norton, 1972, Phys. Rev. C **5**, 1050.
Boyno, J. S., Th. W. Elze, and J. R. Huizenga, 1970, Nucl. Phys. A **157**, 263.
Brack, M., J. Damgaard, A. S. Jensen, H. C. Pauli, V. M. Strutinsky, and C. Y. Wong, 1972, Rev. Mod. Phys. **44**, 320.
Brack, M., T. Ledergerber, and H. C. Pauli, 1974, Nucl. Phys. **234**, 185.
Braid, T. H., R. R. Chasman, J. R. Erskine, and A. M. Friedman, 1965, Phys. Lett. **18**, 149.
Braid, T. H., R. R. Chasman, J. R. Erskine, and A. M. Friedman, 1970, Phys. Rev. C **1**, 275.
Braid, T. H., R. R. Chasman, J. R. Erskine, and A. M. Friedman, 1971, Phys. Rev. C **4**, 247.
Braid, T. H., R. R. Chasman, J. R. Erskine, and A. M. Friedman, 1972, Phys. Rev. C **6**, 1374.
Braid, T. H., J. R. Erskine, and A. M. Friedman, 1976, unpublished.
Brink, D. M. and A. Weiguny, 1968, Phys. Lett. B **26**, 497.
Brockmeier, R. T., S. Wahlborn, E. J. Seppi, and F. Boehm, 1965, Nucl. Phys. **63**, 102.
Brown, G. E., 1967, *Unified Theory of Nuclear Models and Forces* (North-Holland, Amsterdam).
Brown, G. E., 1972, *Many Body Problems* (North-Holland, Amsterdam).
Brown, G. E. and M. Bolsterli, 1959, Phys. Rev. Lett. **3**, 472.
Brown, G. E., J. H. Gunn, and P. Gould, 1963, Nucl. Phys. **46**, 598.
Browne, E. and F. Asaro, 1968, Lawrence Radiation Laboratory Nucl. Chem. Annual Report UCRL-18667, 1.
Browne, E. and F. Asaro, 1969, Lawrence Radiation Laboratory Nucl. Chem. Annual Report UCRL-19530, 8.
Browne, E. and F. Asaro, 1973, Phys. Rev. C **7**, 2546.
Browne E. and F. R. Femenia, 1971, Nucl. Data A **10**, 81.
Bunker, M. E., D. C. Hoffman, C. J. Orth, and J. W. Starner, 1967, Nucl. Phys. A **97**, 593.
Bunker, M. E. and C. W. Reich, 1971, Rev. Mod. Phys. **43**, 348.
Casten, R. F., W. R. Kane, J. R. Erskine, A. M. Friedman, and D. S. Gale, 1976, Phys. Rev. C **14**, 912.
Chasman, R. R., 1964, Phys. Rev. **134**, 279B.
Chasman, R. R., 1970, Phys. Rev. C **1**, 2144.
Chasman, R. R., 1971, Phys. Rev. C **3**, 1803.
Chasman, R. R., 1972, Phys. Rev. Lett. **28**, 1275.
Chasman, R. R., 1972, Phys. Rev. C **5**, 29.
Chasman, R. R., 1972, talk delivered at Third International Symposium on the Transplutonium Elements, Argonne, Illinois, 20–22 October, unpublished.
Chasman, R. R., 1976, Phys. Rev. C **14**, 1935.
Chasman, R. R. and J. W. Durso, 1975, Nucl. Phys. A **255**, 45.
Chasman, R. R., and J. O. Rasmussen, 1959, Phys. Rev. **115**, 1527.
Chepurnov, V. A. and P. E. Nemirovskii, 1963, Nucl. Phys. **49**, 90.
Chetham-Strode, A., Jr., R. J. Silva, J. R. Tarrant, and I. R. Williams, 1968, Nucl. Phys. A **107**, 645.
Church, E. L. and J. Weneser, 1956, Phys. Rev. **104**, 1382.
Cline, J. E., 1968, Nucl. Phys. A **106**, 481.
Damgaard, J., H. C. Pauli, V. V. Pashkevitch, and V. M. Strutinsky, 1969, Nucl. Phys. A **135**, 432.
Dancoff, S. M., 1950, Phys. Rev. **78**, 382.
Dang, G. D. and A. Klein, 1965, Phys. Rev. **143**, 735.
Dang, G. D. and A. Klein, 1966, Phys. Rev. **147**, 689.
Daniels, W. R., D. C. Hoffman, F. O. Lawrence, and C. J. Orth, 1968, Nucl. Phys. A **107**, 569.
Da Providencia, J., 1974, Nucl. Phys. A **224**, 262.
Davidson, J. P., 1968, *Collective Models of the Nucleus* (Academic, New York).
Davidson, J. P., D. A. Close, and J. J. Malanify, 1974, Phys. Rev. Lett. **32**, 337.
Davies, D. W. and J. M. Hollander, 1965, Nucl. Phys. **68**, 161.
De Shalit, A. and H. Feshbach, 1974, *Theoretical Nuclear Physics*, Vol. I, *Nuclear Structure* (Wiley, New York).
Dietrich, K., H. J. Mang, and J. H. Pradal, 1966, Phys. Rev. **135**, 22B.
Dittner, P. F., C. E. Bemis, Jr., D. C. Hensley, R. J. Silva, and C. D. Goodman, 1971, Phys. Rev. Lett. **26**, 1037.
Dorain, P. B., C. A. Hutchison, and E. Wong, 1957, Phys. Rev. **105**, 1307.
Ehrling, G. and S. Wahlborn, 1972, Phys. Scr. **6**, 94.
Elbek, B. and P. O. Tjøm, 1969, in *Advances in Nuclear Physics*, edited by M. Baranger and E. Vogt (Plenum, New York and London), Vol. III.
Eliot, J. P., 1958, Proc. R. Soc. Lond. A **245**, 128.
Eliot, J. P., 1958, Proc. R. Soc. Lond. A **245**, 562.
Ellis, Y. A., and M. R. Schmorak, 1972, Nucl. Data B **8**, 345.
Elze, Th. W., T. V. Egidy, and J. R. Huizenga, 1969, Nucl. Phys. A **128**, 564.
Elze, Th. W. and J. R. Huizenga, 1969, Nucl. Phys. A **133**, 10.
Elze, Th. W. and J. R. Huizenga, 1970, Nucl. Phys. A **149**, 585.
Elze, Th. W. and J. R. Huizenga, 1970, Phys. Rev. C **1**, 328.
Elze, Th. W. and J. R. Huizenga, 1971, Phys. Rev. C **3**, 234.
Elze, Th. W. and J. R. Huizenga, 1975, Z. Phys. A **272**, 119.
Engelkemeir, D., 1969, Phys. Rev. **181**, 1675.
Erskine, J. R., 1965, Phys. Rev. **138**, 66B.
Erskine, J. R., 1966, BANDMIX program for Coriolis calculations, unpublished.
Erskine, J. R., 1972, Phys. Rev. C **5**, 959.
Erskine, J. R., 1972, talk delivered at Third International Symposium on the Transplutonium Elements, Argonne, Illinois, 20–22 October, unpublished.
Erskine, J. R., G. Kyle, R. R. Chasman, and A. M. Friedman, 1975, Phys. Rev. C **11**, 561.
Erskine, J. R., A. M. Friedman, and D. S. Gale, 1976, to be published; Bull. Am. Phys. Soc. **20**, 97 (1975).
Eskola, P., K. Eskola, M. Nurmia, and A. Ghiorso, 1970, Phys. Rev. C **2**, 1058.
Ewan, G. T., J. W. Knowles, and D. R. MacKenzie, 1957, Phys. Rev. **108**, 1308.
Ewan, G. T., J. S. Geiger, R. L. Graham, and D. R. MacKenzie, 1959, Phys. Rev. **116**, 950.
Faessler, A. and R. K. Sheline, 1966, Phys. Rev. **148**, 1003.
Faust, J., R. Marrus, and W. A. Nierenberg, 1965, Phys. Lett. **16**, 71.
Ferrel, R. A., 1957, Phys. Rev. **107**, 1631.
Fields, P. R., I. Ahmad, R. K. Sjoblom, R. F. Barnes, and E. P. Horwitz, 1968, J. Inorg. Nucl. Chem. **30**, 1345.
Fields, P. R., I. Ahmad, A. M. Friedman, J. Lerner, and D. N. Metta, 1971, Nucl. Phys. A **160**, 460.
Friedman, A. M. and J. Milsted, 1966, Phys. Lett. **21**, 179.
Friedman, A. M., I. Ahmad, J. Milsted, and D. W. Engelkemeir, 1969, Nucl. Phys. A **127**, 33.
Friedman, A. M., K. Katori, D. Albright, and J. P. Schiffer, 1974, Phys. Rev. C **9**, 760.
Fröman, P. O., 1957, K. Dan. Vidensk. Selsk. Mat.-Fys. Skr. **1**, No. 3.
Fuller, G. H. and V. W. Cohen, 1969, Nucl. Data A **5**, 433.
Gareev, F. A., S. P. Ivanova, and L. A. Kalinkin, 1967, JINR Dubna preprint P4-3326.
Gareev, F. A., S. P. Ivanova, and V. V. Pashkevitch, 1969, JINR Dubna preprint E4-4704.
Gareev, F. A., S. P. Ivanova, L. A. Malov, and V. G. Soloviev, 1971, Nucl. Phys. A **171**, 134.
Gerstenkorn, S., P. Lue, J. Verges, D. W. Engelkemeir, J. E. Gindler, and F. S. Tomkins, 1974, J. Phys. (Paris) **35**, 483.
Glas, D. and U. Mosel, 1973, Nucl. Phys. A **216**, 563.

Glendenning, N. K., 1975, Rev. Mod. Phys. **47**, 659.
Goodman, L. S., H. Diamond, and H. E. Stanton, 1975, Phys. Rev. A **11**, 499.
Gorman, D. G. and F. Asaro, 1971, Phys. Rev. C **3**, 746.
Gottfried, K., 1956, Phys. Rev. **103**, 1017.
Gove, N. B. and M. J. Martin, 1971, Nucl. Data A **10**, 206.
Green, I. M. and S. A. Moszkowski, 1965, Phys. Rev. **139**, 790B.
Griffin, J. J. and J. A. Wheeler, 1957, Phys. Rev. **108**, 311.
Griffin, R. E., A. D. Jackson, and A. B. Volkov, 1971, Phys. Lett. B **36**, 281.
Grotdal, T., L. Løset, K. Nybø, and T. F. Thorsteinsen, 1973, Nucl. Phys. A **211**, 541.
Gustafson, C., I. L. Lamm, B. Nilsson, and S. G. Nilsson, 1967, Ark. Fys. **36**, 613.
Hager, R. S. and E. C. Seltzer, 1968, Nucl. Data A **4**, 1.
Hamamoto, I., 1974, Phys. Rep. **10** C, No. 2.
Harada, K., 1964, Phys. Lett. **10**, 80.
Haxel O., J. H. D. Jensen, and H. E. Suess, 1950, Z. Phys. **128**, 295.
Hendrie, D. L., 1973, Phys. Rev. Lett. **31**, 478.
Hill, D. L. and J. A. Wheeler, 1953, Phys. Rev. **89**, 1102.
Hoekstra, W. and A. H. Wapstra, 1969, Phys. Rev. Lett. **22**, 859.
Hoff, R. W., 1972, talk delivered at Third International Symposium on the Transplutonium Elements, Argonne, Illinois, 20–22 October, unpublished.
Hoff, R. W., 1975, in *Proceedings of the Fourth International Symposium on the Transplutonium Elements*, Baden-Baden, 13–15 September, edited by W. Müller and R. Lindner (North-Holland, Amsterdam), 341.
Hoff, R. W., J. E. Evans, L. G. Mann, J. F. Wild, and R. W. Lougheed, 1971, Bull. Am. Phys. Soc. **16**, 494.
Hoffman, D. C. and B. J. Dropesky, 1958, Phys. Rev. **109**, 1282.
Hoffman, D. C., F. O. Lawrence, and W. R. Daniels, 1969, Nucl. Phys. A **131**, 551.
Højeberg, M. and S. G. Malmskog, 1970, Nucl. Phys. A **141**, 249.
Holtz, M. D. and J. M. Hollander, 1970, Lawrence Berkeley Laboratory Nucl. Chem. Annual Report UCRL-20425, 6.
Holzworth, G., 1972, Nucl. Phys. A **185**, 268.
Hornshøj, P., P. Tidemand-Petersson, R. Kaezarowski, B. Kotlinska, and J. Zylicz, 1975, Nucl. Phys. A **248**, 406.
Hubbs, J. C. and R. Marrus, 1958, Phys. Rev. **110**, 287.
Hutchison, C. A., Jr., and B. Weinstock, 1960, J. Chem. Phys. **32**, 56.
Immele, J. D. and G. L. Struble, 1973, Nuovo Cimento Lett. **7**, 41.
Immele, J. D. and G. L. Struble, 1975, UCRL preprint 77519.
Ivanova, S. P., A. L. Komov, L. A. Malov, and V. G. Soloviev, 1972, JINR Dubna preprint E4-6663.
Jäger, U., H. Münzel, and G. Pfennig, 1973, Phys. Rev. C **7**, 1627.
James, A. N., P. T. Andrews, P. Kirkby, and B. G. Lowe, 1969, Nucl. Phys. A **138**, 145.
Jancovici, B. and D. H. Schiff, 1964, Nucl. Phys. **58**, 678.
Kerman, A. K., 1956, K. Dan. Vidensk. Selsk. Mat.-Fys. Medd. **30**, No. 15.
Kerman, A. K., 1959, in *Nuclear Reactions*, edited by P. M. Endt and M. Demeur (North-Holland, Amsterdam), Vol. I, 427.
Kerman, A. K., R. D. Lawson, and M. H. MacFarlane, 1961, Phys. Rev. **124**, 162.
Kern, J. and D. Duc, 1974, Phys. Rev. C **10**, 1554.
Kisslinger, L. S. and R. A. Sorensen, 1960, K. Dan. Vidensk. Selsk. Mat.-Fys. Medd. **32**, No. 9.
Kisslinger, L. S. and R. A. Sorensen, 1963, Rev. Mod. Phys. **35**, 853.
Kjällquist, K., 1958, Nucl. Phys. **9**, 163.
Ko, C. M., H. C. Pauli, M. Brack, and G. E. Brown, 1974, Nucl. Phys. A **236**, 269.
Kolb, D., R. Y. Cusson, and R. W. Schmitt, 1974, Phys. Rev. C **10**, 1529.
Komov, A. L., L. A. Malov, and V. G. Soloviev, 1971, JINR Dubna preprint P4-5693.
Kroger, L. A. and C. W. Reich, 1976, Nucl. Phys. A **259**, 29.
Krpić, D. K., I. V. Anicin, and R. B. Vukanovic, 1973, Nucl. Data A **11**, 553.
Kumar, K., 1975, in *Electromagnetic Interactions in Nuclear Spectroscopy*, edited by W. D. Hamilton (North-Holland, Amsterdam) 55, 119.
Kunz, P., 1969, Univ. of Colorado, Zero-range DWBA code DWUCK, unpublished.
Lamm, I. L., 1969, Nucl. Phys. A **125**, 504.
Lande, A., 1965, Ann. Phys. **31**, 525.
Lane, A. M., 1964, *Nuclear Theory* (Benjamin, New York).
Lederer, C. M., J. K. Poggenburg, F. Asaro, J. O. Rasmussen, and I. Perlman, 1966, Nucl. Phys. **84**, 481.
Lederer, C. M., J. M. Hollander, and I. Perlman, 1967, *Table of Isotopes* (Wiley, New York).
Macefield, B. E. F. and R. Middleton, 1964, Nucl. Phys. **59**, 561.
Major, J. K. and L. C. Biedenharn, 1954, Rev. Mod. Phys. **26**, 321.
Malov, L. A. and V. G. Soloviev, 1966, JINR Dubna preprint E-2857.
Mang, H. J., J. K. Poggenburg, and J. O. Rasmussen, 1965, Nucl. Phys. **64**, 353.
Mang, H. J., J. O. Rasmussen, and M. Rho, 1966, Phys. Rev. **141**, 941.
Manning, T. E., M. Fred, and F. S. Tomkins, 1956, Phys. Rev. **102**, 1109.
Marrus, R., W. A. Nierenberg, and J. Winocur, 1961, Nucl. Phys. **23**, 90.
Marshalek, E. R., 1974, Nucl. Phys. A **224**, 221.
Marumori, T., 1960, Prog. Theor. Phys. **24**, 331.
Marumori, T., M. Yamamura, and A. Tokunaga, 1964, Prog. Theor. Phys. **31**, 1009.
Mattuck, R. D., 1967, *A Guide to Feynman Diagrams in Many Body Problems* (McGraw Hill, London).
Mayer, M. G., 1949, Phys. Rev. **75**, 1969.
Migdal, A. B., 1962, Nucl. Phys. **30**, 239.
Migdal, A. B., 1967, *Theory of Finite Fermi Systems and Applications to Atomic Nuclei* (Interscience, New York).
Migdal. A. B., 1968, *Nuclear Theory: The Quasiparticle Method* (Benjamin, New York).
Mills, R., 1969, *Propagators for Many-Particle Systems* (Gordon and Breach, New York).
Milner, W. T., C. E. Bemis, Jr., and F. K. McGowan, 1976, private communication.
Møller, P., S. G. Nilsson, and J. R. Nix, 1974, Nucl. Phys. A **229**, 292.
Moss, J. M,, Y. D. Terrien, R. M. Lombard, C. Brassard, and J. M. Loiseaux, 1971, Phys. Rev. Lett. **26**, 1488.
Moszkowski, S. A., 1955, Phys. Rev. **99**, 803.
Moszkowski, S. A., 1957, in *Handbuch der Physik*, edited by S. Flugge (Springer, Berlin) Vol. 39, 411.
Moszkowski, S. A., 1965, in *Alpha-, Beta-, and Gamma-Ray Spectroscopy*, edited by K. Siegbahn (North-Holland, Amsterdam) Vol. II, 881.
Mottelson, B. R., 1959, Nordita publication No. 20.
Mottelson, B. R., 1976, Rev. Mod. Phys. **48**, 375.
Mottelson, B. R. and S. G. Nilsson, 1959, K. Dan. Vidensk. Selsk. Mat.-Fys. Skr. **1**, No. 8.
Myers, W. D. and W. J. Swiatecki, 1966, Nucl. Phys. A **81**, 1.
Nathan, O. and S. G. Nilsson, 1965, in *Alpha-, Beta-, and Gamma-Ray Spectroscopy*, edited by K. Siegbahn (North-Holland, Amsterdam).
Nemirovskii, P. E., 1963, *Contemporary Models for the*

Atomic Nucleus,(Pergamon, Oxford).
Nemirovskii, P. E. and V. A. Chepurnov, 1966, Sov. J. Nucl. Phys. **3**, 730.
Neergård, K. and P. Vogel, 1970, Nucl. Phys. A **149**, 209,217.
Nierenberg, W. A. and I. Lindgren, 1965, in *Alpha-, Beta-, and Gamma-Ray Spectroscopy*, edited by K. Siegbahn (North-Holland, Amsterdam) Vol. II, 1263.
Nielsen, B. S. and M. E. Bunker, 1975, Nucl. Phys. A **245**, 376.
Nilsson, S. G., 1955, K. Dan. Vidensk. Selsk. Mat.-Fys. Medd. **29**, No. 16.
Nilsson, S. G. and J. O. Rasmussen, 1958, Nucl. Phys. **5**, 617.
Nilsson, S. G. and O. Prior, 1961, K. Dan. Vidensk. Selsk. Mat.-Fys. Medd. **32**, No. 16.
Nilsson, S. G., C. F. Tsang, A. Sobiczewski, Z. Szymanski, S. Wycech, C. Gustafson, I. Lamm, P. Møller, and B. Nilsson, 1969, Nucl. Phys. A **131**, 1.
Ogle, W., S. Wahlborn, R. Piepenbring, and S. Fredriksson, 1971, Rev. Mod. Phys. **43**, 424.
Osnes, E., J. Rekstad, and O. Gjøtterud, 1975, Nucl. Phys. A **253**, 45.
Parry, W. E., 1973, *The Many-Body Problem* (Clarendon, Oxford).
Pauli, H. C., 1973, Phys. Rep. 7C, No. 2, 35.
Perdrisat, C. F., 1966, Rev. Mod. Phys. **38**, 41.
Perey, F. and B. Buck, 1962, Nucl. Phys. **32**, 353.
Perlman, I. and J. O. Rasmussen, 1957, in *Handbuch der Physik*, edited by S. Flügge (Springer, Berlin) Vol. 42, 109.
Pilger, R. C., F. S. Stephens, F. Asaro, and I. Perlman, 1964, in *The Nuclear Properties of the Heavy Elements*, edited by E. K. Hyde, I. Perlman, and G. T. Seaborg, (Prentice-Hall, Englewood Cliffs, N. J.), 727.
Poggenburg, J. K., H. J. Mang, and J. O. Rasmussen, 1969, Phys. Rev. **181**, 1697.
Porter, F. T., I. Ahmad, M. S. Freedman, R. F. Barnes, R. K. Sjoblom, F. Wagner, Jr., and P. R. Fields, 1972, Phys. Rev. C **5**, 1738.
Porter, F. T., I. Ahmad, M. S. Freedman, J. Milsted, and A. M. Friedman, 1974, Phys. Rev. C **10**, 803.
Preston, M. A., 1947, Phys. Rev. **71**, 865.
Prior, O., 1959, Ark. Fys. **16**, 15.
Quentin, Ph., 1973, J. Phys. (Paris) **34**, C4-101.
Rainwater, J., 1950, Phys. Rev. **79**, 432.
Rainwater, J., 1976, Rev. Mod. Phys. **48**, 385.
Rasmussen, J. O., 1954, Ark. Fys. **7**, 185.
Rasmussen, J. O., 1965, in *Alpha-, Beta-, and Gamma-Ray Spectroscopy*, edited by K. Siegbahn (North-Holland, Amsterdam), Vol. I, 701.
Rassey, A. J., 1958, Phys. Rev. **109**, 949.
Richardson, R. W., 1966, Phys. Rev. **141**, 949.
Richardson, R. W. and N. Sherman, 1964, Nucl. Phys. **52**, 22.
Rickey, F. A., E. T. Jurney, and H. C. Britt, 1972, Phys. Rev. C **5**, 2072.
Ring, P., H. J. Mang, and B. Banerjee, 1974, Nucl. Phys. A **225**, 141.
Röper, P., 1966, Z. Phys. **195**, 316.
Rost, E., 1967, Phys. Rev. **154**, 994.
Rowe, D. J., 1970, *Nuclear Collective Motion* (Methuen, London).
Satchler, G. R., 1964, Nucl. Phys. **55**, 1.
Schulz, H., H. J. Wiebike, and F. A. Gareev, 1972, Nucl. Phys. A **180**, 625.
Seeger, P. A. and W. M. Howard, 1975, Nucl. Phys. A **238**, 491.
Seelerman-Eggebut, W., G. Pfennig, and H. Munzel, 1974, *Chart of Nuclides* (Kernforschungzintum, Karlsruhe).
Sheline, R. K., W. N. Shelton, T. Udagawa, E. T. Jurney, and M. T. Motz, 1966, Phys. Rev. **151**, 1011.
Shirley, V. G. and C. M. Lederer, 1975, in *Hyperfine Interactions Studied in Nuclear Reactions and Decays*, edited by E. Karlsson and R. Wäpling (Almquist and Wiksell, Stockholm-New York).
Siemssen, R. H. and J. R. Erskine, 1966, Phys. Rev. **146**, 911.
Solinski, A. J., D. G. Raich, J. O. Rasmussen, and E. R. Rauscher, 1973, Lawrence Berkeley Laboratory Nucl. Chem. Annual Report LBL-2366, 172.
Soloviev, V. G., 1958, Nucl. Phys. **9**, 655.
Soloviev, V. G., 1961, K. Dan. Vidensk. Selsk. Mat.-Fys. Skr. **1**, No. 11.
Soloviev, V. G., 1963, in *Selected Topics in Nuclear Theory* (IAEA, Vienna), 233.
Soloviev, V. G. and P. Vogel, 1967, Nucl. Phys. A **92**, 449.
Sorensen, B., 1967, Nucl. Phys. A **97**, 1.
Sorensen, B., 1968, Nucl. Phys. A **119**, 65.
Stephens, F. S., 1975, Rev. Mod. Phys. **47**, 43.
Stephens, F. S., F. Asaro, and I. Perlman, 1959, Phys. Rev. **113**, 212.
Stephens, F. S., M. D. Holtz, R. M. Diamond, and J. O. Newton, 1968, Nucl. Phys. A **115**, 129.
Strutinsky, V. M., 1967, Nucl. Phys. A **95**, 420.
Tamm, I., 1945, J. Phys. (USSR) **9**, 449.
Tamura, T., D. R. Bès, R. A. Broglia, and S. Landowne, 1970, Phys. Rev. Lett. **25**, 1507.
Tamura, T., 1971, Univ. of Texas, code NEPTUNE, unpublished.
Thompson, R. C., J. R. Huizenga, and Th. W. Elze, 1976, Phys. Rev. C **13**, 638.
Ton, H., S. Roodberger, J. Brasz, and J. Blok, 1970, Nucl. Phys. A **155**, 245.
Townes, C. H., H. M. Foley, and W. Low, 1949, Phys. Rev. **76**, 1415.
Vander Sluis, K. L., 1956, Oak Ridge National Laboratory Report ORNL-2236, p. 35.
Van Hise, J. R. and D. W. Engelkemeir, 1968, Phys. Rev. **171**, 1325.
Van Rij, W. I. and S. H. Kahana, 1972, Phys. Rev. Lett. **28**, 50.
Vañó, E., R. Gaeta, L. Gonzalez, and C. F. Liang, 1975, Nucl. Phys. A **251**, 225.
Vergnes, M. N. and R. K. Sheline, 1963, Phys. Rev. **132**, 1736.
Von Egidy, T., Th. W. Elze, and J. R. Huizenga, 1970, Nucl. Phys. A **145**, 306.
Von Egidy, T., Th. W. Elze, and J. R. Huizenga, 1975, Phys. Rev. C **11**, 529.
Von Egidy, T., O. W. B. Schult, D. Rabenstein, J. R. Erskine, O. A. Wasson, R. E. Chrien, D. Breitig, R. P. Sharma, H. A. Baader, and H. R. Koch, 1972, Phys. Rev. C **6**, 266.
Wahlborn, S., 1962, Nucl. Phys. **37**, 554.
Wahlborn, S., 1966, Ark. Fys. **31**, 33.
Wong, C. W., 1975, Phys. Rep. **15C**, No. 5, 283.
Woods, R. D. and D. S. Saxon, 1954, Phys. Rev. **95**, 577.
Wyatt, P. J., J. G. Wills, and A. E. S. Green, 1960, Phys. Rev. **119**, 1031.
Yamazaki, T. and J. M. Hollander, 1966, Nucl. Phys. **84**, 505.
Yates, S. W., I. Ahmad, A. M. Friedman, F. J. Lynch, and R. E. Holland, 1975, Phys. Rev. C **11**, 599.
Yates, S. W., R. R. Chasman, A. M. Friedman, I. Ahmad, and K. Katori, 1975, Phys. Rev. C **12**, 442.